Journal of Environmental Chemical Engineering 13 (2025) 117529

Contents lists available at ScienceDirect

Journal of Environmental Chemical Engineering

journal homepage: www.elsevier.com/locate/jece

Photocatalysis for sustainable energy and environmental protection in construction: A review on surface engineering and emerging synthesis

Kailun Chen [a], Wenkui Dong [a], Yuhan Huang [b], Fazhou Wang [c], John L. Zhou [b], Wengui Li [a,*]

[a] Centre for Infrastructure Engineering and Safety, School of Civil and Environmental Engineering, The University of New South Wales, NSW 2052, Australia
[b] Centre for Green Technology, School of Civil and Environmental Engineering, University of Technology Sydney, NSW 2007, Australia
[c] State Key Laboratory of Silicate Materials for Architectures, Wuhan University of Technology, Wuhan 430070, China

ARTICLE INFO

Keywords:
Photocatalytic technology
Toxic intermediates
Low-carbon synthesis
Surface modification
Defect engineering
Catalyst deactivation

ABSTRACT

The sustained growth in global energy demand and escalating environmental crises resulting from fossil fuel consumption underscore the urgent need for sustainable technologies. Photocatalysis, which harnesses solar energy to drive redox reactions for concurrent clean fuel production and pollutant degradation, has demonstrated significant potential for diverse applications. However, conventional photocatalysts are hindered by intrinsic limitations such as restricted visible-light absorption, rapid electron–hole recombination, and insufficient structural stability. In addition, extrinsic challenges, including mass transfer constraints, catalyst deactivation, and the formation of toxic by-products, further impede practical implementation. Existing reviews typically address these issues in isolation or focus on single materials (e.g., TiO_2), thereby lacking a comprehensive, state-of-the-art perspective. To fill this gap, this review systematically summarizes and critically evaluates the key bottlenecks hindering the practical application of photocatalytic technologies. It provides an in-depth overview of advanced surface functionalization and interfacial engineering strategies designed to overcome these limitations, including ferroelectric polarization, hydrogel-supported composite structures, defect engineering, and heterojunction/homojunction systems, while thoroughly elucidating the synergistic effects among these strategies. Furthermore, the review highlights emerging low-carbon and scalable synthetic approaches such as green biosynthesis, microfluidics, plasma-assisted electrolysis, and mechanochemistry, by comparing their potential for industrial-scale production. Finally, it outlines future research directions, emphasizing the pivotal roles of machine learning, interdisciplinary integration, and scalable manufacturing in transitioning photocatalytic innovations from laboratory settings to industrial applications. Overall, this review offers a comprehensive analytical framework and strategic insights to facilitate the transformation of photocatalysis from laboratory research to practical industrial-scale implementation.

1. Introduction

The world faces an unprecedented nexus of energy demand and environmental degradation. Accelerated industrialization and population growth have driven a steep rise in energy consumption, while continued reliance on fossil fuels not only exhausts finite resources but also releases large quantities of pollutants and greenhouse gases, exacerbating climate change as well as air and water quality crises [1]. Photocatalysis has proven to be a compelling strategy to address these intertwined challenges [2]. By harnessing solar photons to drive redox reactions that emulate artificial photosynthesis, photocatalytic systems can simultaneously generate carbon-neutral fuels and degrade

Abbreviation: VB, Valence band; E^-, Electrons; CB, Conduction band; H^+, Hole pairs; $O_2^{\bullet-}$, Superoxide radicals; •OH, Hydroxyl radicals; RP, Red phosphorus; RH, Relative humidity; PVA, Polyvinyl alcohol; SA, Alginate; CMC, Carboxymethyl cellulose; K, Potassium K; B, Boron; $TiCl_4$, Titanium tetrachloride; HAp, Hydroxyapatite; OVs, oxygen vacancies; UV, ultraviolet; E^-/h^+, electron–hole; G-C_3N_4, graphitic carbon nitride; Apd, acetamiprid; VOCs, Volatile organic compounds; DMS, Dimethyl sulfide; GO, Graphene oxide; CQD, carbon quantum dot; RGO, Reduced graphene oxide; $NiTiO_3$, Nickel titanate; COF, Covalent organic framework; ALD, Atomic layer deposition; Tr, Tartrazine; $BiVO_4$, Bismuth vanadate; ROS, Reactive oxygen species; MB, Methylene blue; MOFs, Metal–organic frameworks; HER, Hydrogen evolution reaction; DFT, Density functional theory; MCC, Microcrystalline cellulose; TCH, Tetracycline hydrochloride; QDs, Quantum dots; RhB, Rhodamine B; LDH, Layered double hydroxide; PVD, Physical vapor deposition; DIW, Direct ink writing.

* Correspondence to: School of Civil and Environmental Engineering, The University of New South Wales, NSW 2052, Australia.
E-mail address: wengui.li@unsw.edu.au (W. Li).

https://doi.org/10.1016/j.jece.2025.117529
Received 15 February 2025; Received in revised form 23 April 2025; Accepted 9 June 2025
Available online 10 June 2025

contaminants under mild conditions [3–5]. With further efficiency gains, such systems are poised to satisfy global energy needs while mitigating environmental impacts, positioning photocatalysis at the forefront of next-generation green technologies [2].

As shown in Fig. 1(a), under light irradiation, a photocatalyst absorbs energy ($h\nu \geq Eg$), which excites valence band (VB) electrons (e^-) to transition to the conduction band (CB), forming photogenerated electron–hole (e^-/h^+) pairs. The photogenerated electrons can react with O_2 to produce superoxide radicals ($O_2\bullet^-$), while the photogenerated h^+ can oxidize H_2O or OH^- to generate hydroxyl radicals (•OH). These active species can efficiently degrade pollutants or drive redox reactions, thereby achieving both the degradation of environmental contaminants and energy conversion [6]. As a green technology that uses light energy to drive chemical reactions, photocatalysis has shown broad application prospects in multiple fields, as illustrated in Fig. 1(b). In terms of pollution control, photocatalysis can effectively degrade organic pollutants [7,8], remove nitrogen oxides from the air [9], and reduce heavy metal ions in water [10]. In the field of energy conversion, photocatalytic technology can be used for water splitting to produce hydrogen or for the synthesis of hydrogen peroxide as an energy source [11,12], as well as for carbon dioxide reduction [13]. Furthermore, this technology can also be applied in resource recovery [14] and nitrogen fixation [15].

Despite these attractive prospects, current photocatalytic systems suffer from several fundamental limitations that hinder their practical performance. A wide-bandgap semiconductor (such as TiO_2 or ZnO) typically absorbs only ultraviolet (UV) (a small ~5 % fraction of the solar spectrum) and thus has limited visible-light absorption, severely underutilizing available sunlight [16,17]. Moreover, rapid e^-/h^+ recombination following photoexcitation in such materials drastically lowers the external quantum efficiency by annihilating most photogenerated carriers before they can reach surface redox sites[18]. In

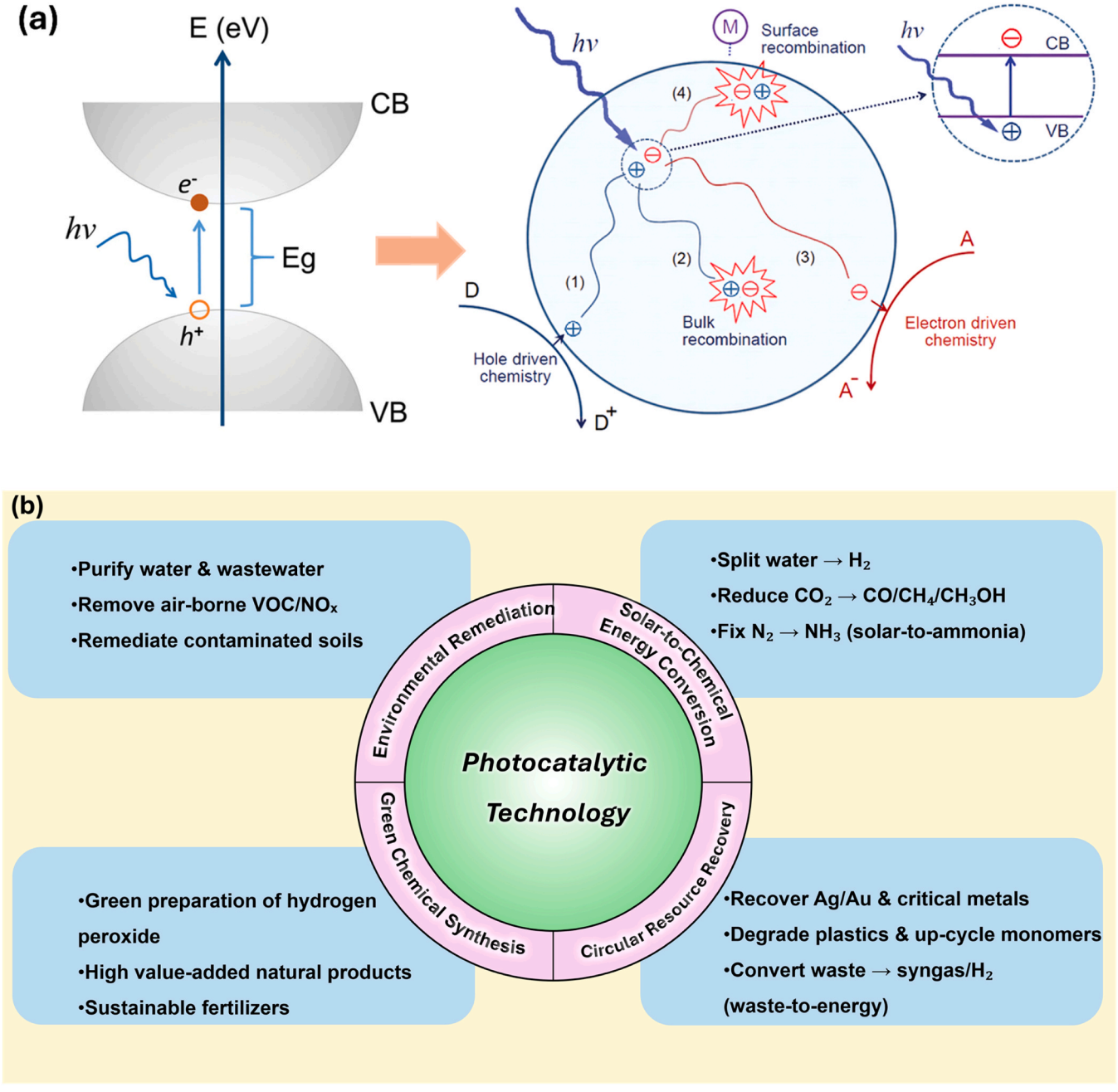

Fig. 1. Photocatalytic technology: (a) Photocatalytic technology reaction mechanism[6]; (b) Prospects for the application of photocatalytic technology.

addition, many intrinsic and extrinsic factors influence photocatalytic performance. The semiconductor's band structure controls the balance between light-harvesting and redox power [19], while operating conditions such as temperature and pH can change reaction kinetics and pathways [20]. Likewise, factors like gas flow rate and concentration, as well as the relative humidity of the environment, significantly affect the mass transfer rate of the reactants [21,22]. Thus, achieving high photocatalytic efficiency is a multifaceted problem involving both material properties and reaction environment, and suboptimal values in any of these aspects can bottleneck the overall performance.

To overcome the common limitations of photocatalysts, such as narrow light absorption ranges, rapid carrier recombination, and poor structural stability, research strategies have shifted from traditional single doping or co-catalyst addition to more sophisticated surface structural engineering[23,24]. Among these, semiconductor structure engineering, including the construction of Type-II, Z-scheme, or S-scheme heterojunctions, as well as homojunctions formed by coupling different crystal facets of the same semiconductor, significantly enhances the separation efficiency of photogenerated e^-/h^+ [25,26]. Defect engineering, such as intentional elemental doping, the introduction of oxygen vacancies (OVs), or lattice strain, enables the formation of intermediate energy states within the bandgap, thereby effectively prolonging carrier lifetime without compromising redox capability[27]. Furthermore, ferroelectric interface engineering leverages intrinsic electric fields to direct photogenerated charges in opposite directions, effectively suppressing carrier recombination and enhancing photocatalytic efficiency [28]. Recently, hydrogel-based surface functionalization strategies have also attracted considerable attention; embedding photocatalysts such as TiO_2 into hydrophilic polymer gel networks maintains excellent nanoparticle dispersion and optical transparency, improves pollutant adsorption at catalytic sites, and prevents particle agglomeration, thus significantly improving the photocatalytic activity and recyclability of the materials [29]. Nevertheless, integrating multiple modifications in a controlled manner and ensuring stability of the resulting complex systems remain non-trivial. There is a need for a comprehensive understanding of how different modifications can be synergistically combined and what fundamental limits might be approached through these enhancements. Also, although numerous strategies boost photocatalytic rates in the laboratory, these gains seldom persist under practical conditions. In real-scale reactors, external mass transfer resistance and sub-optimal photon penetration can mask the intrinsic merits of an upgraded catalyst [30]. Moreover, photocatalysts may gradually deactivate due to surface contamination, leaching of active components, or photo corrosion, causing long-term operational efficiency to decline by 50 % or more, despite high initial catalytic performance [31]. More complicatedly, incomplete mineralization may lead to the formation of toxic intermediates; for example, excessive NO_2 produced during the photocatalytic oxidation of NO_x can significantly diminish the overall environmental benefits [32].

In recent years, various innovative strategies have emerged in fields such as interface regulation and new material synthesis. However, the synergistic mechanisms and practical application effects of these strategies have not yet been systematically evaluated. Therefore, a comprehensive review that systematically addresses these unresolved challenges and recent advancements is urgently needed to provide clear guidance for future research. Compared with previous reviews, this review systematically examines the critical bottlenecks in practical photocatalytic applications, such as mass transfer limitations, catalyst deactivation, and toxic intermediate formation, and critically assesses state-of-the-art mitigation strategies. It further integrates interface engineering techniques, including ferroelectric polarization interfaces, hydrogel-based composite structures, homojunction construction, and defect engineering, clearly elucidating how the synergy among these diverse strategies enhances photocatalytic activity and stability across various semiconductor systems. Such systematic and integrative analysis moves beyond conventional reviews that typically focus exclusively on TiO_2-based materials or singular modification methods such as doping. Additionally, building upon a thorough overview of traditional photocatalyst fabrication methods, this review introduces emerging low-carbon synthesis technologies, such as green biological synthesis, microfluidics, and plasma-assisted electrolysis, and comparatively evaluates their distinctive advantages in terms of precise structural control and potential scalability. Finally, by closely coupling theoretical insights with experimental findings, this review provides an in-depth mechanistic understanding of how structural modifications precisely influence charge dynamics and reaction pathways, offering novel theoretical perspectives and experimental validations of the "structure–performance" relationships. Overall, this integrative perspective establishes a unified framework linking fundamental mechanisms with practical engineering solutions, providing valuable insights and strategic directions for advancing photocatalysis research and its industrial-scale implementation.

This review systematically discusses the critical intrinsic factors and operational parameters controlling photocatalytic performance in Section 2. Subsequently, Section 3 explores a variety of surface modification and functionalization strategies designed to improve photocatalyst efficiency, with particular emphasis on synergistic mechanisms such as cation-anion defect synergies and homo-/heterojunction interfacial interactions. This section systematically summarizes these strategies and elucidates how such synergistic effects enhance light absorption, facilitate charge separation, and improve catalytic efficiency. Section 4 addresses the principal challenges encountered in the practical implementation of photocatalysts and reviews recent advancements in reactor design and materials engineering that aim to mitigate these limitations. Section 5 further outlines emerging preparation techniques for photocatalysts, emphasizing their unique advantages in precisely controlling catalyst composition and structure to overcome the inherent limitations of traditional preparation methods. Finally, the paper concludes by providing a forward-looking perspective, clearly identifying research opportunities and future directions essential for advancing photocatalytic materials and technologies toward practical applications. Through this comprehensive overview, readers will gain insights into the latest progress and evolving trends in photocatalysis, bridging fundamental concepts and innovative engineering approaches.

2. Factors affecting photocatalytic efficiency

2.1. Band gap and optical property effects on photocatalytic activity

The bandgap width of a photocatalyst controls the balance between its light-harvesting capacity and the redox reactivity of the photoexcited carriers [33]. Narrow bandgap materials in Fig. 2(a) can absorb lower-energy, longer-wavelength photons in the visible region, promoting e^- transitions from the VB to the CB, whereas wider bandgap materials require higher-energy UV photons for excitation [34]. Generally, a smaller bandgap enables the utilization of a larger portion of the solar spectrum (i.e., visible light), but this is often accompanied by a higher rate of e^-/h^+ recombination and diminished oxidative power of photogenerated h^+ [35]. In contrast, larger bandgaps allow for more energetic charge carriers with higher redox potentials, but the activation is mainly limited to the UV range of sunlight (about 3–5 %) [36]. For example, TiO_2 (3.2 eV) and ZnO (3.2 eV) are wide-bandgap photocatalysts that absorb only UV irradiation ($\lambda < 400$ nm) and exhibit excellent photocatalytic activity under UV light but offer limited visible-light responsiveness [17,37]. Conversely, narrow-bandgap photocatalysts such as CdS (2.4 eV) and g-C_3N_4 (2.7 eV) extend absorption into the visible region [38]. Notably, CdS was activated by sunlight (380–780 nm) to effectively degrade organic dyes such as Congo red, whereas TiO_2 showed significant pollutant decomposition only under UV illumination [39]. Nonetheless, these visible-light-responsive materials frequently experience rapid e^-/h^+ recombination, diminishing their overall efficiency [35]. On the other hand, a broad bandgap, such as that

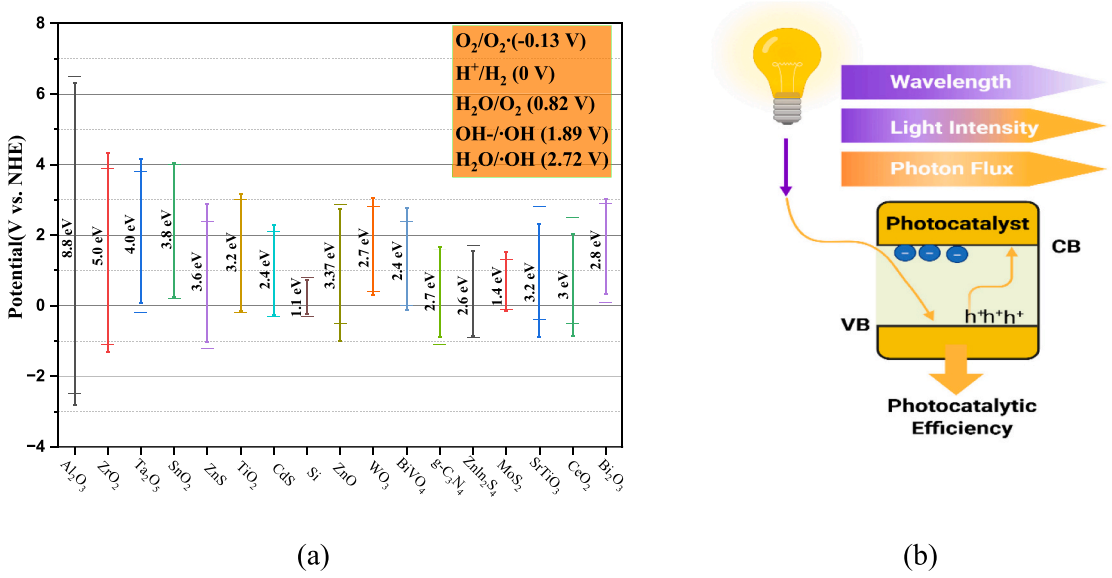

Fig. 2. Effect of band gap on photocatalytic performance [42,47,48].

observed in alumina Al_2O_3 (8.8 eV), showed negligible activity under low energy visible or even UV light [40], but under high-energy γ-irradiation, Al_2O_3 became an effective catalyst for degrading 4-chlorophenol [41]. Therefore, the interplay between bandgap width and photocatalytic performance underscores the importance of tailoring the bandgap to maximize light absorption while still providing sufficient carrier energy to drive the desired redox reactions.

Moreover, the CB and VB potentials of photocatalysts play a decisive role in their catalytic performance [42], as shown in Fig. 2(a). When a photocatalyst absorbs light energy, e^- is excited to the CB (leaving h^+ in the VB); if the CB potential is more negative than the $O_2/O_2\bullet^-$ redox potential (−0.13 V vs. NHE), these electrons can reduce oxygen to form $O_2\bullet^-$, which accelerates pollutant degradation and suppresses e^-/h^+ recombination. For instance, CdS (−1.4 V vs. NHE) was more effective at generating $O_2\bullet^-$ than WO_3 (+0.39 V vs. NHE), thus exhibiting higher photocatalytic activity[43]. Meanwhile, a sufficiently positive VB enables holes to directly oxidize pollutants or react with H_2O/OH^- to form •OH [44,45]. In this regard, WO_3, which had a higher VB potential compared to MoO_3 and TiO_2, showed stronger oxidative capacity in degrading Remazol Black B [46]. These examples illustrate that a photocatalyst's bandgap determines which portion of the light spectrum can be utilized for excitation, thereby governing its activity under various illumination conditions.

Even if the bandgap is suitable, photocatalytic efficiency is still highly dependent on the optical characteristics. Recent studies suggest that photocatalytic efficiency depends on the properties of the radiation source (e.g., wavelength, spectral distribution), the total irradiance, and the photon flux in Fig. 2(b) [49–52]. Different photocatalysts exhibit unique optimal absorption ranges according to their bandgap; for example, titanate-based materials showed superior activity in the UV region, whereas visible-light-responsive catalysts such as goethite could better exploit the larger visible component of solar irradiation [49]. Previous studies [53–55] have demonstrated that greater light intensity (i.e., total irradiance) accelerated photocatalytic reactions by providing more energy to the catalyst, whereas photon flux determined the number of photons available per unit time, thus influencing quantum efficiency; however, excessively high photon flux might saturate active sites and induce photodegradation, revealing a non-linear relationship between photon flux and catalytic efficiency. Consequently, optimizing light sources and irradiance conditions based on the catalyst's bandgap, morphology, and pollutant characteristics is crucial for achieving efficient energy conversion.

A particular study elaborated on the impact of light on photocatalyst performance [56] and examined how different radiation schemes significantly influenced the photocatalytic performance of TiO_2-based samples in organic degradation, as shown in Fig. 3. By comparing the performance of acetamiprid (Apd) and tartrazine (Tr) under different lighting conditions, it was found that Apd achieved the highest efficiency (50.3 %) under the lighting condition using three UV-A sources and one Vis source, while Tr's efficiency was 46.6 %. Additionally, photocatalytic efficiency was influenced not only by total irradiance but also by the type of radiation source, with lower efficiencies observed at irradiance intensities of 8.6, 12.9, and 17.6 W/m^2, and higher efficiencies at 12.3 and 12.9 W/m^2. However, merely increasing photon flux did not effectively enhance photocatalytic efficiency, as it would exceed the energy threshold corresponding to the catalyst's effective bandgap.

In addition to TiO_2, photocatalysts with narrower bandgaps, such as graphitic carbon nitride (g-C_3N_4), bismuth vanadate ($BiVO_4$), and $ZnIn_2S_4$, display heightened sensitivity to visible light and can utilize photons with wavelengths extending to 500 nm or even beyond. As photons with sub-bandgap energies cannot excite charge carriers and any excess energy from high-energy photons is lost as heat, optimal light management should balance adequate excitation against the risk of carrier recombination and saturation under intense illumination. Indeed, while g-C_3N_4 demonstrated improved pollutant degradation rates with increasing photon flux, strong illumination induced recombination losses that diminish overall efficiency gains [57]. Similarly, Pihosh et al. [58] observed a sublinear correlation between photocurrent and light intensity in $BiVO_4$ photoanodes at room temperature, driven primarily by carrier recombination under intense illumination. Moreover, Chong et al. [59] confirmed the critical impact of radiation-source spectral characteristics on photocatalytic activity. By introducing sulfur vacancy defects in $ZnIn_2S_4$, they expanded the photocatalyst's absorption into the visible, red, and even the spectral response range in the near-infrared region. This broadened spectral response allows more effective utilization of the incident photon flux, enabling two-step electron excitation and thereby enhancing both the generation and utilization of photogenerated carriers. In summary, tailoring a photocatalyst's bandgap and aligning the illumination wavelength and intensity accordingly allowed maximum photon utilization and minimizes carrier losses, thereby markedly enhancing photocatalytic performance.

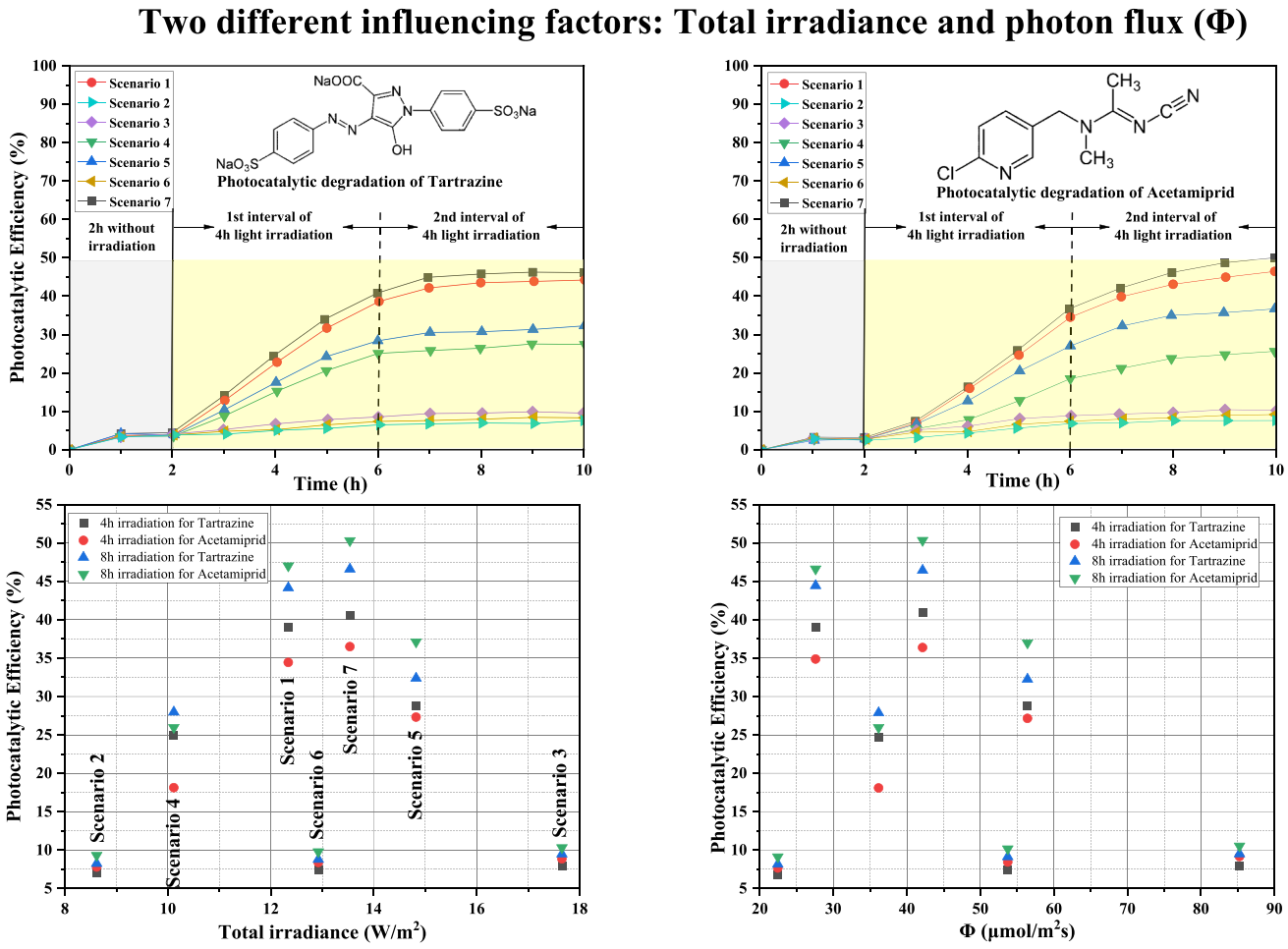

Irradiation Scenarios	UV-A Sources	UV-B+C Sources	Vis Sources	Total Irradiance (W/m2)
Scenario 1	4	0	0	12.3
Scenario 2	0	4	0	8.6
Scenario 3	0	0	4	17.6
Scenario 4	2	2	0	10.1
Scenario 5	2	0	2	14.8
Scenario 6	0	2	2	12.9
Scenario 7	3	0	1	13.5

Fig. 3. Influence of optical properties on photocatalytic performance [56].

2.2. *The effect of temperature*

Temperature plays a pivotal role in photocatalytic processes by modifying reaction rates and mechanisms through multiple pathways, including enhanced charge transport and modified adsorption–desorption equilibria in Fig. 4(a). In the case of TiO_2-based photocatalysts, Barakat et al. [60] demonstrated that increasing the reaction temperature up to 55 °C improved the degradation rate of organic pollutants. Similarly, Kim et al. [61] observed an increase in H_2 production from Pt/TiO_2 suspensions over the temperature range of 298–323 K. These findings highlight that elevated reaction temperatures help surmount energy barrier activation, boosting both carrier mobility and charge-transfer efficiency. However, excessively high temperatures (500–700 °C) may trigger structural instability in the photocatalyst, thereby diminishing its long-term activity [62,63]. Moreover, synergistic photochemical and thermochemical effects under solar illumination, particularly those tied to localized surface plasmon resonance, can substantially accelerate reaction rates [64], indicating that a judicious balance of thermal input is crucial.

Chen et al. [65] provided further insights by examining the photocatalytic performance of TiO_2 for methylene blue (MB) degradation at various temperatures; their results in Fig. 4(b) revealed that photocatalytic efficiency at 50 °C surpassed that at other temperatures. Kinetic analyses confirmed that the reaction rate constant positively correlated with temperature-driven enhancements. Beyond the extensively studied TiO_2 system, emerging materials such as g-C_3N_4-based composites, metal–organic frameworks (MOFs), and $BiVO_4$ also exhibit pronounced temperature-dependent photocatalytic activity. For instance, raising the reaction temperatures from approximately 20 °C to 50 °C in g-C_3N_4@CdO/ZnO photocatalysts accelerated dye degradation by facilitating molecular collisions and expediting surface reactions [66], while MOFs often showed higher hydrogen evolution rates at elevated temperatures owing to thermally activated surface sites [67]. Similarly, $BiVO_4$-based systems displayed optimal operating windows where

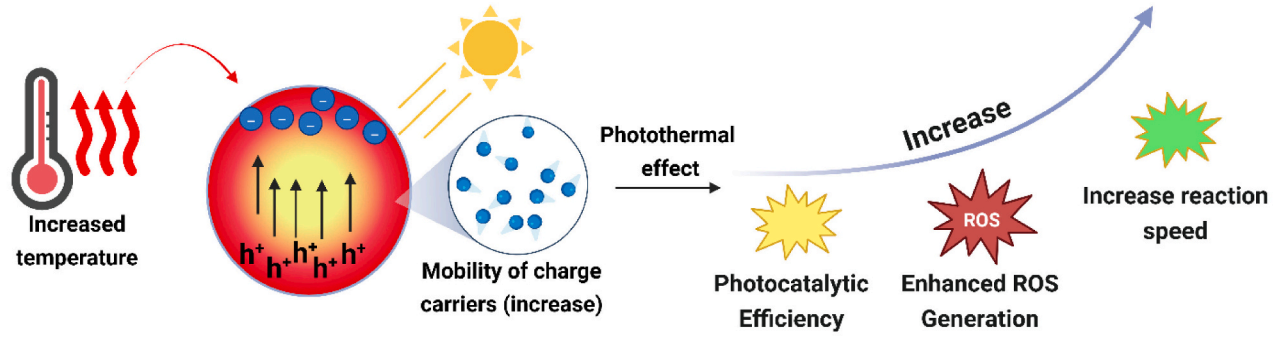

(a)

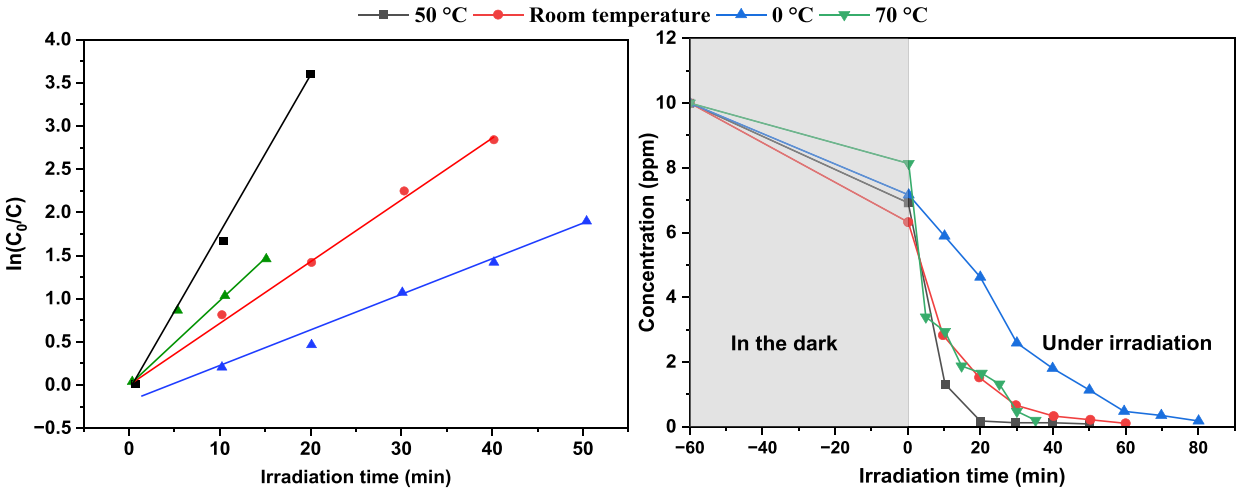

(b)

Fig. 4. Photothermal effects and temperature-dependent performance in photocatalytic degradation: (a) Schematic illustration of the photothermal enhancement mechanism; (b) Influence of temperature on photocatalytic performance [65].

moderate heating improved pollutant degradation [68]. In $ZnIn_2S_4$--based photocatalysts, particularly those integrated with photothermal components, temperature could strongly influence charge-transport dynamics, surface adsorption, and reaction kinetics [69].

2.3. The effect of pH

pH exerts an influence on photocatalytic reaction rates and pathways by modulating both photocatalyst surface charge and the ionization state of reactants. In the photocatalytic degradation of organic pollutants in aqueous systems, varying the pH changes pollutant dissociation and catalyst surface charge, thereby impacting adsorption and overall degradation efficiency in Fig. 5(a) [70]. For instance, in oxide-based photocatalysts such as TiO_2, the initial solution pH dictated whether the surface was positively charged ($pH < pH_{ZC} \approx 7.1$) or negatively charged ($pH > pH_{ZC}$) [71]. Under acidic conditions ($pH < pH_{ZC}$), TiO_2 more readily adsorbed negatively charged species (e.g., dye molecules), leading to enhanced degradation rates. Rosa et al. [72] demonstrated that increasing the pH weakened TiO_2 adsorption of rhodamine B (RhB), with the highest degradation achieved at $pH = 3$ in Fig. 5(b). By contrast, in alkaline media, many dyes became deprotonated and negatively charged, while the catalyst surface was also negatively charged, resulting in electrostatic repulsion that diminished both adsorption and degradation efficiency. A similar trend has been reported by Hanafi et al. [73], who observed that dye degradation decreased at higher pH. By contrast, under acidic conditions below pH_{ZC} of charge of $EGZrO_2$, the positively charged surface strongly attracted anionic dyes and accelerated their decay. These findings collectively underscore that tuning the pH can be an effective strategy to regulate both the mechanism and efficiency of photocatalytic pollutant removal in water.

During photocatalytic hydrogen evolution, variations in solution pH modulate the band-edge positions relative to the H^+/H_2 redox potential and alter the electric double layer (zeta potential), thereby influencing charge separation and reaction kinetics [74]. In general, acidic conditions offer a high concentration of protons that favor the hydrogen evolution reaction (HER), resulting in enhanced H_2 generation rates [75]. For example, Fe-doped g-C_3N_4 achieved its highest H_2 yield in mildly acidic to neutral solutions ($pH \approx 3$–7); at $pH < 3$, photocatalyst stability deteriorated, whereas at $pH > 7$, a lack of protons increased e^-/h^+ recombination, ultimately reducing H_2 production [76]. Nonetheless, the optimal pH can vary considerably among different photocatalysts. A recent study [77] on single-atom catalysts anchored on red phosphorus (RP) illustrated that no single pH was universally ideal: Ni-RP exhibited consistently high hydrogen evolution over a broad pH range due to favorable band alignment, while Cu-RP, Fe-RP, and Co-RP performed best in acidic media owing to strong surface proton binding. Under neutral or alkaline conditions, these RP-based catalysts rely on enhanced H_2O adsorption as the proton source for H_2 production.

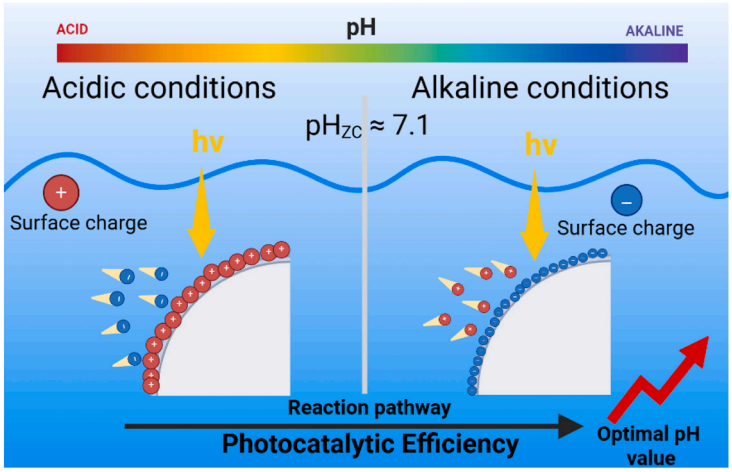

(a)

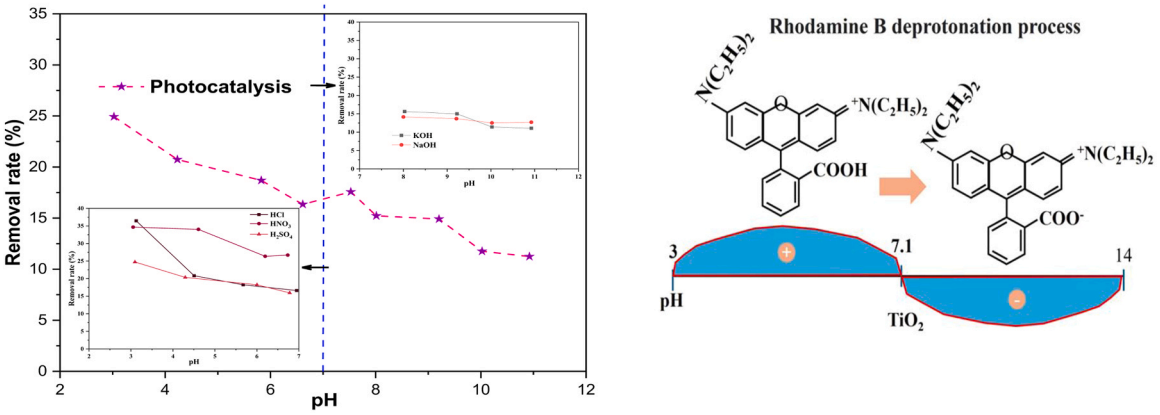

(b)

Fig. 5. Effect of solution pH on photocatalytic (a) mechanism and (b) performance [72].

Furthermore, certain photocatalysts could display dual maxima under both strongly acidic and strongly alkaline conditions. For instance, Ag–La–$CaTiO_3$ perovskite showed two distinct peaks in H_2 evolution at around pH= 4 and pH= 10 under visible-light irradiation [78]. Hence, pH optimization is indispensable for maximizing hydrogen evolution performance across diverse photocatalyst systems.

During photocatalytic CO_2 reduction, the solution pH dictates CO_2 speciation in water and thus has an influence on the reaction pathways and outcomes. The primary dissolved species would change with pH, from H_2CO_3 under strongly acidic conditions (pH $\leq$ 3) to HCO_3^- and CO_3^{2-} in more alkaline media (pH $\geq$ 10) [79]. This trend has also been experimentally verified; for instance, Yoshino et al. [80] reported that under visible-light irradiation, a Z-scheme powder photocatalyst ($CuGaZnS_2/BiVO_4$) produced negligible CO at the natural pH (around 4) of CO_2-saturated water. However, a slight increase in pH to approximately 5–6 could improve CO production, highlighting that even subtle pH adjustments could shift reduction pathways and efficiency. In addition to pH-based regulation of CO_2 speciation, researchers have exploited tailored photocatalyst structures to further refine product selectivity. For example, a Sn(II)-based MOF achieved > 99 % selectivity in reducing CO_2 to formate under visible-light illumination, with an apparent quantum efficiency of up to 9.8 % at 400 nm [81]. This study highlights the great potential of MOF materials in steering reaction selectivity, even in the absence of externally imposed pH control, thereby enabling highly selective CO_2 conversion pathways.

2.4. The effect of gas flow rate and concentration and relative humidity

Gas flow rate, pollutant concentration, and relative humidity (RH) are interdependent parameters that collectively regulate the efficiency of gas-phase photocatalytic processes. In a study on the degradation of volatile organic compounds (VOCs) by TiO_2 (Fig. 6), Alireza et al. [82] demonstrated that optimal photocatalytic activity typically occurred at moderate RH (around 20 %), where adsorbed water provided the necessary •OH radicals without excessively blocking active sites. In contrast, high relative humidity significantly reduced the photocatalytic efficiency by intensifying the competition for reactive sites and promoting the formation of structured water layers through hydrogen bonding, which hindered the adsorption of VOCs on the TiO_2 surface [83]. Regarding gas flow rate, increasing the flow enhanced mass transfer and thereby accelerated reaction kinetics; however, excessively high flow rates reduced the residence time of pollutants, limiting effective adsorption [84]. Consequently, the flow rate should be reasonably optimized based on the reactor configuration and the physicochemical properties of the target pollutants. Also, higher pollutant concentrations adversely affected photocatalytic performance by saturating TiO_2 active sites and promoting competitive adsorption of reaction by-products, ultimately decreasing overall degradation efficiency [85].

The g-C_3N_4, MOFs, MXenes, and $BiVO_4$ have been observed to exhibit similar performance trends but have significant differences. For

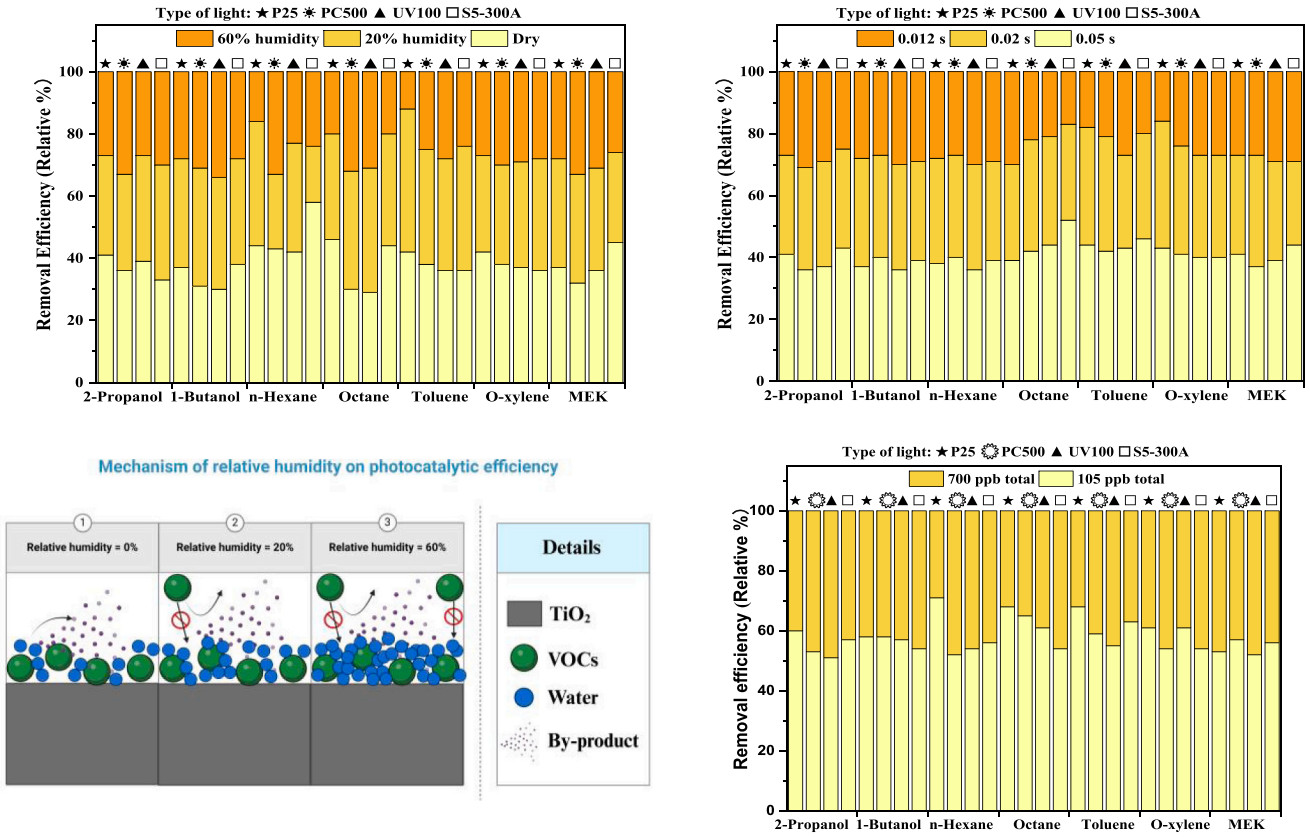

Fig. 6. Factors affecting photocatalytic efficiency: Gas flow rate, concentration and relative humidity [82].

instance, a Ni/Ag–g-C_3N_4 catalyst on the Ni foam showed optimal formaldehyde degradation at approximately 60 % RH, significantly higher than the typical RH range for TiO_2, demonstrating its excellent humidity tolerance. The porous and heterojunction-rich structure of this composite effectively facilitated formaldehyde adsorption and catalytic reactions, delaying the inhibition caused by competitive water vapor adsorption [86]. In MOF-based photocatalysts, the porous framework buffers fluctuations in pollutant concentration or flow rate by adsorption. For example, increasing RH to 60 % significantly enhanced the photocatalytic degradation of dimethyl sulfide (DMS) by UiO-66/TiO_2 due to optimal hydroxyl radical formation; however, further increase to 90 % RH reduced efficiency as excess water competes with DMS for active sites [87]. Similarly, incorporating high–surface-area carriers (e.g., activated carbon or porous clays) has been shown to increase VOC adsorption and retention, mitigating adverse effects of short residence times and high humidity. For example, an activated-carbon-loaded $BiVO_4$–$BiPO_4$–g-C_3N_4 photocatalyst maintained approximately 85.6 % toluene removal at 60 % RH, about 2.4 times higher than its carbon-free counterpart, owing to enhanced toluene adsorption under moist conditions [88]. In addition, tailoring the availability of active sites and the charge-transfer kinetics can preserve reactivity under varying operational conditions. MXene–semiconductor heterostructures serve as a great case: a $Ti_3C_2T_x$ MXene/ZnO composite provided abundant surface sites and superior charge separation, enabling around 91 % formaldehyde degradation, a reaction rate about 2.7 times higher than that of pristine ZnO. Such efficient utilization of photogenerated charge carriers ensures the formation of greater amounts of •OH and O_2^{-}• prior to recombination, thereby sustaining high removal efficiencies even under elevated VOC loads or faster gas flow rates [89].

In summary, while TiO_2 remains the benchmark, achieving maximal performance under balanced humidity, moderate pollutant concentrations, and sufficient contact times, newer materials have demonstrated even greater efficacy under comparable conditions. By offering higher adsorption capacities and more robust generation of reactive radicals, photocatalysts such as g-C_3N_4, MOFs, MXenes, and $BiVO_4$ typically exhibit superior tolerance to high humidity and pollutant concentrations, as well as sustained activity at higher flow rates.

3. Strategies for surface modification and functionalization of photocatalysts

To overcome limitations such as low visible-light response, and rapid recombination of photogenerated charges, catalyst aggregation, significant research efforts have recently shifted toward developing innovative interfacial engineering strategies and functional composite structures. These advanced modification approaches extend beyond traditional co-catalyst deposition and elemental doping, incorporating novel methodologies such as integration with ferroelectric interface engineering, hydrogel-based composites, the construction of homogeneous or heterogeneous structures, and lattice defect engineering. Specifically, integrating ferroelectric materials harnesses their robust internal polarization field to enhance charge separation and directional charge flow at the interface. Meanwhile, coupling photocatalysts with porous hydrogel matrices can significantly mitigate nanoparticle aggregation, enhance the interaction between pollutants and catalytic sites, and simplify catalyst recovery, resulting in superior photocatalytic activity and stability. Furthermore, by implementing doping strategies to engineer homogeneous structures or constructing heterostructures, the interfacial band alignment can be precisely modulated, and built-in electric fields can be generated, thereby promoting the efficient separation and migration of photogenerated charge carriers. Lastly, creating OVs or other point defects introduces mid-gap states, extending light absorption into the visible range and offering active sites that suppress charge-carrier recombination. The following subsections summarize the latest progress in these strategies, highlighting how each approach can be synergistically combined to achieve higher photocatalytic activity.

3.1. Ferroelectric interfaces in photocatalysis

Ferroelectric materials can enhance photocatalytic performance, primarily through polarization-induced modulation of the semiconductor band structure. The spontaneous polarization inherent in these materials generates internal electric fields, causing band bending and energy-level shifts at surfaces and interfaces, effectively altering local Fermi levels [90,91]. Such polarization-driven band structure modifications facilitate spatial separation of photogenerated charge carriers, directing e^- and h^+ toward opposite polarization regions, thereby suppressing recombination (Fig. 7) [91]. Essentially, the built-in electric field arising from ferroelectric polarization serves as a potent driving force for charge separation, drawing electrons to negatively polarized surfaces and holes toward positively polarized surfaces [90]. For instance, in single-domain ferroelectric $PbTiO_3$ nanostructures, the partially unscreened depolarization field constitutes the predominant internal field, driving photogenerated electrons and holes to accumulate on opposite crystal facets, thus efficiently achieving spatial charge separation [92].

Based on these mechanisms, recent research has focused on using the spontaneous polarization properties of ferroelectric materials to optimize photocatalytic performance. Investigations into ferroelectric $BiFeO_3$ and $BaTiO_3$, for instance, have demonstrated that strong remanent polarization generated a substantial internal electric field, effectively driving photogenerated e^- and h^+ toward opposite polarization domains, enhancing carrier separation efficiency and suppressing recombination [93]. Burbure et al. [94] exploited this phenomenon by developing a $BaTiO_3/TiO_2$ core–shell heterostructure, in which the polarized $BaTiO_3$ core introduced an internal field that not only increased the active surface area but also significantly improved charge separation, achieving a hydrogen evolution rate approximately twice that of TiO_2. Similarly, constructing oxidation and reduction co-catalysts at oppositely polarized domains of $BaTiO_3$ formed a bipolar charge collection structure, substantially reinforcing the internal electric field. This configuration efficiently realizes spatial separation of electrons and holes within their thermalization length, enabling overall photocatalytic water splitting in pure water[95]. Furthermore, integrating a ferroelectric $BiFeO_3$ interlayer into a $BiVO_4/CuInS_2$ Z-scheme heterojunction exploited the polarization-induced band bending at the semiconductor interface, facilitating Z-scheme charge transfer and significantly enhancing pollutant degradation efficiency [96]. In addition to these heterostructural designs, interfacial engineering and compositional gradients have emerged as pivotal strategies for enhancing carrier separation efficiency in ferroelectric photocatalysis. For example, the positively polarized surface of $PbTiO_3$ single crystals is susceptible to electron trap formation due to abundant Ti vacancy defects, severely limiting their photocatalytic activity. Addressing this challenge, epitaxially growing an ultrathin $SrTiO_3$ layer on the positively polarized $PbTiO_3$ surface effectively passivated these Ti defects, dramatically extending the electron lifetime (from approximately 50 μs to the millisecond range) and establishing highly efficient interfacial electron transfer pathways [97].

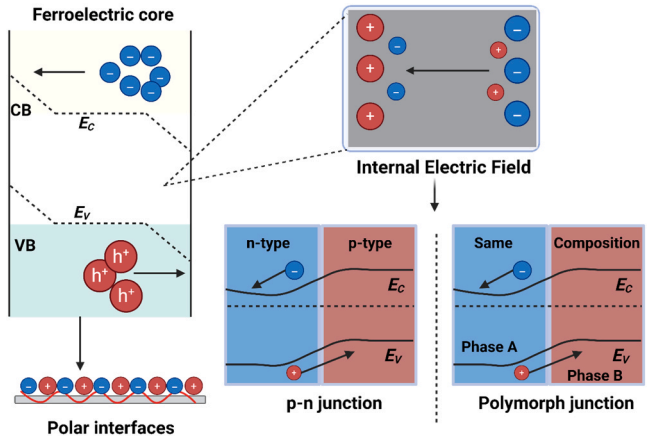

Fig. 7. Schematic representation of charge separation mechanisms in ferroelectric photocatalysts via internal electric fields and interface engineering [91].

Recent theoretical studies have further elucidated the mechanisms by which ferroelectric polarization enhances photocatalytic performance. Density functional theory (DFT) calculations revealed that polarization reversal in two-dimensional $C_2N/\alpha\text{-}In_2Se_3$ heterostructures significantly modulated interfacial band alignment, transforming the system from a conventional type-II heterojunction into an S-scheme heterojunction driven by internal electric fields. This transition simultaneously converted an indirect bandgap (0.63 eV) to a narrower direct bandgap (0.56 eV), improving visible-light absorption and charge separation efficiency [98]. These findings provide theoretical validation that ferroelectric polarization can effectively engineer band gradients in heterostructures, optimizing charge-carrier pathways and enhancing reaction-site selectivity. In addition, first-principles calculations are also used to predict and design new ferroelectric photocatalytic materials. For example, DFT studies on R3c-phase $InVO_3$ demonstrated that spontaneous polarization-induced internal fields effectively suppressed carrier recombination, highlighting its potential in photocatalytic applications [99]. Additionally, theoretical simulations focusing on ferroelectric/semiconductor interfaces illustrated that polarization charges could modify interfacial band structures. Specifically, numerical calculations showed that positive polarization applied at the $TiO_2/SrTiO_3$ interface led to the accumulation of negative charges, intensifying band bending in the TiO_2 side and thereby significantly facilitating carrier separation and transport [100].

In summary, combined experimental investigations and theoretical calculations have underscored the immense potential of ferroelectric polarization-induced internal electric fields in promoting charge separation and modulating band structures in photocatalysts. Future advances in precision interfacial engineering and optimized heterostructure design are expected to facilitate the development of novel high-performance ferroelectric photocatalytic materials, driving both fundamental breakthroughs and practical applications in this burgeoning research field.

3.2. Surface functionalization of photocatalysts through hydrogel-based composites

The TiO_2-hydrogel system consists of TiO_2 immobilized within a hydrophilic, cross-linked polymeric network. Typically, hydrogel matrices such as microcrystalline cellulose (MCC), polyvinyl alcohol (PVA), or alginate (SA) are prepared by dispersing TiO_2 nanoparticles uniformly in a polymer precursor solution, followed by cross-linking through the addition of appropriate agents, such as epichlorohydrin (ECH), to form stable, integrated structures in Fig. 8(a). The resultant porous and highly swellable hydrogel facilitates effective diffusion and adsorption of pollutants near the catalytic sites, while its inherent transparency allows sufficient light penetration to activate the embedded TiO_2 [101,102]. Under UV irradiation, reactive oxygen species (ROS) generated by TiO_2 efficiently oxidized organic pollutants. Importantly, the hydrogel matrix inhibited nanoparticle agglomeration and leaching, enhanced pollutant accessibility, and simplified catalyst recycling [102]. Consequently, TiO_2-hydrogel composites demonstrate significantly improved photocatalytic activity and stability compared with free-standing TiO_2. For instance, a cellulose-based TiO_2-hydrogel composite achieved approximately 90 % degradation of organic dyes within a few hours, maintaining high reusability and retaining about 80 % of its catalytic activity even after five cycles [102]. Overall, the synergistic integration of TiO_2 with the porous and hydrophilic characteristics of hydrogels enhances photon and pollutant accessibility,

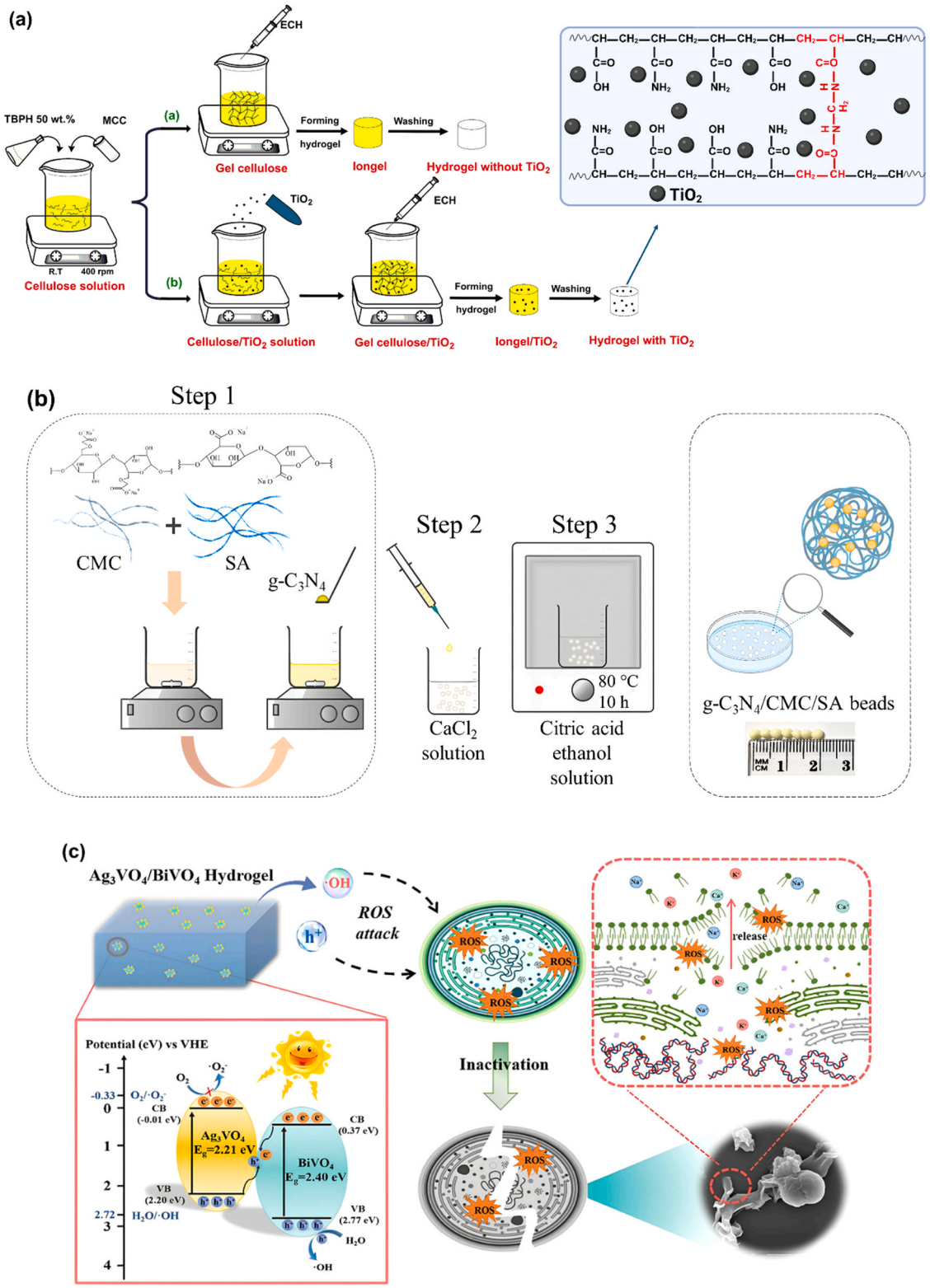

Fig. 8. Schematic illustration of hydrogel-based photocatalytic composite systems: (a) Cellulose hydrogel with TiO_2[102]; (b) g-C_3N_4 immobilized in CMC-alginate hydrogel [103]; (c) Self-floating Ag_3VO_4/$BiVO_4$/PVA composite hydrogel [104]; (d) $BiVO_4$/GO hydrogel composites[105]; (e) CQDs/$BiVO_4$/rGO ternary hydrogel composites[106].

delivering superior degradation performance and convenient catalyst recycling.

In recent years, advancements in hydrogel-based photocatalytic systems have benefited significantly from the integration of novel semiconductor materials and sophisticated interface functionalization strategies, markedly enhancing their photocatalytic activity, selectivity, and durability under visible-light irradiation. For instance, immobilizing g-C_3N_4 nanoparticles within hydrogels composed of cross-linked

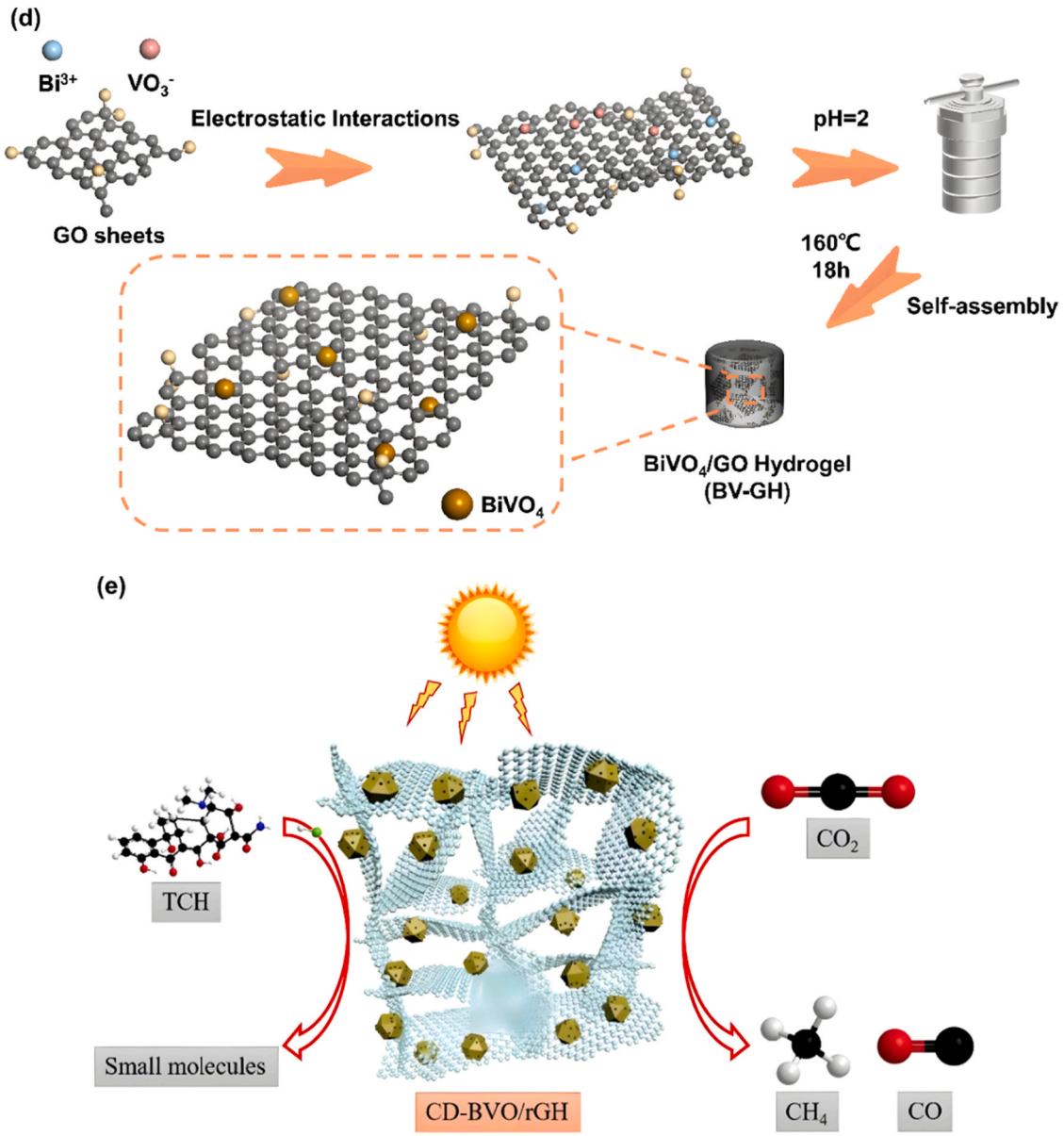

Fig. 8. (*continued*).

carboxymethyl cellulose (CMC) and SA resulted in notable improvements in catalytic efficiency and practical usability in Fig. 8(b); such composite systems have enhanced porosity, improved photostability, and superior photogenerated charge transport efficiency, facilitating effective degradation of dyes with varying charges under natural sunlight; additionally, immobilization of photocatalysts in hydrogels avoids the cumbersome recovery procedures associated with traditional powdered catalysts and eliminates the need for filtration and centrifugation, significantly streamlining wastewater treatment processes [103]. Similarly, integrating $BiVO_4$ into PVA-based hydrogels, particularly when combined with Ag_3VO_4 to form a p-n heterojunction, significantly broadened their applicability in water treatment. The self-floating $Ag_3VO_4/BiVO_4$/PVA composite hydrogels fabricated via a freeze-thaw method exhibited buoyancy and mechanical robustness, optimizing catalyst exposure to light and simplifying retrieval. The efficient charge separation at the heterojunction interface facilitates the rapid generation of ROS, enabling rapid algal cell inactivation under visible-light conditions in Fig. 8(c) [104]. In addition to the Ag_3VO_4/-$BiVO_4$ system, hydrogel composites comprising $BiVO_4$ and graphene oxide (GO) have also been reported. The flexible three-dimensional hydrogel network significantly enhanced intimate interfacial contact between $BiVO_4$ and GO, concurrently increasing local reactant concentrations. Utilizing the exceptional specific surface area, adsorption capacity, and electron-transfer properties of GO, $BiVO_4$/GO hydrogel composites achieved efficient adsorption-enrichment and photocatalytic dye degradation in Fig. 8(d); furthermore, the effective interfacial charge separation promoted the formation of abundant ROS, demonstrating remarkable antibacterial photocatalytic activity under visible light [105]. Additionally, ternary composite systems comprising carbon quantum dot (CQD)-decorated $BiVO_4$ nanoparticles supported within reduced graphene oxide (rGO) hydrogels (CQDs/$BiVO_4$/rGO) had further improved photocatalytic performance in Fig. 8(e). Benefiting from the photon up-conversion capability of CQDs and the efficient electron-transfer network of rGO hydrogels, these composites exhibited not only high-efficiency degradation of tetracycline hydrochloride (TCH) under visible light, but also outstanding photocatalytic activity for CO_2 reduction [106]. In summary, integrating multifunctional hydrogels with diverse advanced photocatalysts has significantly enhanced the catalytic performance, stability, and practical applicability of the resulting composite systems. This approach effectively

addresses the recovery challenges associated with conventional powdered photocatalysts, while interfacial engineering and heterostructure design strategies improve photocatalytic efficiency and broaden the scope of potential applications.

3.3. Heterogeneous (homogeneous) junction structure

Heterostructures consist of two or more different semiconductor materials or metals, creating unique interfacial properties that facilitate effective charge separation through built-in electric fields formed by band offsets [107]. Electron diffusion between semiconductors with differing Fermi levels generates an interfacial electric field, effectively promoting separation of photogenerated carriers (Fig. 9) [108].

For instance, Guo et al. [109,110] synthesized porous Ag-loaded ZnO heterostructures, significantly enhancing electron transfer and photocatalytic stability due to reduced e^-/h^+ recombination facilitated by Ag^+/Ag^0 conversion on the ZnO surface. Similarly, Xiong et al. [111] proposed α-Fe_2O_3/Bi_2O_3 heterojunctions, particularly emphasizing the face-to-face interface model, which exhibited significantly enhanced photocatalytic efficiency attributed to improved charge separation and interfacial electron transfer capabilities.

Homojunction photocatalysts, composed of identical materials with variations in crystal phases or doping (such as PN or NN junctions), effectively optimize charge carrier separation and transfer, thus enhancing photocatalytic efficiency without lattice mismatch or foreign interfaces [26]. Shen et al. [112] designed $WO_3/W_{18}O_{49}$ homojunction photocatalysts, demonstrating significantly enhanced adsorption and photocatalytic stability, owing to effective charge separation within the homogenous structure. Similarly, Wang et al. [113] reported excellent pollutant degradation and robust cyclic stability of TiO_2 quantum dots (QDs) and nanosheet homojunctions, attributed to optimized interfacial interactions and minimal lattice distortion.

In practical photocatalytic applications, heterojunction and homojunction structures exhibit different characteristics. Heterojunction photocatalysts typically exhibit superior activity and selectivity due to efficient charge separation and synergistic interfacial reactions [114,115]. For instance, the Bi_2MoO_6/In_2S_3 heterojunction achieved effective CO_2 reduction through a specifically constructed S-scheme interface, delivering approximately 94 % CO selectivity with CO evolution rates enhanced by 6–8 times compared to single components. This improvement resulted from the internal electric field at the heterointerface promoting directed electron transfer, significantly enhancing catalytic reduction capability and reducing CO_2 emissions [116]. Similarly, Lai et al. [117] developed an S-vacancy-rich In_2S_3/In_2O_3 heterojunction, attaining an exceptional CH_4 selectivity of 95.93 %, far surpassing single-semiconductor performance. This enhanced CO_2 conversion arose from directional electron transfer across the heterointerface, accelerating multielectron reduction pathways and elevating reaction rates and product selectivity. In comparison, homojunction designs excel in crystal lattice matching, significantly reducing interfacial lattice distortions and thus enhancing long-term photostability and recyclability [118,119]. For example, a tetragonal/orthorhombic Bi_2WO_6 homojunction synthesized via in situ bismuth-induced phase transformation demonstrated outstanding photocatalytic performance. It completely

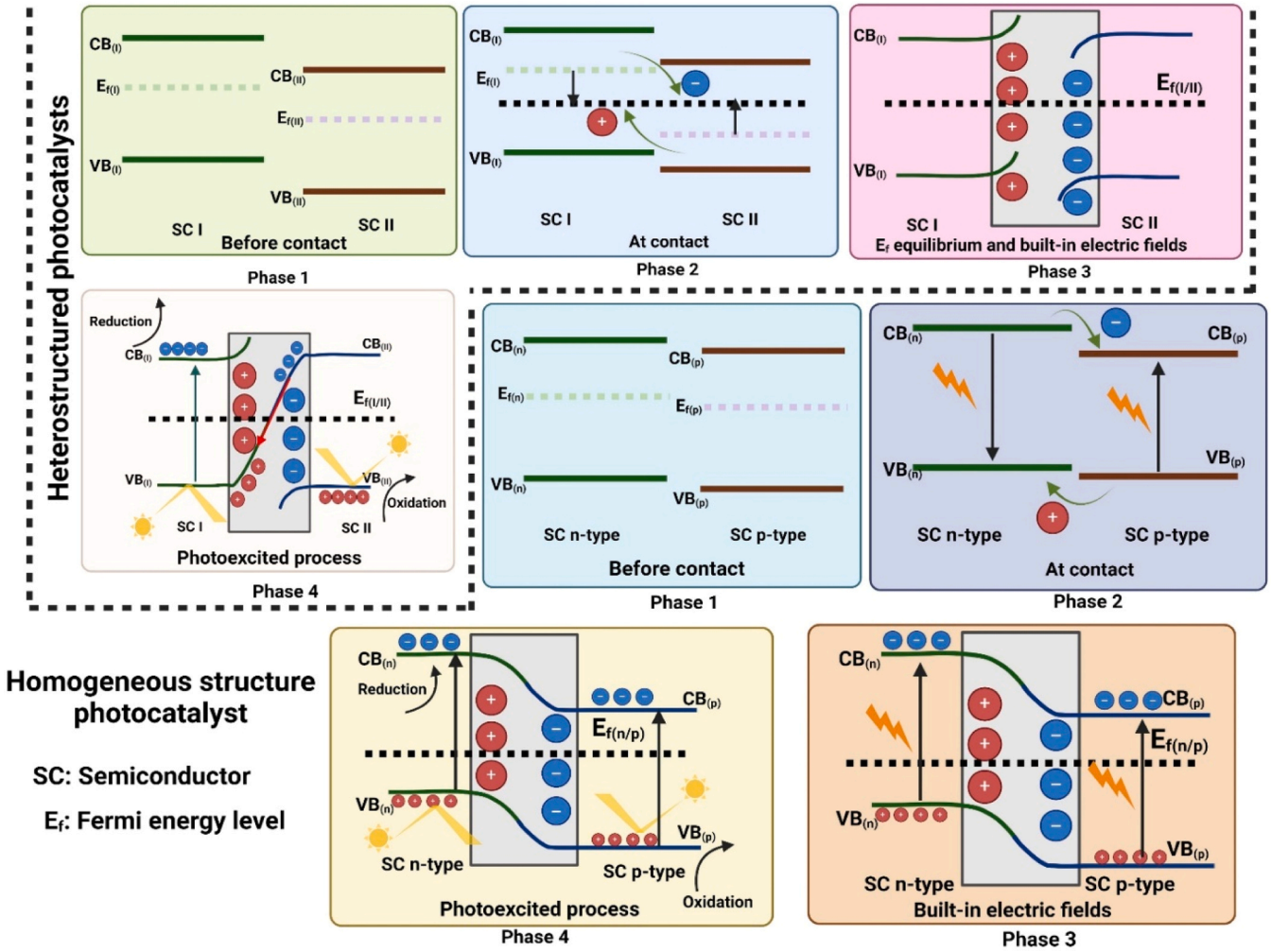

Fig. 9. Mechanism of Charge Transfer in Heterogeneous and Homogeneous Structured Photocatalysts under Photoexcitation [26,108].

degraded Rhb under simulated solar irradiation over five consecutive cycles without significant activity decline, indicating excellent long-term stability and recyclability due to effective charge carrier separation and reduced e^-/h^+ recombination at the homojunction interface [120]. Similarly, phosphate-functionalized g-C_3N_4 homojunction hydrogel microspheres maintained high degradation efficiency for the antibiotic tetracycline even after 20 reuse cycles, with negligible structural alterations. This superior stability was attributed to efficient charge separation within the homojunction, significantly suppressing electron-hole recombination and ensuring prolonged catalytic efficiency [121]. In summary, heterojunctions are optimal for reactions demanding high activity and selectivity, such as CO_2 reduction, whereas homojunctions are advantageous for long-term stability and repeated-use scenarios in environmental purification.

However, in practical applications, heterojunction photocatalysts often suffer from interfacial lattice mismatch and limited structural stability, while homojunction photocatalysts may exhibit suboptimal charge carrier separation efficiency [26,122]. To overcome these inherent limitations, recent research has focused on integrating heterojunction and homojunction architectures, aiming to develop hybrid systems that simultaneously achieve enhanced charge separation and improved long-term stability. For instance, Guo et al. [123] developed a novel multijunction photocatalyst by combining twin $BiPO_4$ (a homojunction composed of two phases of monoclinic $BiPO_4$) with BiOCl, resulting in a composite material with a stepped band structure. This design incorporated both homojunction and heterojunction elements. The photocatalytic performance of this composite was significantly improved, showing multiple times higher photocatalytic activity for organic pollutants such as methyl orange and acetaminophen compared to the original $BiPO_4$. The study confirmed that the synergy between homojunction and heterojunction optimized the transfer and separation of charge carriers, thereby enhancing photocatalytic efficiency. Similarly, Sun et al. [124] investigated a novel photocatalyst composed of mesoporous TiO_2 combined with $CsPbBr_3$ perovskite QDs of varying sizes. These perovskite QDs were in-situ generated within the mesoporous TiO_2, forming both type II homojunctions and Z-scheme heterojunctions. The coexistence of these structures facilitated the efficient transfer of photogenerated electrons from TiO_2 to $CsPbBr_3$, significantly suppressing charge carrier recombination and enhancing photocatalytic activity. This composite material achieved a degradation efficiency of 97.7 % for RhB under light irradiation.

3.4. Defect engineering (lattice defects)

Defect engineering, as an advanced photocatalyst modification strategy, significantly enhances the catalytic efficiency of semiconductor photocatalysts by introducing various defects into the lattice structure, such as point defects, line defects, plane defects, vacancies, doping, or dislocations. By altering atomic coordination numbers and electronic structures, as well as promoting interfacial interactions between different components and leveraging the synergistic effects of multiple defects, defect engineering not only adjusts the band structure and increases carrier mobility but also imparts multifunctionality to photocatalysts. Among these, lattice defects can be categorized into OVs modification [125,126], interstitial doping, cation vacancies, and lattice disorder [127].

Precise modulation of defect types and concentrations, particularly OVs, is crucial for optimizing the optical and electronic properties of photocatalytic materials (Fig. 10). OVs, defined as the absence of oxygen atoms in the metal oxide lattice, typically form under high-temperature or reductive conditions, and can be categorized as surface, subsurface, and bulk oxygen vacancies depending on their spatial positions [125]. These vacancies introduce new defect states within the bandgap, thereby reducing the bandgap width and extending visible-light absorption, significantly enhancing the solar energy utilization and photocatalytic performance. Additionally, OVs elevate the Fermi level, enhance electron delocalization and electrical conductivity, and act as effective pathways for electron transport, thus facilitating electron transfer [125,128–130]. For instance, in TiO_2, the formation of OVs led to localized electron occupancy at positions previously occupied by O^{2-} ions, generating shallow donor states approximately 0.75–1.18 eV below CB. This lowers the h^+ generation energy and induces e^- redistribution among neighboring Ti atoms [126]. Moreover, Ranjbari et al. [131] reported that OVs in ZnO effectively reduced its bandgap from 3.22 eV to 3.07 eV, substantially improving photocatalytic activity toward organic dye degradation. They further discovered that reduced ZnO exhibited outstanding photocatalytic efficiency across varying pH values, similarly attributed to bandgap narrowing and enhanced visible-light utilization [132].

In addition to traditional oxides such as TiO_2 and ZnO, many photocatalysts also enhance their performance through the design of OVs. For example, the introduction of OVs in $BiVO_4$ effectively disrupted lattice symmetry, leading to the formation of defect dipoles. These defect dipoles enhanced the internal electric field, significantly

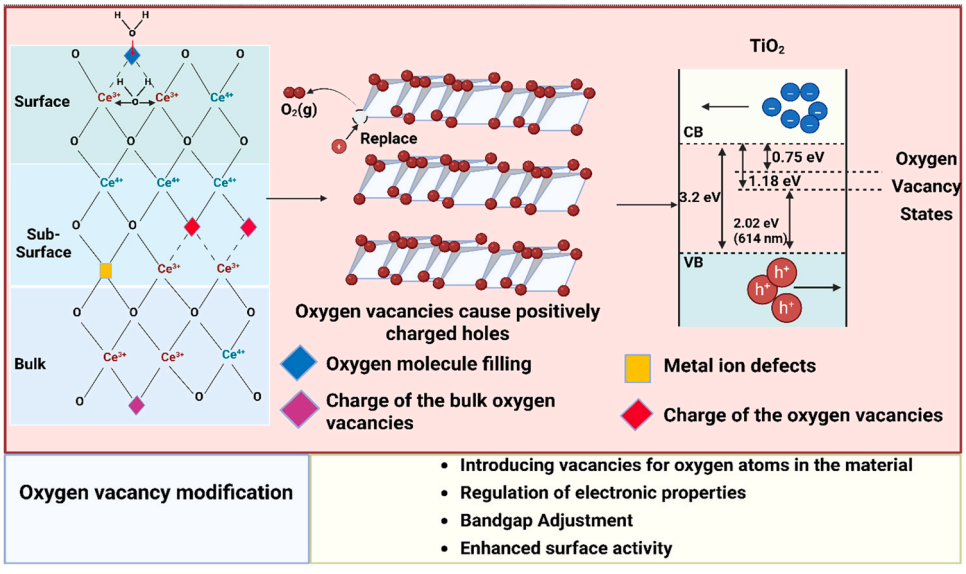

Fig. 10. Schematic illustration of OVs engineering in metal oxide photocatalysts[125].

facilitating the separation and transfer of photogenerated charge carriers. Consequently, OV-engineered $BiVO_4$ photoanodes showed an enhancement in charge transfer efficiency and increased photocurrent, thereby boosting the performance of photoelectrochemical systems in solar fuel generation [133]. Likewise, surface OVs in bismuth oxyhalides (e.g., BiOBr) not only extended the visible-light absorption range but also served as electron-rich active sites to facilitate the adsorption and activation of molecular oxygen, thereby generating $\bullet O_2^-$[134]. This mechanism effectively suppresses the recombination of photogenerated electron-hole pairs, substantially enhancing the photocatalytic degradation efficiency toward organic dyes and other pollutants. Such findings underscore that tailoring anion vacancies (oxygen or chalcogen vacancies) in photocatalytic materials (e.g. $BiVO_4$, BiOBr, $Bi_2O_2CO_3$) is a powerful strategy to broaden light absorption and facilitate charge separation for enhanced photocatalysis[135]. Notably, careful control of OVs concentration was crucial, as excessive vacancies could act as recombination centers if not optimally introduced[136].

Metal cation vacancies (cation defects) are prevalent within semiconductor lattices and represent an effective defect-engineering strategy. These vacancies typically induce shifts in CB edges or introduce acceptor states, thereby enhancing charge transport performance [137]. Unlike anion vacancies, such as OVs, which predominantly affect VB structures and promote h^+ transport, cation vacancies significantly increase CB electron density and facilitate electron mobility and conductivity due to their distinct orbital distribution and unique electronic structure. For instance, incorporating Zn vacancies into $ZnIn_2S_4$-based Z-scheme heterojunctions not only increased carrier density and separation efficiency but also broadened visible-light absorption, thus enhancing photocatalytic hydrogen evolution and pollutant degradation performance [138]. Similarly, a recent study [139] found that the introduction of Cu cation vacancies into $ZnIn_2S_4/Cu_{1.81}S$ heterojunctions significantly improved electronic transport efficiency by inducing electron delocalization and adjusting electron density around neighboring atoms, thereby accelerating CO_2 protonation processes. In rutile-type p-TiO_2, Ti vacancies facilitate electron transport and generate localized active sites for nitrogen reduction, directly influencing catalytic activity [140]. Additionally, the introduction of metal cation vacancies into Bi_2O_3 and WO_3 significantly enhanced their hole mobilities by approximately 270 % and 430 %, respectively. This enhancement was especially pronounced in WO_3, where the incorporation of tungsten vacancies led to a more than 4.4-fold increase in photocurrent density during photoelectrochemical water splitting [141]. Nevertheless, due to the relatively high formation energy of metal cation vacancies, their controlled incorporation remains challenging from a materials design perspective, particularly regarding material stability and durability under highly oxidative conditions. Thus, precise modulation of cation vacancy concentrations to optimize charge transport without compromising structural integrity represents a critical pathway toward developing highly efficient photocatalytic materials.

Introducing defect engineering strategies involving OVs and metal-cation vacancies into photocatalysts can synergistically enhance their photocatalytic performance, primarily by modulating electronic structures and improving charge-carrier dynamics [142]. OVs typically serve as electron donors, forming mid-gap states that extend visible-light absorption and provide active reduction sites. Conversely, metal-cation vacancies function as shallow acceptors, facilitating hole migration. The complementary interaction between these two vacancy types improves charge separation and transport, effectively suppressing e^-/h^+ recombination [143]. For instance, the simultaneous introduction of surface tungsten vacancies and OVs significantly enhanced the photocatalytic activity of Bi_2WO_6; the synergistic interplay of these dual vacancies not only reduced the resistance to charge transfer, accelerating photogenerated charge separation and migration, but also introduced defect states within the bandgap, narrowing the energy gap and prolonging carrier lifetimes, thus enabling highly efficient pollutant degradation [144]. Similarly, in Nb-doped SnO_2, the doping of Nb introduced donor states, while accompanying OVs bridged the gap between the donor states and the conduction band, effectively elevating the conduction-band edge. Such dual-defect synergy significantly narrowed the bandgap and prolonged the carrier lifetime by inhibiting e^-/h^+ recombination, substantially improving photocatalytic efficiency [145]. This cooperative enhancement has also been demonstrated in other vacancy-engineered photocatalysts. For example, in situ formation of adjacent Ti and OVs as paired active sites significantly accelerated electron and proton transport, synergistically enhancing CO_2 adsorption and protonation processes. This strategy achieved 100 % selective conversion of CO_2 to CH_4, with methane production rates nearly 80-fold higher compared to TiO_2. Despite these promising findings, the precise synthesis and control of anion–cation dual vacancies remain challenging. Achieving atomic-scale adjacency between oxygen and metal-cation vacancies is crucial for maximizing their synergistic effects but remains particularly difficult [146]. Typically, this requires carefully designed synthetic routes coupled with specialized post-processing techniques to reliably generate and stabilize such atomic-level co-vacancy structures.

Interstitial doping involves the incorporation of foreign atoms into the interstitial positions of the crystal lattice. This improvement primarily originates from optimized electronic structures, creation of novel active sites, and enhanced charge-carrier dynamics [147–149]. For instance, g-C_3N_4, which typically suffers from rapid charge recombination, exhibited substantially improved photocatalytic activity upon dual doping with potassium (K) and boron (B). Specifically, interstitially positioned K^+ ions expanded interlayer spacing and enhanced electrical conductivity, while substitutional incorporation of B atoms introduced new intermediate electronic states; these modifications facilitated effective charge separation, reduced electron–hole recombination, and extended carrier lifetimes; additionally, this co-doping approach enhanced visible-light absorption, promoted efficient electron transfer toward reactants, and lowered the energetic barrier for CO_2 reduction reactions, ultimately elevating the overall catalytic efficiency [150]. In addition to the above-mentioned dual doping strategy, the performance of the photocatalyst can also be effectively improved by doping with a single element. A recent study [151] demonstrated that interstitial doping with phosphorus, combined with in situ protonation, enhanced photocatalytic hydrogen production in g-$C_{3-x}N_4$. This doping strategy introduced shallow electron trap states that effectively prolonged the lifetime of electrons, reduced unwanted deep trapping, and enhanced charge separation. Similarly, metal-interstitial doping systems, such as Ga-doped CdS catalysts, have been reported to lower valence band positions and formation energies, thereby broadening the VB width and significantly improving charge-carrier separation and migration capabilities [152]. These findings underscore the efficacy of carefully selecting appropriate interstitial dopants to enhance photocatalyst performance while avoiding detrimental lattice strain and excessive carrier recombination.

Combining interstitial doping and metal cation vacancies as a modification strategy has emerged as a promising new approach to enhance the performance of photocatalysts. This method is expected to create a synergistic effect on the structure and performance of photocatalysts, thereby improving their photocatalytic efficiency. Previous studies have shown [153,154] that interstitial metals, by providing additional electrons, could effectively alter the electronic structure of the material and enhance its light-responsive range. At the same time, metal cation vacancies enhanced the chemical activity of the material's surface by creating defect sites and increasing active sites. The synergistic effect between these two modification methods lied in the interaction between the electron supply from the interstitial metals and the charge imbalance introduced by the metal cation vacancies. Additionally, the introduction of interstitial metals improved the thermal stability and structural integrity of the material, while metal cation vacancies offered more kinetic advantages for the reactions. Therefore, this combination not only optimized the electronic properties but also

strengthened the surface reaction performance. Chen et al. [127] significantly improved the photocatalytic CO_2 reduction performance of WO_3 by employing an in-situ modification strategy that created metal cation vacancies and interstitial metals through acid treatment (Fig. 11). The synergistic effect of these two modification methods primarily resulted from their complementary actions: metal cation vacancies provided more active sites and defect levels, facilitating the effective separation of photogenerated electrons; meanwhile, the introduction of interstitial metals enhanced the electron transport speed, inhibiting the recombination of electrons and holes. The combined effect of these structural modifications led to a significant reduction in the bandgap and an extension of the light absorption range, thereby enhancing photocatalytic activity.

Lattice distortion, referring to the local or whole structural deformation in crystals caused by doping, strain, or amorphization, induces alterations in lattice parameters and atomic arrangements [155–157]: primarily, it modulates band structures to extend optical absorption into the visible region; furthermore, such distortions introduce numerous catalytically active defect sites, facilitating chemical reactions; additionally, it efficiently suppresses e^-/h^+ recombination, boosts charge carrier migration, and enhances surface adsorption capabilities.

In TiO_2, doping-induced lattice distortion establishes a potential gradient between CB and VB (Fig. 12), improving e^-/h^+ separation efficiency and photocatalytic activity [158]. Xu et al. [159] demonstrated that lattice distortion in TiO_2 elevated the VB maximum by approximately 0.14 eV, directly influencing electronic structure and carrier dynamics, thus enhancing overall photocatalytic performance. Moreover, in black TiO_2, synergistic effects between lattice disorder and Ti^{3+} defects enabled efficient solar-driven hydrogen generation [160].

Lattice distortion has shown immense potential in emerging materials such as bismuth-based oxides and perovskite oxides. In Bi_2WO_6, doping with rare-earth elements (e.g., Sm, La, Ce, Eu) or Sn^{4+} ions induced significant lattice distortion and local structural deformation, reducing grain size, increasing specific surface area, and extending visible-light absorption, consequently enhancing pollutant degradation efficiency [161]. Similarly, introducing approximately 2 % Cu^{2+} into $NiTiO_3$ induced moderate static lattice distortion, effectively reducing the bandgap and enhancing charge carrier separation, thereby tripling the carrier mobility and markedly improving photocatalytic and electrocatalytic activities [162]. A recent study [163] further highlighted that lattice distortion in medium-entropy perovskite oxide ($La_{0.5}Sr_{0.5}Fe_{0.5}Ti_{0.5}O_3$) significantly reduced the bandgap, broadened visible-light absorption, increased surface-active site density, and promoted efficient charge carrier separation, boosting the photocatalytic degradation of organic pollutants under visible light irradiation. Although the precise mechanisms by which lattice distortion impacts carrier dynamics and recombination remain incompletely understood, strategic manipulation of lattice distortion and surface disorder has emerged as a crucial approach in designing high-performance photocatalysts.

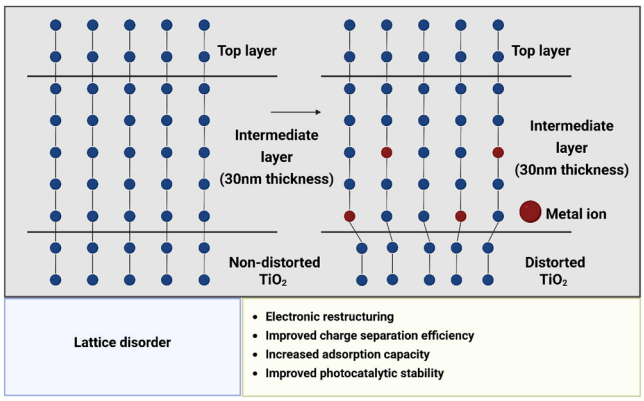

Fig. 12. Schematic illustration of lattice disorder induced by metal-ion doping in TiO_2 [158].

In summary, defect engineering has emerged as a pivotal strategy for enhancing the performance of photocatalysts. Through precise manipulation of lattice defects, including OVs, metal cation vacancies, interstitial doping, and lattice distortion, it becomes possible to tailor electronic structures and charge-carrier dynamics. Particularly, atomic-scale synergistic arrangements of anion and cation vacancies concurrently introduce donor and acceptor states, improving charge separation and transport efficiency. Furthermore, the cooperative interplay between metal cation vacancies and interstitial metal doping enhances surface-active site density and accelerates carrier migration. Additionally, the synergy between lattice distortion and intrinsic defects, such as Ti^{3+} sites, broadens the optical response range and facilitates efficient electron-hole separation. However, the precise synthesis and stabilization of these cooperative defect structures remain challenging. Therefore, future research should aim at a deeper elucidation of structure-activity relationships among various defects and developing robust synthetic methodologies for their controlled implementation.

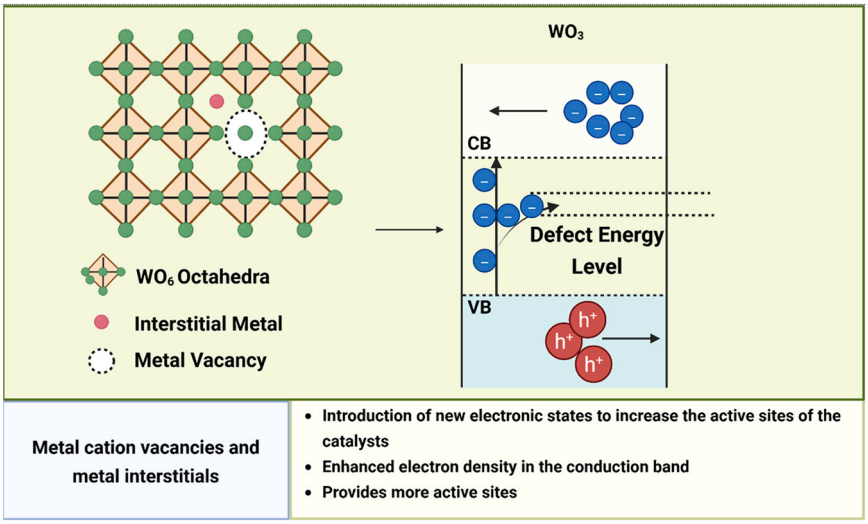

Fig. 11. Schematic illustration of metal cation vacancies and interstitial metal doping in WO_3[127].

4. Challenges in mass transport, catalyst deactivation and toxic intermediates

In previous sections, the latest advances in enhancing photocatalytic performance through surface modification, structural engineering, and related methods have been systematically summarized. Nevertheless, several technical bottlenecks persist in practical applications. These challenges primarily involve: (i) insufficient mass transfer efficiency within reaction systems; (ii) catalyst deactivation over prolonged operation; and (iii) the potential generation of toxic by-products during pollutant degradation. This section therefore provides an in-depth discussion of these three critical issues, highlighting current research progress and potential strategies for mitigation.

4.1. Weak mass transfer

In photocatalytic systems where a solid catalyst is in contact with a gas or a liquid, the mass transfer of reactant molecules from the fluid phase to the catalyst surface is a critical factor in determining the overall rates of the reaction[164]. In the event of sluggish reactant transport relative to the intrinsic surface reaction kinetics, a concentration boundary layer is known to develop in proximity to the catalyst, resulting in the active sites becoming poorly supplied with reactants. Consequently, the process is limited by mass transfer[165]. Indeed, mass transfer limitations are increasingly recognized as a key impediment in photocatalysis that can overshadow the benefits of high catalyst activity. Inefficient mass transfer hinders overall efficiency by limiting the availability of reactant molecules at the photocatalyst's active sites, preventing the catalyst from operating at its full potential. For example, Zhan et al. [166] found that in a water-phase microreactor with a TiO_2-coated catalyst, the degradation rate of a dye was limited by external diffusion to the catalyst surface. Inadequate reactant delivery means active sites on the photocatalyst are under-utilized and photogenerated charge carriers may recombine instead of driving the reaction, wasting the catalyst's potential.

Inadequate mass transfer can result in considerable efficiency declines or even catalyst deactivation if not addressed. In the event of reactants not being adsorbed in a timely manner, the catalytic surface may become unoccupied for a significant period and the reaction will slow down dramatically. For example, in a dye oxidation system, insufficient oxygen transfer from the gas phase caused oxygen to become the limiting reagent, sharply reducing the reaction rate until additional aeration was provided [167]. Also, if products (or reaction intermediates) are not efficiently removed, they can build up and block active sites, which effectively poison the catalyst surface. In gas-phase photocatalytic oxidation of VOCs, Jaison et al. [168] indicated that partial oxidation intermediates (e.g. formic, acetic, and oxalic acids) remained strongly adsorbed on a TiO_2 surface, leading to catalyst deactivation and loss of activity. Such fouling by reaction by-products illustrated how inadequate desorption could cripple photocatalyst efficiency over time.

A recent review has emphasized that improving mass transport in both gas–solid and liquid–solid photocatalytic systems was essential to boost reaction rates and prevent surface fouling[164]. To overcome mass transfer limitations in gas-phase photocatalytic processes in conventional reactors, recent reactor designs aim to increase gas–solid contact and induce vigorous mixing. Fluidized-bed photoreactors have gained attention for gas–solid reactions. By suspending photocatalyst particles in a flowing gas stream, fluidized beds eliminate most external diffusion resistance [30,169]. For example, in a fluidized bed comprising TiO_2-coated beads in Fig. 13(a), the ethylene removal rate was observed to be significantly higher than in a fixed bed catalyst, which can be attributed to the accelerated transport of C_2H_4 to the photocatalyst and the rapid removal of products. This enhanced mass transfer, in conjunction with superior light utilization within the moving bed, led to a substantial enhancement in the degradation rate, which increased from approximately 1.2 μg/min (static) to approximately 10 μg/min in the fluidized system [170].

On the materials side, Schreck et al. [171] demonstrated an effective approach to resolving mass transfer limitations in gas-phase photocatalysis by integrating carefully designed 3D-printed polymeric scaffolds into aerogel photocatalysts in Fig. 13(b). These scaffolds,

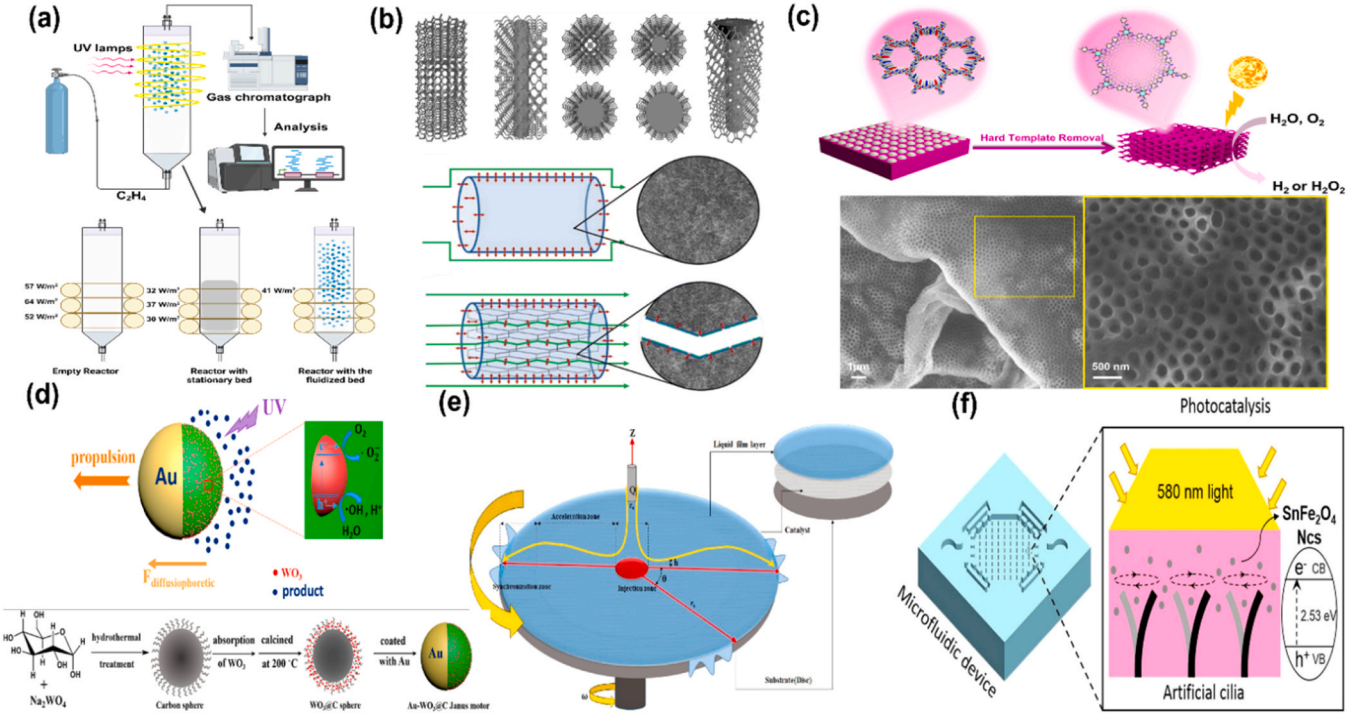

Fig. 13. Representative designs for enhancing mass transfer in photocatalytic systems: (a) fluidized beds [170]; (b) 3D printed scaffolds [171]; (c) hierarchical porous materials [175]; (d) micromotors [176]; (e) spinning disc reactors [179]; (f) magnetically actuated artificial cilia [180].

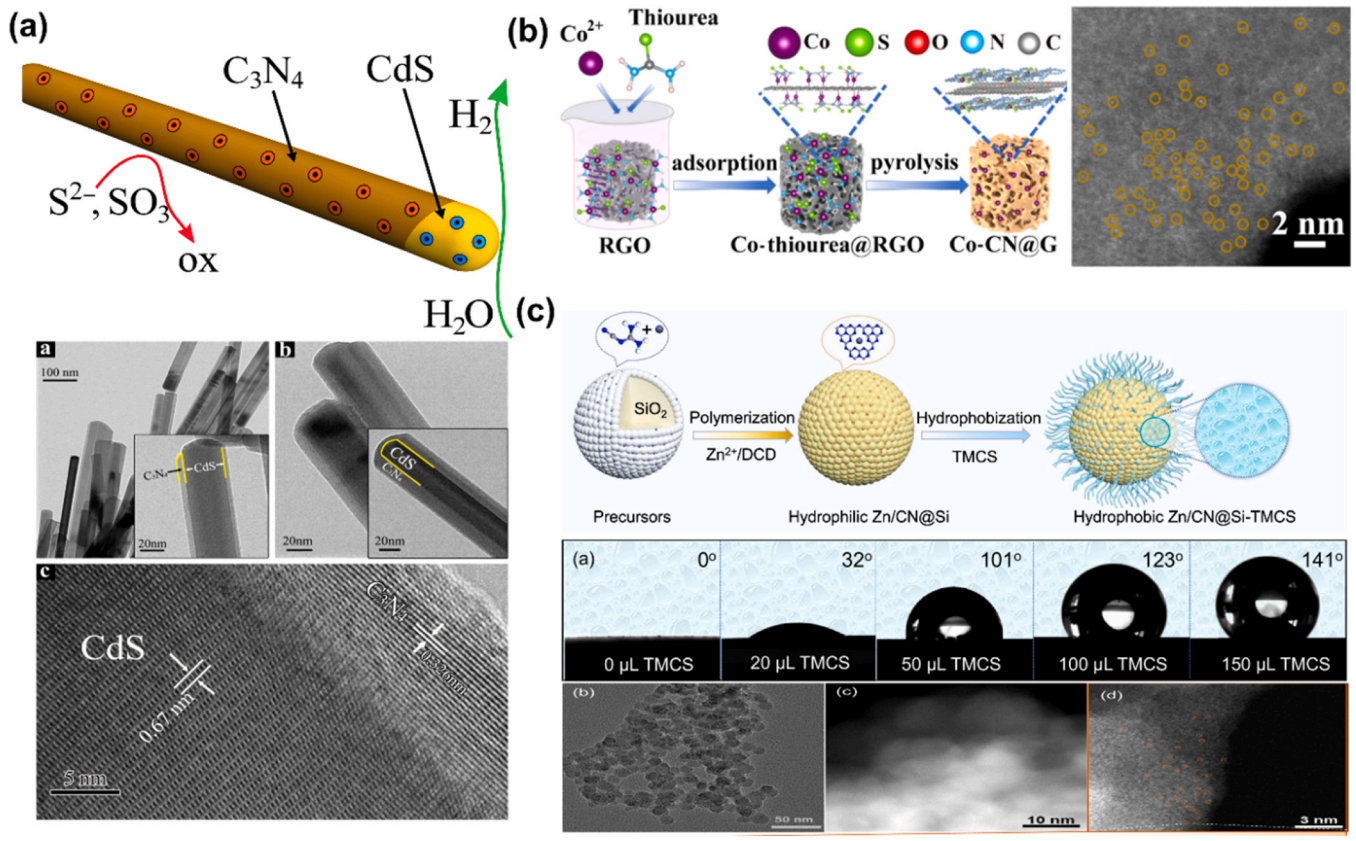

Fig. 14. Advanced approaches to suppress photocatalyst deactivation: (a) core–shell Heterojunctions [189]; (b) single-atom anchoring [192]; (c) surface hydrophobization [193].

structured to enhance mechanical stability and create tailored gas-flow channels, significantly improved gas diffusion within aerogel monoliths. Also, porous and hierarchically structured photocatalysts have proven vital for mitigating internal mass transfer limitations in gas–solid catalysis. Gas-phase reactants often move within catalyst pores; so, an ideal structure balances high surface area (for abundant active sites) with large pore channels (for easy gas flow) [172–174]. Khalil et al. [175] demonstrated that introducing macropores into a microporous covalent organic framework (COF) dramatically improved gas-accessible surface area and diffusion pathways. The resulting hierarchical COF showed a fourfold increase in the photocatalytic H_2 evolution rate compared to its microporous-only analogue in Fig. 13(c). In addition to static structures, dynamic catalyst systems were being explored. For instance, photocatalytic micro-nanomotors in Fig. 13(d) could move autonomously in response to light, stirring the surrounding gas or generating local convection [176,177]. By propelling themselves (via light-driven diffusiophoresis or bubble release), such catalysts prevented local reactant depletion and rapidly dislodged products from the surface.

In liquid-phase photocatalysis, mass transfer limitations usually stem from slow diffusion in liquid and stagnant boundary layers at the solid–liquid interface. If the photocatalyst is immobilized on a surface, reactants from the bulk solution must diffuse through a boundary layer, and products can accumulate near the interface. Conversely, suspending the catalyst as fine particles (a slurry) minimizes diffusion distance but can introduce light attenuation and separation challenges. Reactor configuration is therefore crucial in balancing these factors [178]. A recent spinning disc reactor design has drawn attention for water treatment applications. In this system in Fig. 13(e), the photocatalyst was coated on a rotating disc; as a thin film of polluted water spread radially, the combination of centrifugal force and shear created a highly turbulent, sub-millimeter liquid layer [179]. This configuration was found to reduce mass transfer limitations due to the combination of thin liquid film and flow turbulence, resulting in significantly increased reactant transfer and higher degradation rates. In addition, magnetically actuated artificial cilia have emerged as a promising strategy for enhancing mass transfer in liquid-phase photocatalytic systems, as shown in Fig. 13(f). When integrated into microfluidic reactors and subjected to periodic magnetic excitation, these biomimetic structures induced secondary micro-vortices, thereby significantly improving fluid mixing and continuously renewing the reactant concentration at the catalyst interface [180]. In summary, intelligent reactor design and tailored catalyst morphology go together. By integrating enhanced fluid dynamics (in gas or liquid phase) with advanced porous or dynamic materials, modern photocatalytic systems can overcome mass transfer limitations and achieve substantially higher efficiencies.

4.2. *Photocatalyst deactivation*

Photocatalyst deactivation is another critical issue. During long-term use, photocatalysts often lose their activity due to various degradation mechanisms. A key factor is surface poisoning by reaction intermediate or residual species: partially oxidized compounds and other byproducts tend to strongly adsorb onto active sites, obstructing the adsorption of reactants and suppressing the overall photocatalytic efficiency [181]. Additionally, many catalysts undergo photo-corrosion or self-oxidation/reduction under illumination. For instance, ZnO photocatalysts readily corroded in water, leaching Zn^{2+} into solution with a corresponding loss of activity[182]. Similarly, CdS and other II–VI semiconductors, despite their excellent visible-light absorption, exhibited unsatisfactory photochemical stability and deteriorated into inactive phases during reactions[183]. Developing strategies to mitigate such deactivation is therefore essential.

One effective approach is anchoring photocatalysts on inert supports

Table 1
Comparison of conventional methods of preparing photocatalysts.

Refs.	Methods	Principle (Process)	Typical Applications (Photocatalysts)	Product Characteristics	Advantages	Drawbacks
[226]	PVD	Vaporize source material (e.g. metal oxide or metal target) and condense as a thin film on a substrate under vacuum (e.g. evaporation or sputtering)	Commonly used to deposit oxide semiconductor thin films such as TiO_2 and ZnO, primarily utilized in coatings, electronic, and photocatalytic devices.	Dense, high-purity thin films on substrates (amorphous or polycrystalline depending on conditions)	Uniform composition; precise thickness and stoichiometry control; clean process (low contamination)	High equipment cost; limited scalability; thin-film only (unsuitable for powders); may require post-annealing for crystallinity
[212,213]	Thermal Spraying	Heat and propel precursor powders or molten droplets onto a surface to rapidly form a coating	Oxide photocatalyst coatings (TiO_2, ZnO) on metal or ceramic supports	Thick polycrystalline coatings with strong substrate adhesion; micro- to nano-structured surfaces	Fast coating of large areas; scalable for industrial surface modification; no vacuum needed	High process temperature can induce stresses; rough surface morphology and less nanoscale control; primarily for coatings (not nanoparticles);
[215,216]	Sol–gel	Hydrolysis and polycondensation of metal precursors to form sol-gel, followed by drying and calcination to produce oxides	Widely applied to synthesize oxide-based photocatalysts (TiO_2, ZnO, WO_3) and composite or doped materials for environmental and energy applications	Nanoscale powders, thin films, or porous structures; high chemical homogeneity	Excellent composition and stoichiometry control; suitable for multi-metal systems; synthesis at relatively low temperatures	Potential particle agglomeration and gel shrinkage; time-consuming; organic solvents and reagents required (environmental considerations); careful control needed to avoid film cracking
[217,218]	Hydrothermal	Crystal growth from aqueous solutions at elevated temperature and autogenous pressure in sealed autoclaves	Synthesis of shape-controlled oxide/sulfide nanostructures (e.g., TiO_2, ZnO, $BiVO_4$, CdS).	Highly crystalline nanoparticles with controllable size and anisotropic morphology; no post-calcination required	Direct crystalline phase synthesis; precise shape and size control; suitable for complex morphologies	Batch process with limited scalability; requires high-pressure equipment; lengthy reaction times; challenging for continuous production
[219,220]	Microemulsion	Reaction occurs in nanoscale water droplets dispersed in oil stabilized by surfactants; droplets serve as microreactors for precipitation/hydrolysis	Synthesis of ultrafine, highly uniform oxide nanoparticles (TiO_2, ZnO, Fe_2O_3) and chalcogenide nanomaterials	Uniform, monodisperse nanoparticles; particle size precisely tunable via droplet dimensions; often capped by surfactants	Excellent size and morphology control; narrow particle size distribution (<10 nm achievable); suitable for doped and composite nanoparticles	Low yield; limited scalability; additional washing and calcination steps required for removing organics; high cost due to surfactants; environmental concerns
[214,227]	Gas-phase Oxidation (Flame/Aerosol synthesis)	High-temperature oxidation of volatile precursors (metal chlorides/organometallics) in oxygen-rich flame or aerosol to form oxide nanoparticles	Industrial-scale synthesis of oxide nanopowders (TiO_2, ZnO) for photocatalysis, pigments, and catalysts.	Nano/sub-micron particles; high crystallinity; possible mixed phases (anatase/rutile); typically aggregated with broad size distribution	Continuous, scalable production; rapid synthesis; high purity and crystallinity; minimal residual impurities	Limited morphology and size control; particle aggregation; energy-intensive (1000–3000 °C); toxic/corrosive by-products; high equipment costs

to prevent leaching and aggregation. By immobilizing active sites onto stable matrices, the catalyst can better withstand operational stresses [184,185]. For example, covalent anchoring of a molecular Ru(II) photosensitizer onto rGO resulted in a hybrid photocatalyst exhibiting significantly enhanced photostability, maintaining performance over 24 h of continuous illumination. The graphene support served as a chemically robust scaffold that resisted photodegradation, facilitated heat dissipation, and enhanced charge transfer, thereby mitigating both thermal and chemical degradation pathways of the active Ru complex [186]. Likewise, elemental doping has emerged as a powerful method to bolster the intrinsic stability of semiconductor photocatalysts. Introducing heteroatoms into the lattice (either metal or non-metal dopants) can distort the local structure and electronic configuration in ways that suppress photo corrosive pathways[30,182]. Navarro et al. [187] demonstrated that metal-doped TiO_2 exhibited extended light absorption, improved charge separation, enhanced long-term stability and resistance to deactivation compared to undoped TiO_2. It is worth noting that a recent study on ZnO has shown that doping with trace transition metals (such as Co, Ni, or Cu) reduced Zn^{2+} leaching by 60–85 %, significantly increasing the material's tolerance to photo corrosion [182]. These studies illustrate how tuning the catalyst's composition or support can counteract poisoning and structural breakdown.

Another strategy is the construction of core–shell structures and heterojunctions to protect vulnerable photocatalysts and facilitate charge flow. In core–shell designs, a thin protective shell (usually a more stable oxide, nitride, or carbon layer) surrounds the active core, acting as a physical barrier against corrosive species while still allowing photon absorption and reactant diffusion. This morphology has proven especially beneficial for unstable chalcogenides such as CdS [188]. For example, forming an intimate CdS@g-C_3N_4 core–shell heterojunction was reported to drastically improve the photostability of CdS, as shown in Fig. 14(a): the g-C_3N_4 shell rapidly extracted photogenerated holes from CdS, thereby preventing those holes from oxidizing the CdS itself. By shuttling charges across the interface, the core–shell ensemble enhanced quantum efficiency and hindered photo-corrosion [189]. Such interfacial engineering, effectively an in situ "reconstruction" of the photocatalyst interface, creates a more resilient composite structure. Similarly, Han et al. [190] showed that the growth of a thin MoS_2 shell on CdS nanowires formed a coaxial core–shell structure that could efficiently extract or block charge carriers, thereby mitigating the photo-corrosion of CdS and extending service life of the photocatalyst.

The development of advanced nanoscale engineering techniques has broadened the range of strategies available for improving the long-term durability of photocatalysts. As previously discussed, defect engineering offers a versatile strategy for constructing anchoring sites that stabilize active phases or dopants. OVs and other lattice imperfections can effectively adjust the electronic structure while simultaneously serving as strong binding sites for cocatalysts or isolated atoms, thereby suppressing sintering and leaching. Notably, the field of single atom photocatalysts exemplifies how stability can be achieved even with

atomically dispersed active sites. This is primarily attributed to the strong metal–support interactions that anchor single metal atoms onto robust matrices such as TiO_2, g-C_3N_4, or MOFs [191]. A recent study [192] revealed that, in a photothermal–photocatalytic system based on cobalt single atoms anchored on a sulfur-doped g-C_3N_4/reduced graphene oxide heterostructure (Co–CN@G), the Co atoms were effectively stabilized through Co–N/S coordination environments in Fig. 14(b). This structural configuration enhanced the adsorption and activation of O_2 molecules and ensured excellent photocatalytic stability over extended reaction cycles. Another novel tactic is hydrophobic surface modification to mitigate fouling and unnecessary side reactions. Hydrophobic or omniphobic coatings on photocatalyst surfaces can repel liquid water and organic contaminants, thus limiting the accumulation of deactivating substances. Yu et al. [193] developed an atomically dispersed Zn-based photocatalyst featuring hydrophobic surface functionalization to construct a three-phase (solid–liquid–gas) reaction interface in Fig. 14(c). This design significantly enhanced the mass transport of reactants and products while suppressing the undesired decomposition of peroxide intermediates on the photocatalyst surface. By facilitating the rapid release of hydrophilic reaction products and minimizing their prolonged interaction with active sites, the hydrophobic interface effectively contributes to maintaining the structural and functional integrity of the catalyst during photocatalytic operation.

4.3. Toxic intermediates

During the photocatalytic degradation process, different reaction intermediates can be formed depending on the structure of the pollutant and the degradation pathway. Many of these intermediates have been reported to possess toxicity or pose environmental risks[194]. For instance, common intermediates in the photocatalytic oxidation of gas-phase toluene over TiO_2 included benzoic acid, benzaldehyde, benzyl alcohol, and ring-hydroxylated aromatic compounds, while benzene photocatalytic degradation typically yielded intermediates such as phenol, hydroquinone, and quinone compounds [195]. Most of these intermediates exhibit cytotoxicity, and some are even carcinogenic. Similarly, photocatalytic degradation of complex organic substances frequently generates harmful aldehydes such as formaldehyde and acetaldehyde. Under specific catalytic conditions, formaldehyde may further transform into highly toxic carbon monoxide, increasing potential environmental risks [196]. Another example involved azo dyes; under anaerobic conditions, photocatalytic cleavage of the azo bond generated aromatic amines (such as aniline derivatives), known to have high toxicity [197]. These examples underscore a critical issue: unless photocatalytic processes achieve near-complete mineralization, pollutants may merely convert into other intermediate compounds with potential hazards. Typically, the formation mechanism involves radical species (e.g., •OH, O_2^-, and h^+) attacking parent molecules, causing fragmentation into smaller molecular fragments. However, if the reaction time is insufficient, catalyst activity is limited, or other constituents in water consume reactive substances, these radicals may only partially oxidize pollutants, thereby leading to the accumulation of intermediate products [198–200].

Given the risk associated with generating toxic intermediates in photocatalytic processes, researchers increasingly focus on optimizing reaction pathways to achieve more thorough or selective pollutant degradation, thereby reducing the probability of harmful by-product formation. Generally, previous studies have proposed two complementary strategies: (i) enhancing photocatalyst activity and selectivity to promote pollutant deep mineralization into harmless final products (such as CO_2 and H_2O)[201]; (ii) finely controlling reaction pathways by adjusting photocatalyst composition, structure, or carrier characteristics, thereby facilitating deeper oxidation or conversion of intermediate products and reducing the risk of harmful by-product accumulation [202].

Between these two strategies, controlling photocatalyst selectivity to steer toward safer reaction pathways is especially noteworthy, as it has proven to be an effective approach[203]. Chen et al. [204] employed fluorine doping to regulate the surface charge distribution of $BiVO_4$, thereby directing glyphosate degradation predominantly through C–N bond cleavage. This strategy effectively suppressed the formation of the toxic intermediate aminomethylphosphonic acid, maintaining its yield below 10 %. In situ ATR-FTIR spectroscopy revealed that surface fluorination altered glyphosate's adsorption configuration on the catalyst, prompting preferential adsorption via phosphate groups and consequently shifting the degradation pathway toward less toxic products, such as glycine and phosphate. Overall, this study underscores that controlling surface adsorption can serve as an effective strategy for achieving greener and less toxic photocatalytic degradation.

Another effective strategy involves the rational design of photocatalysts to promote the deep oxidation of intermediates, thereby preventing their accumulation on the photocatalyst surface. For example, Liu et al. [205] investigated the photocatalytic oxidation of gaseous toluene using a ZnTi layered double hydroxide (LDH) catalyst. Compared with TiO_2, which achieved a removal rate of only 10.9 %, ZnTi-LDH exhibited a notably higher toluene removal rate of 75.2 % and generated substantially fewer intermediate products. Gas-phase analyses revealed that, under TiO_2 catalysis, intermediates such as benzaldehyde and benzoic acid tended to accumulate, whereas on ZnTi-LDH surfaces, abundant hydroxyl groups selectively absorbed and activated these key intermediates via hydrogen bonding, driving ring-opening and further deep oxidation. Similarly, doping strategies that introduce OVs or enhance ROS generation can effectively promote the further oxidation of recalcitrant intermediates [206]. For instance, Liu et al. [207] incorporated aluminum into a ZnSn-LDH, synergistically modulating OVs and hydroxyl content at the catalyst surface. This "dual-defect" structure significantly enhanced the photocatalyst's ability to adsorb and activate aromatic VOCs, improved e^-/h^+ separation, and facilitated high-efficiency ROS production. As a result, aromatic ring-opening and subsequent mineralization were greatly accelerated.

Beyond optimizing the structural design of photocatalysts, tailoring reaction pathways to minimize the accumulation of undesirable by-products is also an effective approach. Ma et al. [208] synthesized a Bi_2SiO_5/TiO_2 heterojunction photocatalyst, where a unique interfacial electron-transfer channel (Bi/Si–O–Ti) facilitated the rapid migration of photogenerated electrons to the TiO_2 surface. This enhanced the formation of highly oxidizing •OH radicals, thereby promoting ring-opening oxidation of toluene. Notably, benzoic acid was selectively formed at the Bi_2SiO_5/TiO_2 interface, favoring further rapid ring-opening and reducing the accumulation of other recalcitrant intermediates. Consequently, the Bi_2SiO_5/TiO_2 photocatalyst achieved a toluene mineralization rate of 85.5 %, significantly surpassing the 49.0 % rate observed with TiO_2 and leading to more complete conversion to CO_2. In another strategy, modifying photocatalyst supports or incorporating additives can neutralize or transform hazardous intermediates. In a recent study, Yang et al. [209] doped nitrogen-rich carbon nitride with alkaline-earth metal carbonates (e.g., $BaCO_3/C_3N_5$, $CaCO_3/C_3N_5$), effectively regulating the NO oxidation pathway under photocatalytic conditions. This approach enhanced selective oxidation of NO to NO_3^-, and suppressed the formation and accumulation of toxic NO_2, thereby enabling stable and deep mineralization of pollutants. Overall, recent progress highlights a suite of methodologies, ranging from selective adsorption and catalyst defect engineering to optimized cocatalysts, that researchers are leveraging to suppress toxic by-product formation at its source.

5. Preparation methods for photocatalytic materials

5.1. Conventional preparation methods

Conventional photocatalyst syntheses include a wide range of physical and chemical approaches applicable to common

semiconductors (e.g. TiO_2, ZnO, g-C_3N_4, $BiVO_4$). Physical techniques (such as physical vapor deposition (PVD) [210,211] and thermal spray [212,213]) rely on physical transformations, such as evaporation, sputtering or high-energy milling, to produce films or coatings. These methods are straightforward and often environmentally benign, yielding high-purity products and facile deposition on surfaces. However, purely physical routes struggle with controlling nanoscale particle size and morphology, making them less suited for producing uniform nano powders. As a result, industrial photocatalyst production predominantly uses chemical methods that afford superior control over composition and particle characteristics.

Chemical synthesis methods typically include gas-phase processes and liquid-phase techniques. Among gas-phase methods, flame aerosol or fumed synthesis involves high-temperature oxidation of volatile precursors such as metal chlorides or organometallic compounds, leading to nucleation and formation of oxide nanoparticles, as in the flame hydrolysis of titanium tetrachloride ($TiCl_4$) to produce TiO_2 [214]. This route offered rapid, continuous production of high-purity powders, but tended to produce aggregated nanoparticles with broad size distributions and irregular shapes.

Liquid-phase methods (sol–gel [215,216], hydrothermal [217,218], microemulsion [219,220], etc.) are widely used for both oxide and non-oxide photocatalysts due to their mild conditions and tunability. In sol–gel processing, metal alkoxides or inorganic salt precursors undergo controlled hydrolysis and polycondensation reactions, forming an inorganic polymeric gel network. Subsequent heat treatment transforms this gel into a crystalline metal oxide. This method facilitates molecular-level mixing, leading to highly homogeneous and pure photocatalytic materials, and is suitable for industrial-scale production of both thin films and nano powders[221]. Hydrothermal synthesis, carried out in sealed autoclaves at elevated temperature and autogenous pressure, directly crystallizes materials (such as TiO_2 or $BiVO_4$) from solution, achieving well-defined nanocrystals with controlled phase and morphology without the need for high-temperature calcination [222,223]. Microemulsion methods utilize nanoscopic reactant droplets stabilized by surfactants as "microreactors," confining nucleation and growth to produce extremely uniform nanoparticles with minimal agglomeration [224,225].

Conventional synthesis methods each have distinct advantages and limitations regarding scalability, crystallinity, and morphological control. Chemical methods typically excel in precisely controlling particle size, phase purity, and morphology, whereas physical methods are more suited to fabricating thin films or coating structures. Although most oxide-based photocatalysts can be synthesized via multiple pathways, the optimal process choice is usually dictated by the desired form (powder or thin film), crystallinity requirements, and production scale. Table 1 summarizes the core principles, general advantages, and inherent limitations of these traditional synthesis approaches.

In summary, despite significant advancements, several critical bottlenecks continue to impede the industrial-scale application of photocatalytic technologies. Stability concerns, including particle agglomeration, phase instability, and performance deterioration, frequently emerge during scale-up, particularly in flame aerosol and microemulsion syntheses. Traditional photocatalysts, such as TiO_2 and ZnO, exhibit limited visible-light response, primarily absorbing ultraviolet light, thus restricting their practical efficiency under natural sunlight conditions. While doping and heterostructure strategies have extended their absorption spectra, achieving reproducible and consistent performance at industrial scales remains challenging. Additionally, chemical synthesis methods such as sol–gel and microemulsion processes involve extensive use of organic solvents and surfactants, substantially increasing production costs and environmental impacts during large-scale manufacturing. Similarly, gas-phase oxidation techniques are energy-intensive and pose significant ecological and economic burdens. Furthermore, extensive post-synthesis treatments and catalyst regeneration further increase operational complexity and costs. Effectively addressing these challenges is essential to successfully transitioning photocatalytic materials from laboratory innovation to broad industrial deployment.

5.2. *Novel methods for the preparation of photocatalytic materials*

To effectively address the challenges, recent research has turned to novel synthetic approaches that emphasize green chemistry, refined nanostructure control, and scalability. The following reviews several innovative approaches, including green biosynthesis, plasma-assisted electrolysis, microfluidic continuous-flow reactors, mechanochemistry, atomic layer deposition (ALD), and direct ink writing (DIW) 3D printing technology, demonstrating how each method offers distinct advantages over conventional techniques.

"Green" synthesis strategies use harmless reagents (e.g., plant extracts, biological templates) and waste materials for the preparation of photocatalysts, avoiding toxic solvents and excessive energy inputs. Natural capping agents inherent in these methods mitigate particle

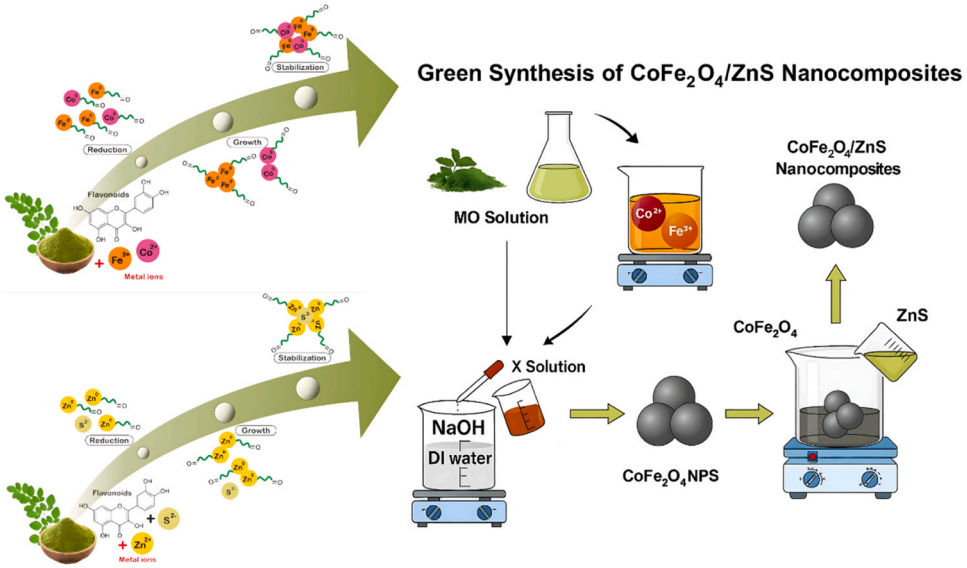

Fig. 15. Green synthesis method of photocatalysts using plant extracts [230].

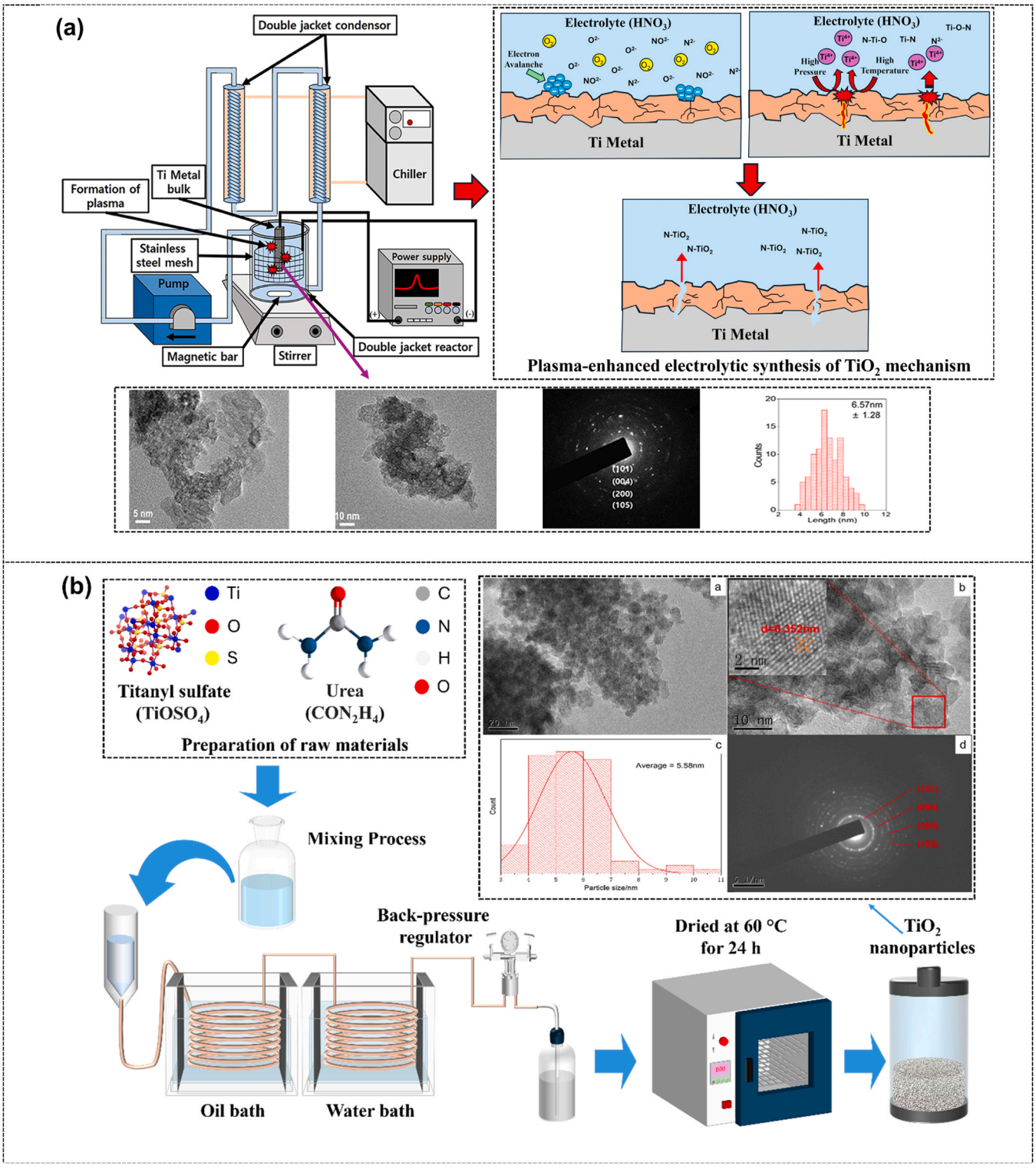

Fig. 16. Innovative photocatalyst synthesis via (a) plasma-assisted electrolysis [231] and (b) microfluidics [232].

aggregation and significantly enhance environmental compatibility [228]. For instance, Gadore et al. [229] introduced an innovative green synthetic route using Ocimum tenuiflorum leaf extract as a stabilizer to fabricate a novel Z-scheme SnS_2/HAp nanocomposite photocatalyst. In this approach, hydroxyapatite (HAp) was sustainably derived from waste fish scales via alkaline extraction, followed by loading of SnS_2 onto HAp through a mild coprecipitation process at 60°C. Compared to conventional methods, this strategy effectively eliminates reliance on costly and highly corrosive chemicals, while simultaneously converting waste into value-added materials, thereby reducing environmental pollutants. In another study, Larasati et al. [230] developed a green synthesis protocol utilizing Moringa oleifera leaf extract as both reducing and stabilizing agents to successfully produce a magnetically separable and reusable $CoFe_2O_4$/ZnS nanocomposite photocatalyst in Fig. 15. $CoFe_2O_4$ and ZnS nanoparticles were separately synthesized via coprecipitation at 60–80°C; ZnS was subsequently uniformly deposited

Fig. 17. Mechanochemical synthesis of doped photocatalytic nanomaterials [234].

onto $CoFe_2O_4$ surfaces through ultrasonic-assisted treatment, forming core-shell structures that effectively reduced particle agglomeration and improved dispersion. This eco-friendly synthesis leverages phenolic and flavonoid compounds from plant extracts to replace hazardous solvents and surfactants typical in chemical synthesis, thus enhancing environmental compatibility and safety.

To enhance the visible-light activity of TiO_2 without the stringent requirements of conventional chemical doping methods, plasma-assisted electrolysis has emerged as a novel and effective "one-pot" synthesis strategy in Fig. 16(a). Kim et al. [231] used a plasma-electrolytic approach utilizing nitric acid as the electrolyte, applying a 500 V alternating current directly to a metallic titanium substrate. Within merely 10 min, uniform N-doped TiO_2 nanoparticles (12.1–24.7 nm) were produced. Compared to traditional liquid-phase methods such as sol-gel or hydrothermal synthesis, this technique significantly simplifies the preparation process by avoiding prolonged reaction and drying steps, thus enabling direct and rapid formation of catalysts from the metallic source. Moreover, adjusting electrolyte concentrations allows precise control over particle size and nitrogen doping levels, enhancing the photocatalytic activity of the resulting materials in the visible spectrum. Another promising synthetic approach was the use of microfluidic continuous-flow reactors in Fig. 16(b). Deng et al. [232] developed a novel microfluidic system comprising a coiled stainless-steel microreactor, facilitating rapid heat and mass transfer, thereby overcoming the inherently sluggish diffusion kinetics of traditional batch reactors. Under conditions of 180°C, anatase TiO_2 nanoparticles (~5 nm) were synthesized within 3.5 min, a remarkable reduction compared to conventional hydrothermal techniques, which typically require several hours or even longer reaction durations.

Mechanochemical synthesis, exemplified by high-energy ball milling, has emerged as a solvent-free and efficient strategy for preparing photocatalytic nanoparticles and doped composites. This technique utilizes mechanical forces to drive solid-state reactions, eliminating

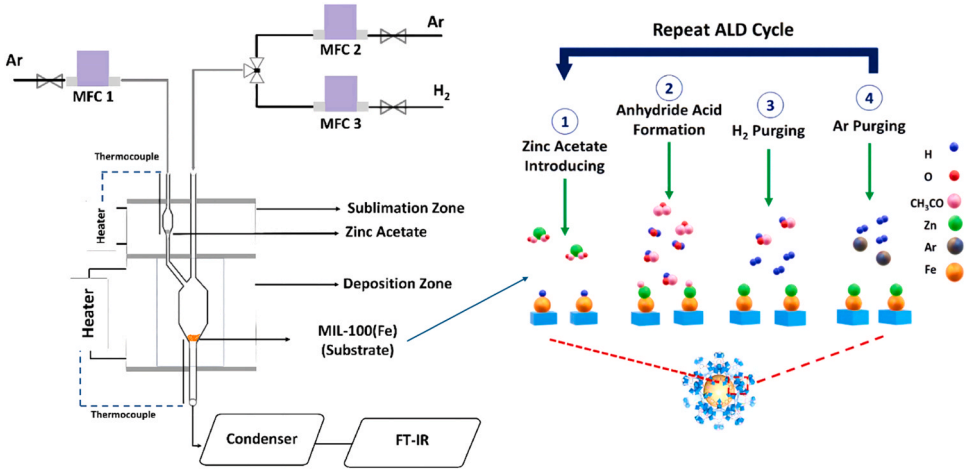

Fig. 18. ALD for precise photocatalyst structuring [240].

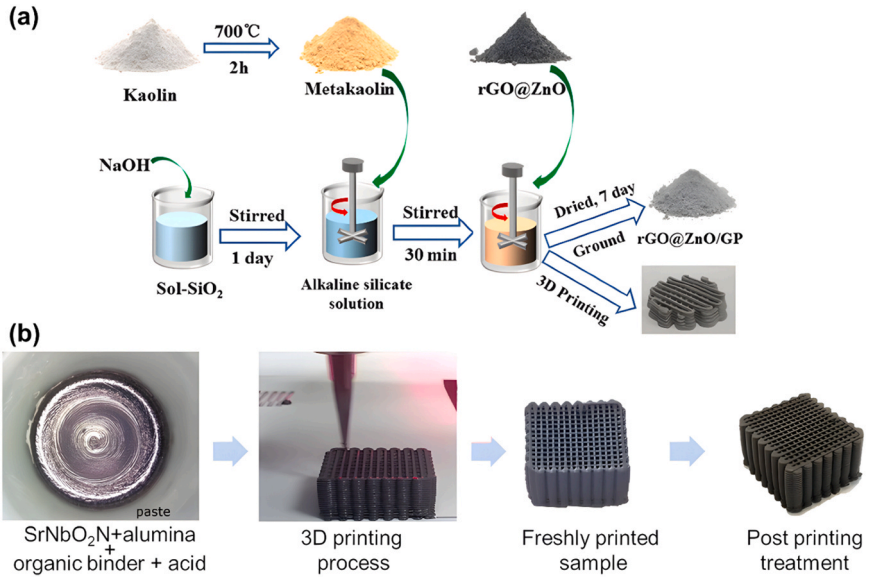

Fig. 19. Advanced photocatalyst architecture fabricated by 3D printing: (a) Liu et al. [244]; (b) Iborra-Torres et al. [245].

extensive solvent use and facilitating the formation of beneficial defects or phase transformations otherwise challenging to achieve through conventional wet-chemical methods [233]. Yang et al. [234] developed a mechanochemically assisted sol–gel approach for synthesizing nickel-doped TiO_2 nanoparticles (Fig. 17). In their procedure, solution A was prepared by mixing tetrabutyl titanate with absolute ethanol, while solution B was formed by combining nickel nitrate, glacial acetic acid, deionized water, and ethanol with pH adjustment. These solutions were subsequently mixed to form a gel, which after drying underwent mechanochemical ball milling (100 rpm, 15 min) using corundum spheres, followed by calcination at 500 °C. The milling process effectively disrupted particle agglomeration within the gel matrix, resolving issues related to uneven precursor mixing, aggregation, and contamination encountered in conventional synthesis methods. Additionally, this mechanochemical route avoided excessively high calcination temperatures, thereby preserving the integrity of the nanocrystalline structure. This one-step, solvent-free method offers simplicity, scalability, and environmental compatibility, thus presenting significant potential for industrial-scale production.

ALD is a gas-phase deposition technology based on surface self-limiting reactions, enabling precise control over thin-film thickness and composition at atomic-level resolution (angstrom-scale) [235]. In recent years, ALD has increasingly gained prominence in photocatalysis, particularly for fabricating conformal coatings [236], doping layers [237], and co-catalyst clusters [238] with unprecedented accuracy. Compared with traditional impregnation or co-precipitation techniques, which often suffer from non-uniform coverage or particle agglomeration, ALD provides uniformity and reproducibility at the nanoscale by enabling atomically precise, layer-by-layer growth. Consequently, it offers a novel route for profound optimization of surface and interfacial properties in photocatalytic materials [236,239]. For instance, Parasa et al. [240] utilized ALD to uniformly deposit ZnO nanoparticles onto MIL-100(Fe) frameworks, yielding highly efficient ZnO/MIL-100(Fe) composite photocatalysts (Fig. 18). MIL-100(Fe) nanocrystals were synthesized via a hydrothermal method (150 °C, 40 h), followed by precise deposition of ZnO using zinc acetate as the ALD precursor at 200 °C over 0.5–2 ALD cycles. Compared to conventional techniques, this ALD-based approach provided atomically accurate control and homogeneous distribution of nanoparticles, effectively mitigating common issues such as nanoparticle agglomeration, non-uniform dispersion, and lattice mismatches at interfaces. Similarly, Saedy et al. [241] utilized ALD to prepare a Cu_xO/TiO_2 composite photocatalyst. Using a fluidized-bed reactor at 250 °C with Cu(I)(hfac)(TMVS) as the copper source and water as the reactant, they achieved precise deposition of uniformly sized Cu_xO nanoclusters (~1.7 nm) onto TiO_2 particle surfaces. This methodology avoided limitations inherent in conventional liquid-phase impregnation and precipitation methods, particularly the challenges in controlling particle size and ensuring dispersion uniformity. Thus, ALD facilitated atomic-level precision and high dispersion of Cu_xO nanoparticles on TiO_2.

3D printing technology has demonstrated great potential in the design and fabrication of photocatalysts. In contrast to traditional photocatalysts prepared primarily as powders, which are prone to aggregation and difficult to recover, 3D printing technology can directly construct integrated monoliths, lattice structures, or films on demand, enabling precise customization of photocatalyst architectures at the macroscopic scale. Importantly, these structured photocatalysts are easier to handle and more readily reusable [242,243]. For example, Liu et al. [244] reported a hybrid approach combining hydrothermal synthesis and DIW 3D printing to fabricate structured rGO@ZnO/geopolymer composite photocatalysts in Fig. 19(a). Initially, rGO-ZnO composites were prepared hydrothermally from ZnO, NaOH, and GO at 180 °C for 12 h. The obtained rGO@ZnO was then mixed with a metakaolin-based geopolymer slurry, dried at 60 °C for 7 days, ground into powder, and subsequently structured into complex geometries using DIW printing. In another study, Iborra-Torres et al. [245] successfully synthesized structured perovskite oxynitride ($SrNbO_2N$) photocatalysts via DIW 3D printing in Fig. 19(b). $SrNbO_2N$ powders synthesized using a polymeric precursor method were combined with Al_2O_3 supports, methylcellulose binder, and nitric acid aqueous solution to formulate printable inks. Following 3D printing, the organic constituents were removed by calcination at 650 °C under air, yielding precisely structured monolithic photocatalysts. Inclusively, these studies illustrate that compared to photocatalyst powders prepared by traditional methods, which suffer from difficulties in recovery, severe aggregation, and low reuse efficiency, photocatalysts fabricated via 3D printing technology exhibit significantly improved structural stability, ease of recovery, and reusability.

In summary, these emerging synthesis strategies for photocatalysts not only adhere to green chemistry principles by minimizing toxic solvents and energy consumption, but also substantially enhance the precision and uniformity of nanostructures through advanced methods such as ALD and microfluidic processing. Furthermore, innovative techniques including plasma-assisted and mechanochemical syntheses significantly simplify preparation procedures, reducing reaction times and associated costs. Also, additive manufacturing technologies such as 3D printing have enabled structural customizability and scalability. These systematic advancements effectively overcome critical bottlenecks associated with traditional photocatalyst preparation methods, laying a robust foundation for the efficient and sustainable development of next-generation photocatalytic materials [246–251].

6. Conclusions and perspectives

This review systematically summarizes the key factors affecting the performance of photocatalysts, elucidating strategies for enhancing photocatalyst activity via surface modification and functionalization. It further provides an in-depth analysis of cutting-edge approaches to overcoming key bottlenecks in practical photocatalytic applications. Notably, emerging synthetic methodologies demonstrate distinct advantages over conventional techniques by effectively mitigating particle agglomeration, enhancing structural stability, broadening visible-light responsiveness, and significantly reducing environmental and economic costs. The main conclusions are as follows:

(1) Achieving superior photocatalytic performance depends critically on the synergistic optimization of intrinsic semiconductor properties and operating conditions. Bandgap energy adjustment, illumination intensity thresholds, and reaction parameters (e.g., temperature and pH) maximize photon utilization efficiency and reaction kinetics. Moreover, interfacial engineering strategies enhance photocatalyst functionality: ferroelectric interface engineering leverages intrinsic polarization-induced electric fields to promote efficient charge carrier separation; hydrogel-based composite systems mitigate nanoparticle aggregation through hydrophilic porous networks, improving catalyst recyclability and stability; heterojunction and homojunction architectures achieve an effective balance between catalytic activity and long-term stability; defect engineering finely modulates electronic structures, broadening spectral response and enhancing carrier mobility. These innovative interfacial and composite structures substantially control charge dynamics, thereby pushing photocatalytic performance beyond traditional limits.

(2) Practical application of photocatalysts remains constrained by three critical bottlenecks: mass transfer limitations, catalyst deactivation, and toxic byproduct formation. Mass transfer limitations cause inadequate reactant availability at active sites, which can be alleviated through advanced reactor designs such as fluidized beds, rotating disk reactors, and magnetically actuated biomimetic cilia to enhance interfacial diffusion. Catalyst deactivation predominantly originates from photochemical corrosion and active-site poisoning; strategies such as using inert supports

or constructing protective heterojunctions (e.g., encapsulation of CdS by g-C_3N_4) substantially improve catalyst stability. Additionally, single-atom catalysts (e.g., cobalt atoms anchored on doped g-C_3N_4) enhance recyclability via strong metal–support interactions. Toxic byproduct formation can be effectively mitigated by precise structural and surface modifications, steering reaction pathways towards complete mineralization.

(3) The integration of fundamental theory and frontier engineering techniques is reshaping the trajectory of next-generation photocatalyst development. Emerging bottom-up synthetic strategies and fabrication processes are overcoming longstanding limitations in precise control of catalyst composition and structural characteristics. Green biosynthesis, plasma-assisted electrolysis, microfluidic continuous-flow reactors, and mechanochemical methods minimize environmental impacts and production costs as well as accelerate catalyst formation and streamline scalable manufacturing. Additionally, ALD enables uniform doping and cocatalyst coatings at angstrom-level precision, while 3D printing facilitates customized photocatalytic architectures, significantly enhancing photon utilization efficiency and catalyst reusability. These cutting-edge methodologies synergistically mitigate critical issues inherent to conventional synthesis, such as particle aggregation, insufficient phase stability, limited visible-light response, and precursor toxicity, laying a robust foundation for industrial-scale production of advanced photocatalysts.

(4) Emerging data-driven methods, particularly machine learning, provide a powerful pathway for accelerating the discovery and optimization of advanced photocatalytic materials. By utilizing predictive algorithms and extensive materials datasets, researchers can rapidly identify high-performance catalyst compositions and structures, surpassing conventional trial-and-error approaches. Concurrently, interdisciplinary integration is poised to unlock novel reaction frontiers. For instance, coupling photocatalysis with electrocatalysis or photothermal catalysis could establish synergistic pathways, enhancing efficiencies beyond the sum of individual processes. Such integrated strategies promise to overcome current performance bottlenecks and revolutionize solar energy conversion.

(5) Another crucial direction lies in developing scalable and environmentally sustainable manufacturing technologies to facilitate the practical deployment of advanced photocatalysts. Techniques such as ALD and 3D printing enable atomic-level precision in catalyst nanostructure fabrication, while remaining fully compatible with high-throughput production requirements. Equally important is reactor engineering: innovative reactor systems that combine efficient light harvesting with enhanced mass transport will ensure optimal convergence of photons and reactants at catalytic active sites, thereby maximizing catalytic turnover rates. These advancements will help bridge the existing gap between laboratory breakthroughs and practical clean-energy technologies.

CRediT authorship contribution statement

Wengui Li: Writing – review & editing, Writing – original draft, Validation, Supervision, Resources, Conceptualization. **John L. Zhou:** Writing – review & editing, Writing – original draft, Validation. **Fazhou Wang:** Writing – review & editing, Writing – original draft, Validation. **Huang Yunan:** Writing – review & editing, Writing – original draft, Validation. **Wenkui Dong:** Writing – review & editing, Writing – original draft, Validation, Supervision. **Kailun Chen:** Writing – review & editing, Writing – original draft, Validation, Methodology, Investigation, Formal analysis, Conceptualization.

Declaration of Competing Interest

The authors declare that they have no known competing financial interests or personal relationships that could have appeared to influence the work reported in this paper.

Acknowledgements

The authors would like to acknowledge the support from Australian Research Council (ARC), Australia (FT220100177, LP230100288, DP220101051, DP220100036, IH200100010).

Data Availability

Data will be made available on request.

References

[1] J. Wang, W. Azam, Natural resource scarcity, fossil fuel energy consumption, and total greenhouse gas emissions in top emitting countries, Geosci. Front. 15 (2024) 101757, https://doi.org/10.1016/J.GSF.2023.101757.
[2] Y. Xia, M. Sayed, L. Zhang, B. Cheng, J. Yu, Single-atom heterogeneous photocatalysts, Chem. Catal. 1 (2021) 1173–1214, https://doi.org/10.1016/J.CHECAT.2021.08.009.
[3] X. Yu, S. Wang, Y. Zhang, X. Yu, X. Zhao, H. Gao, H. Yang, L. Fang, A. Syed, Biochar coupling induced charge transfer switching of a NiAl2O4/NiCr2O4 photocatalyst to enhance photocatalytic degradation of tetracycline hydrochloride, Surf. Interfaces 54 (2024) 105222, https://doi.org/10.1016/J.SURFIN.2024.105222.
[4] M. Gu, L. Duan, Z. Zhang, Y. Jiang, Q. Zhang, L. Zhou, G. Yu, J. Huang, Multi-charge bridge transfer guiding design of photocatalyst with oxygen defects for effective degradation of PFAS in fluoropolymer production wastewater, Chem. Eng. J. 505 (2025) 159124, https://doi.org/10.1016/J.CEJ.2024.159124.
[5] C. Yue, J. Jiang, M. Li, X. Wang, T. Li, Z. Zhao, S. Dong, Accelerating the peroxymonosulfate activation and charge transfer by construction of Fermi energy level-matched CoWO4/g-C3N4 photocatalyst for typical antibiotics degradation, Sep Purif. Technol. 301 (2022) 122020, https://doi.org/10.1016/J.SEPPUR.2022.122020.
[6] Q. Guo, C. Zhou, Z. Ma, X. Yang, Fundamentals of TiO2 Photocatalysis: Concepts, Mechanisms, and Challenges, Adv. Mater. 31 (2019) 1901997, https://doi.org/10.1002/adma.201901997.
[7] Y. Wang, Z. Wang, X. Jia, X. Zhang, H. Xie, Y. Zhang, Performance and mechanism of step-scheme P-doped g-C3N4/Ag3PO4 heterojunction photocatalysts for organic pollutant degradation, Diam. Relat. Mater. 151 (2025) 111865, https://doi.org/10.1016/J.DIAMOND.2024.111865.
[8] P. Rajaram, K.K. Brito, S. Vignesh, M. Srinivasan, Biosynthesis of 2D MnMoO4@g-C3N4 composite photocatalyst for environmental hazardous pollutant degradation with optimizing degradation parameters, Inorg. Chem. Commun. 173 (2025) 113867, https://doi.org/10.1016/J.INOCHE.2024.113867.
[9] P. Alimard, C. Gong, I. Itskou, A. Kafizas, Achieving high photocatalytic NOx removal activity using a Bi/BiOBr/TiO2 composite photocatalyst, Chemosphere 368 (2024) 143728, https://doi.org/10.1016/J.CHEMOSPHERE.2024.143728.
[10] C. Xu, Cu/Cu2O/NH2-MIL-88B (Fe) heterojunction as the photocatalyst to remove hexavalent chromium heavy metal ions in water, RSC Adv. 15 (2025) 2462–2469, https://doi.org/10.1039/D4RA08143A.
[11] S. Zeng, L. Wu, W. Bing, W. Wang, H. Li, X. Zhou, S. Peng, Constructing O doped g-C3N4 nanosheets as photocatalysts for photocatalytic water splitting derived hydrogen isotopic water separation, Sep Purif. Technol. 359 (2025) 130880, https://doi.org/10.1016/J.SEPPUR.2024.130880.
[12] S. Yan, L. Wang, Y. Wu, T. Hou, Y. Li, K. Shen, Photothermal-enabled metal-free polyfuran photocatalysts for efficient solar-to-hydrogen peroxide energy conversion from seawater, Appl. Catal. B Environ. Energy 357 (2024) 124337, https://doi.org/10.1016/J.APCATB.2024.124337.
[13] K. Chen, F. Qu, Z. Sun, S.P. Shah, W. Li, Carbon sequestration, performance optimization and environmental impact assessment of functional materials in cementitious composites, J. CO2 Util. 90 (2024) 102986, https://doi.org/10.1016/J.JCOU.2024.102986.
[14] M. Muscetta, L. Clarizia, R. Andreozzi, R. Marotta, G. Palmisano, G. Policastro, M. Race, M. Verrillo, R. Spaccini, I. Di Somma, From waste to resource: Hydrogen generation and antimicrobial activity of Ag-based photocatalysts recovered from biomedical waste, J. Environ. Chem. Eng. 12 (2024) 114722, https://doi.org/10.1016/J.JECE.2024.114722.
[15] Y. Zhu, Q. Dong, A. Sial, A. Labidi, K. Zhao, X. Li, J. Wang, C. Wang, Mixed-metal MIL-101(Fe/Cr) MOF photocatalyst: Efficient photocatalytic nitrogen fixation by promoting ligand-metal charge transfer, Appl. Catal. O Open 200 (2025) 207030, https://doi.org/10.1016/J.APCATO.2025.207030.
[16] F.X. Jiang, H.Y. Zheng, L.F. Wang, L.J. Yan, Y.N. Wang, X.Y. Chen, X.H. Xu, Enhanced photoelectric performance in a CdO/ZnO/Ag heterostructure thin film photoanode, Vacuum 185 (2021) 109951, https://doi.org/10.1016/J.VACUUM.2020.109951.

[17] H. Khan, M.U.H. Shah, Modification strategies of TiO2 based photocatalysts for enhanced visible light activity and energy storage ability: a review, J. Environ. Chem. Eng. 11 (2023) 111532, https://doi.org/10.1016/J.JECE.2023.111532.
[18] S. Ghasemi, A. Parastesh, M. Padervand, H. Ren, X. Li, A. Labidi, M. Signoretto, E. A. Dawi, T. Hamzehlouyan, E. Lichtfouse, C. Wang, Recent progress on Z- and S-scheme photocatalysis: mechanistic understanding toward green applications, Curr. Opin. Chem. Eng. 47 (2025) 101059, https://doi.org/10.1016/J.COCHE.2024.101059.
[19] M. Khatun, P. Mitra, S. Mukherjee, Effect of band gap and particle size on photocatalytic degradation of NiSnO3 nanopowder for some conventional organic dyes, Hybrid. Adv. 4 (2023) 100079, https://doi.org/10.1016/J.HYBADV.2023.100079.
[20] F. Azeez, E. Al-Hetlani, M. Arafa, Y. Abdelmonem, A.A. Nazeer, M.O. Amin, M. Madkour, The effect of surface charge on photocatalytic degradation of methylene blue dye using chargeable titania nanoparticles, Sci. Rep. 8 (2018) 7104, https://doi.org/10.1038/s41598-018-25673-5.
[21] G. Zhang, Y. Liu, Z. Hashisho, Z. Sun, S. Zheng, L. Zhong, Adsorption and photocatalytic degradation performances of TiO2/diatomite composite for volatile organic compounds: Effects of key parameters, Appl. Surf. Sci. 525 (2020) 146633, https://doi.org/10.1016/J.APSUSC.2020.146633.
[22] Z. Lin, X. Tong, W. Shen, J.C. Roux, H. Xi, Humidity impact on photo-catalytic degradation: Adsorption behavior simulations and catalytic reaction mechanisms for main gaseous pollutants in papermaking industry, J. Clean. Prod. 244 (2020) 118863, https://doi.org/10.1016/J.JCLEPRO.2019.118863.
[23] R. Marschall, Semiconductor composites: Strategies for enhancing charge carrier separation to improve photocatalytic activity, Adv. Funct. Mater. 24 (2014) 2421–2440, https://doi.org/10.1002/adfm.201303214.
[24] Y. Li, S.C.E. Tsang, Recent progress and strategies for enhancing photocatalytic water splitting, Mater. Today Sustain. 9 (2020) 100032, https://doi.org/10.1016/J.MTSUST.2020.100032.
[25] A. Balapure, J. Ray Dutta, R. Ganesan, Recent advances in semiconductor heterojunctions: a detailed review of the fundamentals of photocatalysis, charge transfer mechanism and materials, RSC Appl. Interfaces 1 (2024) 43–69, https://doi.org/10.1039/D3LF00126A.
[26] S.J. Phang, V.L. Wong, L.L. Tan, S.P. Chai, Recent advances in homojunction-based photocatalysis for sustainable environmental remediation and clean energy generation, Appl. Mater. Today 20 (2020) 100741, https://doi.org/10.1016/J.APMT.2020.100741.
[27] X. Yang, Z. Xiang, J. Wu, P. He, Y. Qi, S. Chen, Y. Lu, R. Xie, Z. Liu, C. He, Research progress on the construction of oxygen vacancy defects and application in photocatalytic oxidation of elemental mercury, Fuel 355 (2024) 129440, https://doi.org/10.1016/J.FUEL.2023.129440.
[28] J. An, C. Xu, L. Li, B. Tang, The unique spontaneous polarization property and application of ferroelectric materials in photocatalysis, Nano Res 17 (2024) 3571–3585, https://doi.org/10.1007/s12274-023-6357-8.
[29] E.A. Mohamad, E.M. Sakr, S.A. Mohammed, V.S. John, H.S. Mohammed, Modified TiO2/chitosan-based hydrogel beads for the photocatalytic degradation of dyes and heavy metals for water treatment, Chem. Pap. 79 (2025) 1417–1425, https://doi.org/10.1007/s11696-024-03863-y.
[30] C. Gusmão, P.H. Palharim, L.A. Diniz, G.C. de Assis, T. de Carvalho e Souza, B. Ramos, A.C.S.C. Teixeira, Advances in Fluidized Bed Photocatalysis: Bridging Gaps, Standardizing Metrics, and Shaping Sustainable Solutions for Environmental Challenges, Ind. Eng. Chem. Res 63 (2024) 14967–14982, https://doi.org/10.1021/acs.iecr.4c00821.
[31] M. Xiao, Z. Wang, K. Maeda, G. Liu, L. Wang, Addressing the stability challenge of photo(electro)catalysts towards solar water splitting, Chem. Sci. 14 (2023) 3415–3427, https://doi.org/10.1039/d2sc06981d.
[32] P. Chen, W. Ma, W. He, J. Liao, Q. Xia, A. Jiang, Y. Ma, W. Ai, Y. Wang, W. Zhang, Constructing multiple active sites of Bi2WO6 for efficient photocatalytic NO removal and NO2 inhibition, J. Catal. 434 (2024) 115538, https://doi.org/10.1016/J.JCAT.2024.115538.
[33] T. Xie, S. Sun, Y. Guo, Y. Luo, M. Yang, B. Yang, J. Cui, Fabrication of In–S-co-doped two-dimensional BiOCl coupling with surface hydroxylation toward simultaneously efficient charge separation and redox capability for photocatalytic water remediation, Chemosphere 315 (2023) 137742, https://doi.org/10.1016/J.CHEMOSPHERE.2023.137742.
[34] Y. Mohammed, H.Y. Hafeez, J. Mohammed, A.B. Suleiman, C.E. Ndikilar, M. G. Idris, Hydrogen production via photocatalytic water splitting using spinel ferrite-based photocatalysts: Recent and future perspectives, Energy 4 (2024) 100145, https://doi.org/10.1016/J.NXENER.2024.100145.
[35] X. Ren, R. Chen, S. Ding, N. Fu, Preparation and photocatalytic performance of a magnetically recyclable ZnFe2O4@TiO2@Ag2O p-n/Z-type tandem heterojunction photocatalyst: Degradation pathway and mechanism, Colloids Surf. A Physicochem Eng. Asp. 658 (2023) 130604, https://doi.org/10.1016/J.COLSURFA.2022.130604.
[36] M.T. Ahmed, S.A. Farooqui, S.-H. Hsu, L. Daeun, S.K. Chaerun, Valorizing Glycerol into Valuable Chemicals Through Photocatalytic Processes Utilizing Innovative Nano-Photocatalysts, in: H. Abdullah (Ed.), Solar Light-to-Hydrogenated Organic Conversion: Heterogeneous Photocatalysts, Springer Nature Singapore, Singapore, 2024, pp. 149–234, https://doi.org/10.1007/978-981-99-8114-4_4.
[37] M.Z. Shafiq, W. shahid, A. Khalid, Z.M. Aldhafeeri, M.I. Khan, M. Umar, G. S. Albakri, M. Hasan, S. Hayat, J.R. Choi, Enhanced photocatalytic activity of V2O5/ZnO heterostructures for malachite green dye using solar simulator irradiation, Opt. Mater. (Amst.) 158 (2025) 116458, https://doi.org/10.1016/J.OPTMAT.2024.116458.
[38] J.-Z. Kong, H.-F. Zhai, W. Zhang, S.-S. Wang, X.-R. Zhao, M. Li, H. Li, A.-D. Li, D. Wu, Visible Light-Driven Photocatalytic Performance of N-Doped ZnO/g-C3N4 Nanocomposites, Nanoscale Res Lett. 12 (2017) 526, https://doi.org/10.1186/s11671-017-2297-0.
[39] A. Khan, Zia-ur-Rehman, M. ur Rehman, R. Khan, A. Zulfiqar, A. Waseem, Z. H. Iqbal, Shah, CdS nanocapsules and nanospheres as efficient solar light-driven photocatalysts for degradation of Congo red dye, Inorg. Chem. Commun. 72 (2016) 33–41, https://doi.org/10.1016/J.INOCHE.2016.08.001.
[40] J.C. González-Juárez, J. Jiménez-Becerril, Gamma radiation-induced catalytic degradation of 4-chlorophenol using SiO2, TiO2, and Al2O3, Radiat. Phys. Chem. 75 (2006) 768–772, https://doi.org/10.1016/J.RADPHYSCHEM.2005.12.032.
[41] D. Liu, J. Robertson, Oxygen vacancy levels and interfaces of Al2O3, Micro Eng. 86 (2009) 1668–1671, https://doi.org/10.1016/J.MEE.2009.03.011.
[42] K. Lee, T.H. Kim, T.H. Kim, J. Lee, S. Yu, Enhancement of TOC removal efficiency of sulfamethoxazole using catalysts in the radiation treatment: Effects of band structure and electrical properties of radiocatalysts, Sep Purif. Technol. 312 (2023) 123390, https://doi.org/10.1016/J.SEPPUR.2023.123390.
[43] P. Xia, X. Pan, S. Jiang, J. Yu, B. He, P.M. Ismail, W. Bai, J. Yang, L. Yang, H. Zhang, M. Cheng, H. Li, Q. Zhang, C. Xiao, Y. Xie, Designing a redox heterojunction for photocatalytic “overall nitrogen fixation” under mild conditions, Adv. Mater. 34 (2022) 2200563, https://doi.org/10.1002/adma.202200563.
[44] A. Gnanaprakasam, V.M. Sivakumar, P.L. Sivayogavalli, M. Thirumarimurugan, Characterization of TiO2 and ZnO nanoparticles and their applications in photocatalytic degradation of azodyes, Ecotoxicol. Environ. Saf. 121 (2015) 121–125, https://doi.org/10.1016/J.ECOENV.2015.04.043.
[45] M.A. Barakat, H. Schaeffer, G. Hayes, S. Ismat-Shah, Photocatalytic degradation of 2-chlorophenol by Co-doped TiO2 nanoparticles, Appl. Catal. B 57 (2005) 23–30, https://doi.org/10.1016/J.APCATB.2004.10.001.
[46] M. Hepel, S. Hazelton, Photoelectrocatalytic degradation of diazo dyes on nanostructured WO3 electrodes, Electro Acta 50 (2005) 5278–5291, https://doi.org/10.1016/J.ELECTACTA.2005.03.067.
[47] M.A. Ahmed, S.A. Mahmoud, A.A. Mohamed, Unveiling the photocatalytic potential of graphitic carbon nitride (g-C3N4): a state-of-the-art review, RSC Adv. 14 (2024) 25629–25662, https://doi.org/10.1039/d4ra04234d.
[48] L. Li, D. Ma, Q. Xu, S. Huang, Constructing hierarchical ZnIn2S4/g-C3N4 S-scheme heterojunction for boosted CO2 photoreduction performance, Chem. Eng. J. 437 (2022) 135153, https://doi.org/10.1016/J.CEJ.2022.135153.
[49] R. Acosta-Herazo, M.Á. Mueses, G.L. Puma, F. Machuca-Martínez, Impact of photocatalyst optical properties on the efficiency of solar photocatalytic reactors rationalized by the concepts of initial rate of photon absorption (IRPA) dimensionless boundary layer of photon absorption and apparent optical thickness, Chem. Eng. J. 356 (2019) 839–849, https://doi.org/10.1016/J.CEJ.2018.09.085.
[50] A. Turolla, D. Santoro, J.R. de Bruyn, F. Crapulli, M. Antonelli, Nanoparticle scattering characterization and mechanistic modelling of UV–TiO2 photocatalytic reactors using computational fluid dynamics, Water Res 88 (2016) 117–126, https://doi.org/10.1016/J.WATRES.2015.09.039.
[51] J. Carbajo, A. Tolosana-Moranchel, J.A. Casas, M. Faraldos, A. Bahamonde, Analysis of photoefficiency in TiO2 aqueous suspensions: Effect of titania hydrodynamic particle size and catalyst loading on their optical properties, Appl. Catal. B 221 (2018) 1–8, https://doi.org/10.1016/J.APCATB.2017.08.032.
[52] A. Tolosana-Moranchel, J.A. Casas, J. Carbajo, M. Faraldos, A. Bahamonde, Influence of TiO2 optical parameters in a slurry photocatalytic reactor: Kinetic modelling, Appl. Catal. B 200 (2017) 164–173, https://doi.org/10.1016/J.APCATB.2016.06.063.
[53] T. Matiazzo, V.J.P. Vilar, N. Padoin, C. Soares, CFD and radiation field modeling of the NETmix milli-photocatalytic reactor: Evaluation of illumination systems composed of LEDs with distinct view angles, Chem. Eng. Sci. 285 (2024) 119576, https://doi.org/10.1016/J.CES.2023.119576.
[54] J.L. Coutts, L.H. Levine, J.T. Richards, D.W. Mazyck, The effect of photon source on heterogeneous photocatalytic oxidation of ethanol by a silica–titania composite, J. Photochem. Photobio. A Chem. 225 (2011) 58–64, https://doi.org/10.1016/J.JPHOTOCHEM.2011.09.026.
[55] A. Duta, L. Andronic, A. Enesca, The influence of low irradiance and electrolytes on the mineralization efficiency of organic pollutants using the Vis-active photocatalytic tandem CuInS2/TiO2/SnO2, Catal. Today 300 (2018) 18–27, https://doi.org/10.1016/J.CATTOD.2017.03.018.
[56] A. Enesca, L. Isac, The influence of light irradiation on the photocatalytic degradation of organic pollutants, Materials 13 (11) (2020) 2494, https://doi.org/10.3390/ma13112494.
[57] Z. Abbasi, E.I. García-López, G. Marcì, A. Farrokhnia, M.Z. Shoushtari, Photocatalytic degradation of 4-Nitrophenol by g-C3N4-MCy: Mechanism study and kinetic modeling, J. Photochem. Photobio. A Chem. 407 (2021) 113004, https://doi.org/10.1016/J.JPHOTOCHEM.2020.113004.
[58] Y. Pihosh, I. Turkevych, K. Mawatari, J. Uemura, Y. Kazoe, S. Kosar, K. Makita, T. Sugaya, T. Matsui, D. Fujita, M. Tosa, M. Kondo, T. Kitamori, Photocatalytic generation of hydrogen by core-shell WO3/BiVO4 nanorods with ultimate water splitting efficiency, Sci. Rep. 5 (2015) 11141, https://doi.org/10.1038/srep11141.
[59] W.-K. Chong, B.-J. Ng, Y.J. Lee, L.-L. Tan, L.K. Putri, J. Low, A.R. Mohamed, S.-P. Chai, Self-activated superhydrophilic green ZnIn2S4 realizing solar-driven overall water splitting: close-to-unity stability for a full daytime, Nat. Commun. 14 (2023) 7676, https://doi.org/10.1038/s41467-023-43331-x.
[60] N.A.M. Barakat, M.A. Kanjwal, I.S. Chronakis, H.Y. Kim, Influence of temperature on the photodegradation process using Ag-doped TiO2 nanostructures: Negative

impact with the nanofibers, J. Mol. Catal. A Chem. 366 (2013) 333–340, https://doi.org/10.1016/J.MOLCATA.2012.10.012.
[61] G. Kim, H.J. Choi, H.Il Kim, J. Kim, D. Monllor-Satoca, M. Kim, H. Park, Temperature-boosted photocatalytic H2 production and charge transfer kinetics on TiO2 under UV and visible light, Photochem. Photobiol. Sci. 15 (2016) 1247–1253, https://doi.org/10.1039/c6pp00263c.
[62] M. Ahmadlouydarab, S. Javadi, F.A.A. Darab, Evaluation of Thermal Stability of TiO2 Applied on the Surface of a Ceramic Tile to Eliminate Methylene Blue Using Silica-based Doping Materials, Adv. J. Chem. Sect. A 6 (2023) 352–365, https://doi.org/10.22034/ajca.2023.405496.1379.
[63] L. Velardi, L. Scrimieri, A. Serra, D. Manno, L. Calcagnile, Effect of temperature on the physical, optical and photocatalytic properties of TiO2 nanoparticles, SN Appl. Sci. 2 (2020) 707, https://doi.org/10.1007/s42452-020-2544-3.
[64] K. Nakano, E. Obuchi, M. Nanri, Thermo-photocatalytic decomposition of acetaldehyde over Pt-TiO2/SiO2, Chem. Eng. Res. Des. 82 (2004) 297–301, https://doi.org/10.1205/026387604772992909.
[65] Y.W. Chen, Y.H. Hsu, Effects of reaction temperature on the photocatalytic activity of TiO2 with Pd and Cu cocatalysts, Catalysts 11 (8) (2021) 966, https://doi.org/10.3390/catal11080966.
[66] S. Berhanu, H. Gebremariam, S. Chufamo, The g-C3N4@CdO/ZnO ternary composite: photocatalysis, thermodynamics and acute toxicity studies, Heliyon 8 (2022) e11612, https://doi.org/10.1016/J.HELIYON.2022.E11612.
[67] M.H. Razeghi, O. Gholipour, J.J. Sardroodi, S. Keshipour, A. Hassanzadeh, Magnetic cobalt metal organic framework for photocatalytic water splitting hydrogen evolution, Discov. Nano 19 (2024) 82, https://doi.org/10.1186/s11671-024-04019-3.
[68] R. Che, Y. Zhu, B. Tu, J. Miao, Z. Dong, M. Liu, Y. Wang, J. Li, S. Chen, F. Wang, A meta-analysis of influencing factors on the activity of BiVO4-based photocatalysts, Nanomaterials 13 (6) (2023) 2352, https://doi.org/10.3390/nano13162352.
[69] D. Zhang, D. Zhang, F. Zhao, Y. Zhao, H. Li, J. Liu, X.-Y. Ji, X. Pu, H. Zhang, Synergistic enhancement of photocatalytic hydrogen evolution in ZnIn2S4/CuWO4via an S-scheme heterojunction and the photothermal effect, J. Mater. Chem. A Mater. 12 (2024) 33546–33558, https://doi.org/10.1039/D4TA06654E.
[70] F. Abedini, R. Omidyan, M. Salehi, Theoretical insights on nonradiative deactivation mechanisms of protonated xanthine, J. Photochem. Photobio. A Chem. 385 (2019) 112067, https://doi.org/10.1016/J.JPHOTOCHEM.2019.112067.
[71] M.J. Uddin, M.A. Islam, S.A. Haque, S. Hasan, M.S.A. Amin, M.M. Rahman, Preparation of nanostructured TiO2-based photocatalyst by controlling the calcining temperature and pH, Int Nano Lett. 2 (2012) 19, https://doi.org/10.1186/2228-5326-2-19.
[72] D. Rosa, G. Manetta, L. Di Palma, Experimental assessment of the pH effect and ions on the photocatalytic activity of iron-doped titanium dioxide supported on polystyrene pellets: Batch and continuous tests, Chem. Eng. Sci. 291 (2024) 119918, https://doi.org/10.1016/J.CES.2024.119918.
[73] M.F. Hanafi, N. Sapawe, Effect of pH on the photocatalytic degradation of remazol brilliant blue dye using zirconia catalyst, Mater. Today Proc. 31 (2020) 260–262, https://doi.org/10.1016/J.MATPR.2020.05.746.
[74] O. Ben Abdelhadi, M. El Kassaoui, H. Moatassim, A. Kotbi, M. Balli, O. Mounkachi, M. Jouiad, Unveiling the photocatalytic potential of BiAgOS solid solution for hydrogen evolution reaction, Nanomaterials 14 (23) (2024) 1869, https://doi.org/10.3390/nano14231869.
[75] X. Zou, Y. Zhang, Noble metal-free hydrogen evolution catalysts for water splitting, Chem. Soc. Rev. 44 (2015) 5148–5180, https://doi.org/10.1039/c4cs00448e.
[76] B. Arabacı, R. Bakır, C. Orak, A. Yüksel, Predictive Modeling of Photocatalytic Hydrogen Production: Integrating Experimental Insights with Machine Learning on Fe/g-C3N4 Catalysts, Ind. Eng. Chem. Res 64 (2025) 5184–5199, https://doi.org/10.1021/acs.iecr.4c03919.
[77] L. Lu, M. Sun, T. Wu, Q. Lu, B. Chen, C.H. Chan, H.H. Wong, B. Huang, Transition metal anchored on red phosphorus to enable efficient photocatalytic H2 generation, Front Chem. 11 (2023) 1197010, https://doi.org/10.3389/fchem.2023.1197010.
[78] S. Ragab, M.R. Elkatory, M.A. Hassaan, A. El Nemr, Experimental, predictive and RSM studies of H2 production using Ag-La-CaTiO3 for water-splitting under visible light, Sci. Rep. 14 (2024) 1019, https://doi.org/10.1038/s41598-024-51219-z.
[79] Z. Liu, T. Yi, C. Huang, K.L. Choy, C. Liu, Thermodynamic and kinetics of hydrogen photoproduction enhancement by concentrated sunlight with CO2 photoreduction by heterojunction photocatalysts, Energy AI 6 (2021) 100102, https://doi.org/10.1016/J.EGYAI.2021.100102.
[80] S. Yoshino, A. Iwase, Y. Yamaguchi, T.M. Suzuki, T. Morikawa, A. Kudo, Photocatalytic CO2Reduction Using Water as an Electron Donor under Visible Light Irradiation by Z-Scheme and Photoelectrochemical Systems over (CuGa)0.5ZnS2in the Presence of Basic Additives, J. Am. Chem. Soc. 144 (2022) 2323–2332, https://doi.org/10.1021/jacs.1c12636.
[81] Y. Kamakura, C. Suppaso, I. Yamamoto, R. Mizuochi, Y. Asai, T. Motohashi, D. Tanaka, K. Maeda, Tin(II)-Based Metal–Organic Frameworks Enabling Efficient, Selective Reduction of CO2 to Formate under Visible Light, Angew. Chem. Int. Ed. 62 (2023) e202305923, https://doi.org/10.1002/anie.202305923.
[82] A. Haghighatmamaghani, F. Haghighat, C.S. Lee, Performance of various commercial TiO2 in photocatalytic degradation of a mixture of indoor air pollutants: effect of photocatalyst and operating parameters, Sci. Technol. Built Environ. 25 (2019) 600–614, https://doi.org/10.1080/23744731.2018.1556051.
[83] C. Hägglund, B. Kasemo, L. Österlund, In situ reactivity and FTIR study of the wet and dry photooxidation of propane on anatase TiO2, J. Phys. Chem. B 109 (2005) 10886–10895, https://doi.org/10.1021/jp0442448.
[84] C.S. Jwo, C.C. Chen, H. Chang, T.P. Teng, S.L. Chen, S.C. Huang, Simulating catalyst filter airflow and formaldehyde photocatalysis in the duct, HVAC R. Res. 16 (2010) 497–512, https://doi.org/10.1080/10789669.2010.10390917.
[85] S. Lu, X. Yao, Y. Cheng, L. Zhao, Recent developments and challenges for volatile organic compounds control by the synergistic of adsorption and photocatalysis, Appl. Catal. O Open 193 (2024) 206975, https://doi.org/10.1016/J.APCATO.2024.206975.
[86] Z. Wang, Z. Huang, J. Yu, X. Shao, W. Peng, J. Yu, Y. Jiang, Growth of Ag/g-C3N4 nanocomposites on nickel foam to enhance photocatalytic degradation of formaldehyde under visible light, J. Environ. Sci. 137 (2024) 432–442, https://doi.org/10.1016/J.JES.2023.02.003.
[87] Z. Man, Y. Meng, X. Lin, X. Dai, L. Wang, D. Liu, Assembling UiO-66@TiO2 nanocomposites for efficient photocatalytic degradation of dimethyl sulfide, Chem. Eng. J. 431 (2022) 133952, https://doi.org/10.1016/j.cej.2021.133952.
[88] G.S. Kamble, T.S. Natarajan, S.S. Patil, M. Thomas, R.K. Chougale, P.D. Sanadi, U. S. Siddharth, Y.C. Ling, BiVO4 As a sustainable and emerging photocatalyst: synthesis methodologies, engineering properties, and its volatile organic compounds degradation efficiency, Nanomaterials 13 (9) (2023) 1528, https://doi.org/10.3390/nano13091528.
[89] Y. Zhang, Y. Huang, B. Lin, Z. Chen, X. Xu, M. Pan, Ti3C2TX MXene supported ZnO nanocomposites with highly efficient photocatalytic performance for degradation of VOCs, Diam. Relat. Mater. 133 (2023) 109763, https://doi.org/10.1016/J.DIAMOND.2023.109763.
[90] T. Lv, J. Li, N. Arif, L. Qi, J. Lu, Z. Ye, Y.J. Zeng, Polarization and external-field enhanced photocatalysis, Matter 5 (2022) 2685–2721, https://doi.org/10.1016/j.matt.2022.06.004.
[91] Y. Li, J. Li, W. Yang, X. Wang, Implementation of ferroelectric materials in photocatalytic and photoelectrochemical water splitting, Nanoscale Horiz. 5 (2020) 1174–1187, https://doi.org/10.1039/d0nh00219d.
[92] Y. Liu, S. Ye, H. Xie, J. Zhu, Q. Shi, N. Ta, R. Chen, Y. Gao, H. An, W. Nie, H. Jing, F. Fan, C. Li, Internal-field-enhanced charge separation in a single-domain ferroelectric PbTiO3 photocatalyst, Adv. Mater. 32 (2020) 1906513, https://doi.org/10.1002/adma.201906513.
[93] Y. Nassereddine, M. Benyoussef, B. Asbani, M. El Marssi, M. Jouiad, Recent advances toward enhanced photocatalytic proprieties of BiFeO3-based materials, Nanomaterials 14 (1) (2024) 51, https://doi.org/10.3390/nano14010051.
[94] N.V. Burbure, P.A. Salvador, G.S. Rohrer, Photochemical reactivity of titania films on BaTiO3 substrates: Origin of spatial selectivity, Chem. Mater. 22 (2010) 5823–5830, https://doi.org/10.1021/cm1018025.
[95] Y. Liu, M. Zhang, Z. Wang, J. He, J. Zhang, S. Ye, X. Wang, D. Li, H. Yin, Q. Zhu, H. Jing, Y. Weng, F. Pan, R. Chen, C. Li, F. Fan, Bipolar charge collecting structure enables overall water splitting on ferroelectric photocatalysts, Nat. Commun. 13 (2022) 4245, https://doi.org/10.1038/s41467-022-32002-y.
[96] H. Li, X. Quan, S. Chen, H. Yu, Ferroelectric-enhanced Z-schematic electron transfer in BiVO4-BiFeO3-CuInS2 for efficient photocatalytic pollutant degradation, Appl. Catal. B 209 (2017) 591–599, https://doi.org/10.1016/J.APCATB.2017.03.043.
[97] J. Zhang, Y. Liu, T. Dittrich, Z. Wang, P. Ji, M. Li, N. Ta, H. Zhang, C. Zhen, Y. Xu, D. Li, Z. Feng, Z. Li, Y. Luo, J. Cui, D. Su, Y. Weng, G. Liu, X. Wang, F. Fan, C. Li, Unveiling charge utilization mechanisms in ferroelectric for water splitting, Nat. Commun. 16 (2025) 1515, https://doi.org/10.1038/s41467-025-56359-y.
[98] Y. Zhong, Ferroelectric polarization reversals in C2N/α-In2Se3 van der Waals heterostructures: a conversion from the traditional type-II to S-scheme, Front Chem. 11 (2023) 1278370, https://doi.org/10.3389/fchem.2023.1278370.
[99] Z.Da He, Y.Y. Tan, X.W. Lu, H.K. Xu, X.F. Xu, Y.Da Che, X.D. Yang, G.X. Lai, X. Y. Chen, Exploring the ferroelectric photocatalytic potential of R3c-structured InVO3: a computational study, Mater. Today Commun. 39 (2024) 109368, https://doi.org/10.1016/J.MTCOMM.2024.109368.
[100] M. Gunawan, S. Zhou, D. Gunawan, Q. Zhang, J.N. Hart, R. Amal, J. Scott, N. Valanoor, C.Y. Toe, Ferroelectric materials as photoelectrocatalysts: photoelectrode design rationale and strategies, J. Mater. Chem. A Mater. 13 (2024) 1612–1640, https://doi.org/10.1039/d4ta07812h.
[101] N.X.D. Mai, D. Park, J. Yoon, J. Hur, Comparative study of hydrogel-based recyclable photocatalysts, J. Nanosci. Nanotechnol. 18 (2017) 1361–1364, https://doi.org/10.1166/jnn.2018.14929.
[102] B.C. Nguyen, T.M. Truong, N.T. Nguyen, D.N. Dinh, D. Hollmann, M.N. Nguyen, Advanced cellulose-based hydrogel TiO2 catalyst composites for efficient photocatalytic degradation of organic dye methylene blue, Sci. Rep. 14 (2024) 10935, https://doi.org/10.1038/s41598-024-61724-w.
[103] K. Milošević, D. Lončarević, M. Kalagasidis Krušić, M. Hadnađev-Kostić, J. Dostanić, Eco-Friendly g-C3N4/carboxymethyl cellulose/alginate composite hydrogels for simultaneous photocatalytic degradation of organic dye pollutants, Int J. Mol. Sci. 25 (14) (2024) 7896, https://doi.org/10.3390/ijms25147896.
[104] G. Fan, X. Li, J. Lin, X. Wu, L. Zhang, J. Wu, Y. Wang, Efficient photocatalytic inactivation of Microcystis aeruginosa via self-floating Ag3VO4/BiVO4 hydrogel under visible light, Sep Purif. Technol. 299 (2022) 121803, https://doi.org/10.1016/J.SEPPUR.2022.121803.
[105] R. Wang, Z. Wu, X. Chen, B. Cheng, W. Ou, Water purification using a BiVO4/graphene oxide multifunctional hydrogel based on interfacial adsorption-enrichment and photocatalytic antibacterial activity, Ceram. Int 49 (2023) 9657–9671, https://doi.org/10.1016/J.CERAMINT.2022.11.137.
[106] C. Ma, Z. Xie, W.C. Seo, S.T. Ud Din, J. Lee, Y. Kim, H. Jung, W. Yang, Carbon dot-coupled BiVO4/reduced graphene hydrogel for significant enhancement of

photocatalytic activity: Antibiotic degradation and CO2 reduction, Appl. Surf. Sci. 565 (2021) 150564, https://doi.org/10.1016/J.APSUSC.2021.150564.
[107] J. Low, J. Yu, M. Jaroniec, S. Wageh, A.A. Al-Ghamdi, Heterojunction photocatalysts, Adv. Mater. 29 (2017) 1601694, https://doi.org/10.1002/adma.201601694.
[108] M. Lin, H. Chen, Z. Zhang, X. Wang, Engineering interface structures for heterojunction photocatalysts, Phys. Chem. Chem. Phys. 25 (2023) 4388–4407, https://doi.org/10.1039/d2cp05281d.
[109] W. Guo, H. Liu, Preparation of ZnO/Ag heterostructure material by one-pot method for enhanced photocatalytic performance, Chem. Res Chin. Univ. 33 (2017) 129–134, https://doi.org/10.1007/s40242-017-6098-x.
[110] S. Zhang, Z. He, X. Li, J. Zhang, Q. Zang, S. Wang, Building heterogeneous nanostructures for photocatalytic ammonia decomposition, Nanoscale Adv. 2 (2020) 3610–3623, https://doi.org/10.1039/d0na00161a.
[111] Z. Xiong, Q. Liu, Z. Gao, J. Yang, X. Zhang, Q. Yang, C. Hao, Heterogeneous Interface Design to Enhance the Photocatalytic Performance, Inorg. Chem. 60 (2021) 5063–5070, https://doi.org/10.1021/acs.inorgchem.1c00093.
[112] Y. Shen, Y. Liu, X. Xi, Z. Nie, Immobilized WO3/W18O49 trunk-branch nanostructure: a homojunction improved adsorption and photocatalytic performance, Opt. Mater. 138 (2023) 113681, https://doi.org/10.1016/J.OPTMAT.2023.113681.
[113] X. Wang, R. Xia, E. Muhire, S. Jiang, X. Huo, M. Gao, Highly enhanced photocatalytic performance of TiO2 nanosheets through constructing TiO2/TiO2 quantum dots homojunction, Appl. Surf. Sci. 459 (2018) 9–15, https://doi.org/10.1016/J.APSUSC.2018.06.293.
[114] T. Li, W. Zhou, Y. Lin, F. Yang, F. Deng, X. Tu, Step-scheme heterojunction photocatalyst: preparation, application and future outlook, Curr. Opin. Chem. Eng. 45 (2024) 101042, https://doi.org/10.1016/J.COCHE.2024.101042.
[115] Z. Jiang, Y. Zheng, L. Zhang, L. Xu, Q. Feng, C. Luo, W. Tan, J. Wang, Construction of a novel NH2-MIL-101(Fe)/Zn0.5Cd0.5S heterojunction photocatalyst with improved hydrogen production, Int J. Hydrog. Energy 82 (2024) 703–712, https://doi.org/10.1016/J.IJHYDENE.2024.07.460.
[116] B. Yu, Y. Wu, F. Meng, Q. Wang, X. Jia, M. Wasim Khan, C. Huang, S. Zhang, L. Yang, H. Wu, Formation of hierarchical Bi2MoO6/In2S3 S-scheme heterojunction with rich oxygen vacancies for boosting photocatalytic CO2 reduction, Chem. Eng. J. 429 (2022) 132456, https://doi.org/10.1016/J.CEJ.2021.132456.
[117] K. Lai, Y. Sun, N. Li, Y. Gao, H. Li, L. Ge, T. Ma, Photocatalytic CO2-to-CH4 conversion with ultrahigh selectivity of 95.93% on S-Vacancy Modulated Spatial In2S3/In2O3 Heterojunction, Adv. Funct. Mater. 34 (2024) 2409031, https://doi.org/10.1002/adfm.202409031.
[118] T. Shi, X. Wang, X. Yu, G. Li, L. Wang, S. Li, J. Huang, A. Meng, Z. Li, Rational construction of carbon nitride homojunction photocatalyst for enhanced hydrogen evolution from water splitting, Energy Convers. Manag 300 (2024) 117941, https://doi.org/10.1016/J.ENCONMAN.2023.117941.
[119] H. Wang, M. Li, Z. You, Y. Chen, Y. Liu, An innovative Zn3In2S6/ZnIn2S4 homojunction photocatalyst with enhanced interfacial charge transfer for the highly efficient degradation of tetracycline under visible radiation, J. Environ. Manag. 365 (2024) 121605, https://doi.org/10.1016/J.JENVMAN.2024.121605.
[120] C. Chang, L. Kan, W. Mu, Q. Wang, S.Y. Lu, Tetragonal/orthorhombic-bismuth tungstate homojunction formed through in situ bismuth induced phase transformation as highly efficient photocatalyst for pollutant degradation, J. Colloid Interface Sci. 607 (2022) 269–280, https://doi.org/10.1016/J.JCIS.2021.08.167.
[121] A. Balakrishnan, K. Vijaya Suryaa, M. Chinthala, A. Kumar, Mechanistic insights of PO43− functionalized carbon nitride homojunction hydrogels in photocatalytic-self-Fenton-peroxymonosulfate system for tetracycline degradation, J. Colloid Interface Sci. 669 (2024) 366–382, https://doi.org/10.1016/J.JCIS.2024.04.177.
[122] H. Sudrajat, M. Nobatova, Heterojunction photocatalysts: where are they headed? (Advance Article), RSC Appl. Interfaces (2025), https://doi.org/10.1039/d5lf00037h.
[123] Y. Guo, P. Wang, J. Qian, J. Hou, Y. Ao, C. Wang, Construction of a composite photocatalyst with significantly enhanced photocatalytic performance through combination of homo-junction with hetero-junction, Catal. Sci. Technol. 8 (2018) 486–498, https://doi.org/10.1039/c7cy02027a.
[124] C. Sun, Y. Zhao, Y. Ding, F. Zhang, Z. Deng, K. Lian, Z. Wang, J. Cui, W. Bi, Efficient homojunction/heterojunction photocatalyst via integrating $CsPbBr_3$ Quantum Dot Homojunction with TiO_2 for degradation of organic dyes, ACS Appl. Mater. Interfaces 16 (2024) 24806–24815, https://doi.org/10.1021/acsami.4c04063.
[125] F. Zhan, G. Wen, R. Li, C. Feng, Y. Liu, Y. Liu, M. Zhu, Y. Zheng, Y. Zhao, P. La, A comprehensive review of oxygen vacancy modified photocatalysts: synthesis, characterization, and applications, Phys. Chem. Chem. Phys. 26 (2024) 11182–11207, https://doi.org/10.1039/d3cp06126d.
[126] X. Pan, M.Q. Yang, X. Fu, N. Zhang, Y.J. Xu, Defective TiO2 with oxygen vacancies: synthesis, properties and photocatalytic applications, Nanoscale 5 (2013) 3601–3614, https://doi.org/10.1039/c3nr00476g.
[127] M. Chen, Y. Mao, H. Zhang, M. Ren, D. Wu, X. Zhao, W. Tu, The synergistic promotion effect of in-situ formed metal cationic vacancies and interstitial metals on photocatalytic performance of WO3 in CO2 reduction, ChemCatChem 15 (2023) e202300024, https://doi.org/10.1002/cctc.202300024.
[128] L. Hao, H. Huang, Y. Zhang, T. Ma, Oxygen vacant semiconductor photocatalysts, Adv. Funct. Mater. 31 (2021) 2100919, https://doi.org/10.1002/adfm.202100919.
[129] Y. Feng, Z. Zhang, K. Zhao, S. Lin, H. Li, X. Gao, Photocatalytic nitrogen fixation: Oxygen vacancy modified novel micro-nanosheet structure Bi2O2CO3 with band gap engineering, J. Colloid Interface Sci. 583 (2021) 499–509, https://doi.org/10.1016/J.JCIS.2020.09.089.
[130] Y. Yang, W. Guo, Y. Zhai, Q. Jin, H. Zhao, R. Zhang, Y. Liu, Oxygen-doped and nitrogen vacancy co-modified carbon nitride for the efficient visible light photocatalytic hydrogen evolution, N. J. Chem. 44 (2020) 16320–16328, https://doi.org/10.1039/d0nj03695a.
[131] A. Ranjbari, J. Kim, J. Yu, J. Kim, M. Park, N. Kim, K. Demeestere, P. M. Heynderickx, Effect of oxygen vacancy modification of ZnO on photocatalytic degradation of methyl orange: a kinetic study, Catal. Today 427 (2024) 114413, https://doi.org/10.1016/J.CATTOD.2023.114413.
[132] A. Ranjbari, K. Demeestere, K.H. Kim, P.M. Heynderickx, Oxygen vacancy modification of commercial ZnO by hydrogen reduction for the removal of thiabendazole: characterization and kinetic study, Appl. Catal. B 324 (2023) 122265, https://doi.org/10.1016/J.APCATB.2022.122265.
[133] X. Li, Z. Wang, A. Sasani, A. Baktash, K. Wang, H. Lu, J. You, P. Chen, P. Chen, Y. Bao, S. Zhang, G. Liu, L. Wang, Oxygen vacancy induced defect dipoles in BiVO4 for photoelectrocatalytic partial oxidation of methane, Nat. Commun. 15 (2024) 9127, https://doi.org/10.1038/s41467-024-53426-8.
[134] X.J. Wang, Y. Zhao, F.T. Li, L.J. Dou, Y.P. Li, J. Zhao, Y.J. Hao, A chelation strategy for in-situ constructing surface oxygen vacancy on {001} facets exposed BiOBr nanosheets, Sci. Rep. 6 (2016) 24918, https://doi.org/10.1038/srep24918.
[135] Y. Yu, F. Chen, X. Jin, J. Min, H. Duan, J. Li, Z. Wu, B. Cao, Oxygen vacancies-Rich S-cheme BiOBr/CdS heterojunction with synergetic effect for highly efficient light emitting diode-driven pollutants degradation, Nanomaterials 13 (5) (2023) 830, https://doi.org/10.3390/nano13050830.
[136] S. Corby, L. Francàs, A. Kafizas, J.R. Durrant, Determining the role of oxygen vacancies in the photoelectrocatalytic performance of WO3 for water oxidation, Chem. Sci. 11 (2020) 2907–2914, https://doi.org/10.1039/c9sc06325k.
[137] H. Yu, W. Liu, X. Wang, F. Wang, Promoting the interfacial H2-evolution reaction of metallic Ag by Ag2S cocatalyst: A case study of TiO2/Ag-Ag2S photocatalyst, Appl. Catal. B 225 (2018) 415–423, https://doi.org/10.1016/J.APCATB.2017.12.026.
[138] L. Hou, Z. Wu, C. Jin, W. Li, Q. Wei, Y. Chen, T. Wang, Flower-like dual-defective z-scheme heterojunction g-c3n4/znin2s4 high-efficiency photocatalytic hydrogen evolution and degradation of mixed pollutants, Nanomaterials 11 (10) (2021) 2483, https://doi.org/10.3390/nano11102483.
[139] Y. Sun, K. Lai, X. Shi, N. Li, Y. Gao, L. Ge, Regulating metal cation Cu vacancies on ZnIn2S4/Cu1.81S to achieve high selectivity for the photocatalytic reduction of CO2 to CH4, Appl. Catal. B Environ. Energy 365 (2025) 124907, https://doi.org/10.1016/J.APCATB.2024.124907.
[140] W. Ding, X. Li, S. Su, Z. Liu, Y. Cao, L. Meng, S. Yuan, W. Wei, M. Luo, Cationic vacancy engineering of p-TiO2 for enhanced photocatalytic nitrogen fixation, Nanoscale 15 (2023) 4014–4021, https://doi.org/10.1039/d2nr06821d.
[141] J. Wang, K. Liu, W. Liao, Y. Kang, H. Xiao, Y. Chen, Q. Wang, T. Luo, J. Chen, H. Li, T.S. Chan, S. Chen, E. Pensa, L. Chai, F. Liu, L. Jiang, C. Liu, J. Fu, E. Cortés, M. Liu, Metal vacancies in semiconductor oxides enhance hole mobility for efficient photoelectrochemical water splitting, Nat. Catal. 8 (2025) 229–238, https://doi.org/10.1038/s41929-025-01300-1.
[142] W. Jiang, H. Loh, B.Q.L. Low, H. Zhu, J. Low, J.Z.X. Heng, K.Y. Tang, Z. Li, X. J. Loh, E. Ye, Y. Xiong, Role of oxygen vacancy in metal oxides for photocatalytic CO2 reduction, Appl. Catal. B 321 (2023) 122079, https://doi.org/10.1016/J.APCATB.2022.122079.
[143] Y. He, S. Dai, J. Sheng, Q. Ren, Y. Lv, Y. Sun, F. Dong, In situ fabrication of atomically adjacent dual-vacancy sites for nearly 100% selective CH4 production, Proc. Natl. Acad. Sci. USA 121 (2024), https://doi.org/10.1073/pnas.2322107121.
[144] X. Zhang, Y. Zhang, H. Li, Y. Wang, M. Xiang, W. Yu, H. Huang, H. Ou, Surface cationic and anionic dual vacancies enhancing photocatalytic activity of Bi2WO6, Appl. Surf. Sci. 602 (2022) 154311, https://doi.org/10.1016/J.APSUSC.2022.154311.
[145] J. Liu, D. Zhao, X. Wu, D. Wu, N. Su, Y. Wang, F. Chen, C. Fu, J. Wang, Q. Zhang, Synergistic dual-defect band engineering for highly efficient photocatalytic degradation of microplastics via Nb-induced oxygen vacancies in SnO2 quantum dots, J. Mater. Chem. A Mater. 13 (2025) 4429–4443, https://doi.org/10.1039/d4ta07579j.
[146] S. Hou, X. Gao, X. Lv, Y. Zhao, X. Yin, Y. Liu, J. Fang, X. Yu, X. Ma, T. Ma, D. Su, Decade milestone advancement of defect-engineered g-C3N4 for solar catalytic applications, Nanomicro Lett. 16 (2024) 70, https://doi.org/10.1007/s40820-023-01297-x.
[147] Y. Pang, P. Li, X. Ma, L. Sun, Y. Liu, D. Qu, L. An, Z. Sun, Metal-doped carbon nitride: an all-in-one photocatalyst, EES Catal. 1 (2023) 810–831, https://doi.org/10.1039/D3EY00123G.
[148] Y. Ahmadi, K.H. Kim, Modification strategies for visible-light photocatalysts and their performance-enhancing effects on photocatalytic degradation of volatile organic compounds, Renew. Sustain. Energy Rev. 189 (2024) 113948, https://doi.org/10.1016/J.RSER.2023.113948.
[149] N. Bashir, T. Sawaira, A. Jamil, M. Awais, A. Habib, A. Afzal, Challenges and prospects of main-group metal-doped TiO2 photocatalysts for sustainable water remediation, Mater. Today Sustain. 27 (2024) 100869, https://doi.org/10.1016/J.MTSUST.2024.100869.
[150] G. Fu, W. Zhen, H. Wang, X. Zhou, L. Yang, J. Zhang, Potassium and Boron Co-Doping of g-C3N4 Tuned CO2 Reduction Mechanism for Enhanced Photocatalytic Performance: A First-Principles Investigation, Molecules 29 (22) (2024) 5339, https://doi.org/10.3390/molecules29225339.

[151] W. Wang, L. Du, R. Xia, R. Liang, T. Zhou, H.K. Lee, Z. Yan, H. Luo, C. Shang, D. L. Phillips, Z. Guo, In situ protonated-phosphorus interstitial doping induces long-lived shallow charge trapping in porous C3−xN4 photocatalysts for highly efficient H2 generation, Energy Environ. Sci. 16 (2022) 460–472, https://doi.org/10.1039/d2ee02680e.
[152] J. Yang, R. Liu, S. Huang, Y. Shao, Y. Huang, Y. Yu, Enhanced photocatalytic activity and stability of interstitial Ga-doped CdS: Combination of experiment and calculation, Catal. Today 224 (2014) 104–113, https://doi.org/10.1016/j.cattod.2013.12.016.
[153] A.S. Foster, F. Lopez Gejo, A.L. Shluger, R.M. Nieminen, Vacancy and interstitial defects in hafnia, Phys. Rev. B Condens Matter Mater. Phys. 65 (2002) 1741171–17411713, https://doi.org/10.1103/PhysRevB.65.174117.
[154] A.L. Ivanovsky, V.I. Anisimov, D.L. Novikov, A.I. Lichtenstein, V.A. Gubanov, The influence of structural defects on the electronic properties of interstitial alloys—I. Lattice vacancies, J. Phys. Chem. Solids 49 (1988) 465–477, https://doi.org/10.1016/0022-3697(88)90057-1.
[155] X. Wang, J. Jiang, L. Yang, Q. An, Q. Xu, Y. Yang, H. Guo, Enhanced piezoelectric polarization by subtle structure distortion to trigger efficient photocatalytic CO2RR, Appl. Catal. B 340 (2024) 123177, https://doi.org/10.1016/J.APCATB.2023.123177.
[156] C. Wang, H. Liu, G. Wang, F. Ye, S. Tao, X. Li, P. Qiu, Z. Huang, Ni (II) doping induced lattice distortion in Zn3In2S6/BiOBr-OVs for boosting photocatalytic removal of antibiotics and Cr (VI) performance, Sep Purif. Technol. 324 (2023) 124457, https://doi.org/10.1016/J.SEPPUR.2023.124457.
[157] H. Fu, S. Li, Y. Lin, X. Wu, T. Lin, C. Zhao, M. Gao, C. Lin, Enhancement of piezo–photocatalytic activity in perovskite (Bi0·2Na0·2Ba0·2K0·2La0.2)TiO3 oxides via high entropy induced lattice distortion and energy band reconfiguration, Ceram. Int 50 (2024) 9159–9168, https://doi.org/10.1016/J.CERAMINT.2023.12.232.
[158] M. Nishikawa, S. Yuto, T. Nakajima, T. Tsuchiya, N. Saito, Effect of Lattice Distortion on Photocatalytic Performance of TiO2, Catal. Lett. 147 (2017) 292–300, https://doi.org/10.1007/s10562-016-1928-x.
[159] Y. Xu, S. Wu, P. Wan, J. Sun, Z.D. Hood, Introducing Ti3+ defects based on lattice distortion for enhanced visible light photoreactivity in TiO2 microspheres, RSC Adv. 7 (2017) 32461–32467, https://doi.org/10.1039/c7ra04885h.
[160] X. Chen, L. Liu, F. Huang, Black titanium dioxide (TiO2) nanomaterials, Chem. Soc. Rev. 44 (2015) 1861–1885, https://doi.org/10.1039/c4cs00330f.
[161] M. Liu, M. Bao, H. Cao, X. Yu, S.Q. Zhao, Rare earth induced lattice distortion of Bi2WO6 to effectively improve photocatalytic performance: Experimental and DFT calculations, Opt. Mater. (Amst.) 155 (2024) 115798, https://doi.org/10.1016/J.OPTMAT.2024.115798.
[162] S. Chaudhary, K.P.S. Parmar, R. Brajpuriya, B.S. Rawat, A. Vij, Lattice Distortion Creates Enhancements in Photocatalytic and Electrocapacitive Performance of Sol–Gel-Derived Cu-Doped NiTiO3, Energy Technol. 13 (2024) 2401138, https://doi.org/10.1002/ente.202401138.
[163] H. Shen, C. Ma, Z. Qi, J. Ding, D. Li, B. Ma, X. Zhang, G. Cao, Y. Lu, Exceptional visible-light photocatalytic activity induced by lattice distortion in medium-entropy perovskite oxide La0.5Sr0.5Fe0.5Ti0.5O3, J. Environ. Chem. Eng. 13 (2025) 115753, https://doi.org/10.1016/j.jece.2025.115753.
[164] B. Dai, Y. Zhou, X. Xiao, Y. Chen, J. Guo, C. Gao, Y. Xie, J. Chen, Fluid Field Modulation in Mass Transfer for Efficient Photocatalysis, Adv. Sci. 9 (2022) 2203057, https://doi.org/10.1002/advs.202203057.
[165] D. Uner, B. Ipek, On the Limits of Photocatalytic Water Splitting, in: M. Eyvaz, E. Yüksel (Eds.), Water Chemistry, IntechOpen, Rijeka, 2019, https://doi.org/10.5772/intechopen.89235.
[166] X. Zhan, C. Yan, Y. Zhang, G. Rinke, G. Rabsch, M. Klumpp, A.I. Schäfer, R. Dittmeyer, Investigation of the reaction kinetics of photocatalytic pollutant degradation under defined conditions with inkjet-printed TiO2films-from batch to a novel continuous-flow microreactor, React. Chem. Eng. 5 (2020) 1658–1670, https://doi.org/10.1039/d0re00238k.
[167] A. Chaudhuri, S.D.A. Zondag, J.H.A. Schuurmans, J. Van Der Schaaf, T. Noël, Scale-Up of a Heterogeneous Photocatalytic Degradation Using a Photochemical Rotor-Stator Spinning Disk Reactor, Org. Process Res Dev. 26 (2022) 1279–1288, https://doi.org/10.1021/acs.oprd.2c00012.
[168] A. Jaison, A. Mohan, Y.C. Lee, Recent Developments in Photocatalytic Nanotechnology for Purifying Air Polluted with Volatile Organic Compounds: Effect of Operating Parameters and Catalyst Deactivation, Catalysts 13 (2) (2023) 407, https://doi.org/10.3390/catal13020407.
[169] Y. Cao, D. Ji, J. Zhu, Q. Zhu, C. Wang, Z. Gao, Design of a novel fluidized bed photoreactor and equipment parameters optimization and application in removing aniline, Int. J. Environ. Sci. Technol. (2024), https://doi.org/10.1007/s13762-024-06178-3.
[170] P. Rychtowski, P. Miadlicki, B. Prowans, B. Tryba, High performance fluidized bed photoreactor for ethylene decomposition, Pol. J. Chem. Technol. 24 (2022) 50–56, https://doi.org/10.2478/pjct-2022-0014.
[171] M. Schreck, N. Kleger, F. Matter, J. Kwon, E. Tervoort, K. Masania, A.R. Studart, M. Niederberger, 3D printed scaffolds for monolithic aerogel photocatalysts with complex geometries, Small 17 (2021) 2104089, https://doi.org/10.1002/smll.202104089.
[172] Y. Ding, C. Wang, N. Han, M. Liu, R. Zheng, L.-H. Chen, J. Zhong, B.-L. Su, Two-dimensional hierarchically porous C $_3$ N $_4$ for photocatalysis: perspective and challenges, Chem. Synth. 4 (2024) 59, https://doi.org/10.20517/cs.2024.23.
[173] M. Sigl, M. Egger, F. Warchomicka, D. Knez, M. Dienstleder, H. Amenitsch, G. Trimmel, T. Rath, ZnIn2S4 thin films with hierarchical porosity for photocatalysis, J. Mater. Chem. A Mater. 12 (2024) 28965–28974, https://doi.org/10.1039/d4ta04237a.
[174] P. Haghighi, F. Haghighat, TiO2-based photocatalytic oxidation process for indoor air VOCs removal: A comprehensive review, Build. Environ. 249 (2024) 111108, https://doi.org/10.1016/J.BUILDENV.2023.111108.
[175] I.E. Khalil, P. Das, H. Küçükkeçeci, V. Dippold, J. Rabeah, W. Tahir, J. Roeser, J. Schmidt, A. Thomas, Hierarchical porous covalent organic frameworks: the influence of additional macropores on photocatalytic hydrogen evolution and hydrogen peroxide production, Chem. Mater. 36 (2024) 8330–8337, https://doi.org/10.1021/acs.chemmater.4c01298.
[176] Q. Zhang, R. Dong, Y. Wu, W. Gao, Z. He, B. Ren, Light-Driven Au-WO3@C janus micromotors for rapid photodegradation of dye pollutants, ACS Appl. Mater. Interfaces 9 (2017) 4674–4683, https://doi.org/10.1021/acsami.6b12081.
[177] T. Dong, M. Sun, K. Hu, Q. Wang, C. Lu, J. Kou, Self-propelled jet carbon micromotor enhanced photocatalytic performance for water splitting, Int J. Hydrog. Energy 46 (2021) 17187–17196, https://doi.org/10.1016/J.IJHYDENE.2021.02.153.
[178] P. Pandey, K.P. K, S. Mohanan, A. Surenjan, Photocatalytic Reactor Modelling Incorporating Computational Fluid Dynamics (CFD) for Water and Air purification: A Concise Review, Process Integr. Optim. Sustain. 9 (2025) 471–485, https://doi.org/10.1007/s41660-024-00479-3.
[179] S. Fallahizadeh, M. Gholami, M.R. Rahimi, H.R. Rajabi, S. Djalalinia, A. Esrafili, M. Farzadkia, M. Kermani, The spinning disc reactor for photocatalytic degradation: a systematic review, Heliyon 10 (2024) e32440, https://doi.org/10.1016/J.HELIYON.2024.E32440.
[180] T.C. Li, B. Panigraphi, W.T. Chen, C.Y. Chen, C.Y. Chen, Hydrodynamic benefits of artificial cilia distribution towards photodegradation processes, Sens Actuators A Phys. 313 (2020) 112184, https://doi.org/10.1016/j.sna.2020.112184.
[181] X. Li, Y. Chen, Y. Tao, L. Shen, Z. Xu, Z. Bian, H. Li, Challenges of photocatalysis and their coping strategies, Chem. Catal. 2 (2022) 1315–1345, https://doi.org/10.1016/J.CHECAT.2022.04.007.
[182] Z. Warren, J. Wenk, D. Mattia, Increased photocorrosion resistance of ZnO foams via transition metal doping, RSC Adv. 13 (2023) 2438–2450, https://doi.org/10.1039/d2ra06730g.
[183] L. Zhang, P. Li, L. Feng, X. Chen, J. Jiang, S. Zhang, A. Zhang, G. Chen, H. Wang, Controllable fabrication of visible-light-driven CoSx/CdS photocatalysts with direct Z-scheme heterojunctions for photocatalytic Cr(VI) reduction with high efficiency, Chem. Eng. J. 397 (2020) 125464, https://doi.org/10.1016/J.CEJ.2020.125464.
[184] T. Giannakis, S.K. Zervou, T.M. Triantis, C. Christophoridis, E. Bizani, S. V. Starinskiy, P. Koralli, G. Mousdis, A. Hiskia, M. Kandyla, Enhancing the photocatalytic activity of immobilized TiO2 using laser-micropatterned surfaces, Appl. Sci. 14 (7) (2024) 3033, https://doi.org/10.3390/app14073033.
[185] S. Sun, M. Li, Y. Xue, H. Yang, Immobilized photocatalysts with varied macroscopical supports of different morphologies: A review, J. Environ. Chem. Eng. 12 (2024) 113636, https://doi.org/10.1016/J.JECE.2024.113636.
[186] S. Hennessey, R. González-Gómez, K. McCarthy, C.S. Burke, C. Le Houérou, N. K. Sarangi, P. McArdle, T.E. Keyes, F. Cucinotta, P. Farràs, Enhanced photostability and photoactivity of ruthenium polypyridyl-based photocatalysts by covalently anchoring onto reduced graphene oxide, ACS Omega 9 (2024) 13872–13882, https://doi.org/10.1021/acsomega.3c08800.
[187] L.K. Tinoco Navarro, C. Jaroslav, Enhancing photocatalytic properties of TiO2 photocatalyst and heterojunctions: a comprehensive review of the impact of biphasic systems in aerogels and xerogels synthesis, methods, and mechanisms for environmental applications, Gels 9 (12) (2023) 976, https://doi.org/10.3390/gels9120976.
[188] V. Navakoteswara Rao, H. Kwon, Y. Lee, P. Ravi, C. Won Ahn, K. Kim, J.M. Yang, Synergistic integration of MXene nanosheets with CdS@TiO2 core@shell S-scheme photocatalyst for augmented hydrogen generation, Chem. Eng. J. 471 (2023) 144490, https://doi.org/10.1016/J.CEJ.2023.144490.
[189] J. Zhang, Y. Wang, J. Jin, J. Zhang, Z. Lin, F. Huang, J. Yu, Efficient visible-light photocatalytic hydrogen evolution and enhanced photostability of core/shell CdS/g-C3N4 nanowires, ACS Appl. Mater. Interfaces 5 (2013) 10317–10324, https://doi.org/10.1021/am403327g.
[190] B. Han, S. Liu, N. Zhang, Y.J. Xu, Z.R. Tang, One-dimensional CdS@MoS2 core-shell nanowires for boosted photocatalytic hydrogen evolution under visible light, Appl. Catal. B 202 (2017) 298–304, https://doi.org/10.1016/J.APCATB.2016.09.023.
[191] B. Xia, Y. Zhang, J. Ran, M. Jaroniec, S.-Z. Qiao, Single-atom photocatalysts for emerging reactions, ACS Cent. Sci. 7 (2021) 39–54, https://doi.org/10.1021/acscentsci.0c01466.
[192] W. Wang, Q. Song, Q. Luo, L. Li, X. Huo, S. Chen, J. Li, Y. Li, S. Shi, Y. Yuan, X. Du, K. Zhang, N. Wang, Photothermal-enabled single-atom catalysts for high-efficiency hydrogen peroxide photosynthesis from natural seawater, Nat. Commun. 14 (2023) 2493, https://doi.org/10.1038/s41467-023-38211-3.
[193] B. Yu, Y. Zhao, G. Li, R. Deng, R. Liu, L. Zhang, W. Wang, W. Liu, B. Qiao, Hydrophobic Zn single-atom catalyst for efficient photosynthesis of hydrogen peroxide, CCS Chem. (2024) 1–12, https://doi.org/10.31635/ccschem.024.202404694.
[194] E. Masternak, W. Baran, E. Adamek, Photocatalytic degradation of lincosamides in the presence of commercial pigments: kinetics, intermediates, and predicted ecotoxicity, Int J. Mol. Sci. 25 (24) (2024) 13370, https://doi.org/10.3390/ijms252413370.
[195] O. d'Hennezel, P. Pichat, D.F. Ollis, Benzene and toluene gas-phase photocatalytic degradation over H2O and HCL pretreated TiO2: by-products and mechanisms, J. Photochem. Photobio. A Chem. 118 (1998) 197–204, https://doi.org/10.1016/S1010-6030(98)00366-9.

[196] Q. Geng, H. Wang, R. Chen, L. Chen, K. Li, F. Dong, Advances and challenges of photocatalytic technology for air purification, Natl. Sci. Open 1 (2022) 20220025, https://doi.org/10.1360/nso/20220025.
[197] A.P. Chowdhury, K.S. Anantharaju, K. Keshavamurthy, S.L. Rokhum, Recent advances in efficient photocatalytic degradation approaches for azo dyes, J. Chem. 24 (2023) 9780955, https://doi.org/10.1155/2023/9780955.
[198] H. Zhou, H. Wang, C. Yue, L. He, H. Li, H. Zhang, S. Yang, T. Ma, Photocatalytic degradation by TiO2-conjugated/coordination polymer heterojunction: preparation, mechanisms, and prospects, Appl. Catal. B Environ. Energy 344 (2024) 123605, https://doi.org/10.1016/J.APCATB.2023.123605.
[199] Z. Rao, G. Lu, L. Chen, A. Mahmood, G. Shi, Z. Tang, X. Xie, J. Sun, Photocatalytic oxidation mechanism of Gas-Phase VOCs: unveiling the role of holes, •OH and •O2−, Chem. Eng. J. 430 (2022) 132766 https://doi.org/10.1016/J.CEJ.2021.132766.
[200] K. Lv, X. Guo, X. Wu, Q. Li, W. Ho, M. Li, H. Ye, D. Du, Photocatalytic selective oxidation of phenol to produce dihydroxybenzenes in a TiO2/UV system: hydroxyl radical versus hole, Appl. Catal. B 199 (2016) 405–411, https://doi.org/10.1016/J.APCATB.2016.06.049.
[201] H. Yu, M. Wang, J. Yan, H. Dang, H. Zhu, Y. Liu, M. Wen, G. Li, L. Wu, Complete mineralization of phenolic compounds in visible-light-driven photocatalytic ozonation with single-crystal WO3 nanosheets: Performance and mechanism investigation, J. Hazard Mater. 433 (2022) 128811, https://doi.org/10.1016/J.JHAZMAT.2022.128811.
[202] S. Zhao, C. Jia, X. Shen, R. Li, L. Oldham, B. Moss, B. Tam, S.D. Pike, N. Harrison, E.A. Ahmad, A. Kafizas, The aerosol-assisted chemical vapour deposition of Mo-doped BiVO 4 photoanodes for solar water splitting: an experimental and computational study, J. Mater. Chem. A Mater. 12 (2024) 26645–26666, https://doi.org/10.1039/d4ta02605e.
[203] V. Van Pham, T.Q. Nguyen, H.V. Le, T.M. Cao, Visible light photocatalytic NOx removal with suppressed poisonous NO2 byproduct generation over simply synthesized triangular silver nanoparticles coupled with tin dioxide, Nanoscale Adv. 6 (2024) 2380–2389, https://doi.org/10.1039/d4na00035h.
[204] Y. Chen, Y. Huang, H. Tian, L. Ye, R. Li, C. Chen, Z. Dai, D. Huang, Fluorine-doped BiVO4 photocatalyst: Preferential cleavage of C−N bond for green degradation of glyphosate, J. Environ. Sci. 127 (2023) 60–68, https://doi.org/10.1016/J.JES.2022.04.013.
[205] Y. Liu, S. Chen, K. Li, J. Wang, P. Chen, H. Wang, J. Li, F. Dong, Promote the activation and ring opening of intermediates for stable photocatalytic toluene degradation over Zn-Ti-LDH, J. Colloid Interface Sci. 606 (2022) 1435–1444, https://doi.org/10.1016/J.JCIS.2021.08.146.
[206] Z. Nie, C. Sui, X. Xie, S.Q. Ni, L. Kong, Y. Wang, J. Zhan, Fe vacancies in FeOCl enhanced reactive oxygen species generation for photocatalytic elimination of emerging pollutants, Appl. Catal. B Environ. Energy 347 (2024) 123819, https://doi.org/10.1016/J.APCATB.2024.123819.
[207] B. Liu, B. Zhang, B. Liu, Z. Hu, W. Dai, J. Zhang, F. Feng, B. Lan, T. Zhang, H. Huang, Surface hydroxyl and oxygen vacancies engineering in ZnSnAl LDH: synergistic promotion of photocatalytic oxidation of aromatic VOCs, Environ. Sci. Technol. 58 (2024) 4404–4414, https://doi.org/10.1021/acs.est.3c08860.
[208] H. Ma, X. Wang, R. Jin, T. Tan, X. Zhou, R. Fang, Y. Shen, F. Dong, Y. Sun, Promote hydroxyl radical and key intermediates formation for deep toluene mineralization via unique electron transfer channel, J. Colloid Interface Sci. 630 (2023) 704–713, https://doi.org/10.1016/j.jcis.2022.10.160.
[209] C. Yang, J. Li, J. Zhang, G. Yu, J. Yang, M. Zhu, Stable and efficient selective photochemical conversion of nitric oxide into nitrates via earth-alkaline-carbonate-doped N-rich carbon nitride, Adv. Funct. Mater. (2025) 2501291, https://doi.org/10.1002/adfm.202501291.
[210] M. Kumar, K.K. Parashar, S.K. Tandi, T. Kumar, D.C. Agarwal, A. Pathak, Fabrication of Ag:TiO2 nanocomposite thin films by sol-gel followed by electron beam physical vapour deposition technique, J. Spectrosc. 1 (2013) 491716, https://doi.org/10.1155/2013/491716.
[211] W. Liu, H. Tang, D. Liu, Combining density functional theory and CFD-PBM model to predict TiO2 nanoparticle evolution during chemical vapor deposition, Chem. Eng. J. 454 (2023) 140174, https://doi.org/10.1016/J.CEJ.2022.140174.
[212] F. Wang, X. Qian, X. Li, J. Ye, Z. Han, Y. Chen, G. Liu, J. Li, Optical–thermal properties of reduced TiO2 microspheres prepared by flame spraying, Mater. Lett. 151 (2015) 82–84, https://doi.org/10.1016/J.MATLET.2015.03.030.
[213] P. Shi, H. Sun, G. Yi, W. Wang, S. Wan, Y. Yu, Q. Wang, Tribological behavior and mechanical properties of thermal sprayed TiO2–ZnO and TiOx ceramic coatings, Ceram. Int 49 (2023) 18662–18670, https://doi.org/10.1016/J.CERAMINT.2023.02.243.
[214] T. Ishigaki, Y. Nakada, N. Tarutani, T. Uchikoshi, Y. Tsujimoto, M. Isobe, H. Ogata, C. Zhang, D. Hao, Enhanced visible-light photocatalytic activity of anatase-rutile mixed-phase nano-size powder given by high-temperature heat treatment, R. Soc. Open Sci. 7 (2020) 191539, https://doi.org/10.1098/rsos.191539.
[215] R.S.B. Utomo, J. Sentanuhady, M.A. Muflikhun, TiO2–SiO2 nanocomposite via a novel sol-gel method with the addition of an energy monitoring device: Synthesized, characterization and anti-bacterial applications, Ceram. Int 50 (2024) 23367–23378, https://doi.org/10.1016/J.CERAMINT.2024.04.059.
[216] O. Sadek, S. Touhtouh, M. Rkhis, R. Anoua, M. El Jouad, F. Belhora, A. Hajjaji, Synthesis by sol-gel method and characterization of nano-TiO2 powders, Mater. Today Proc. 66 (2022) 456–458, https://doi.org/10.1016/J.MATPR.2022.06.385.
[217] T. Feng, F.K. Yam, Photoelectrochemical properties of anatase TiO2 nanostructures prepared by hydrothermal method: Effect of illumination and external bias on charge transport, Ceram. Int 50 (2024) 19886–19897, https://doi.org/10.1016/J.CERAMINT.2024.03.116.
[218] T. Feng, F.K. Yam, A comparative study of TiO2 nanostructures prepared by one-step and two-step hydrothermal method: Physical and photoelectrochemical properties, Phys. B Condens Matter 684 (2024) 415996, https://doi.org/10.1016/J.PHYSB.2024.415996.
[219] K.Do Kim, H.T. Kim, Comparison of the growth mechanism of TiO2-coated SiO2 particles prepared by sol–gel process and water-in-oil type microemulsion method, Colloids Surf. A Physicochem Eng. Asp. 255 (2005) 131–137, https://doi.org/10.1016/J.COLSURFA.2004.12.036.
[220] A. Zielińska, E. Kowalska, J.W. Sobczak, I. Łacka, M. Gazda, B. Ohtani, J. Hupka, A. Zaleska, Silver-doped TiO2 prepared by microemulsion method: Surface properties, bio- and photoactivity, Sep Purif. Technol. 72 (2010) 309–318, https://doi.org/10.1016/J.SEPPUR.2010.03.002.
[221] G. Lofrano, F. Ubaldi, L. Albarano, M. Carotenuto, V. Vaiano, F. Valeriani, G. Libralato, G. Gianfranceschi, I. Fratoddi, S. Meric, M. Guida, V. Romano Spica, Antimicrobial Effectiveness of Innovative Photocatalysts: A Review, Nanomaterials 12 (16) (2022) 2831, https://doi.org/10.3390/nano12162831.
[222] Y. Hu, W. Chen, J. Fu, M. Ba, F. Sun, P. Zhang, J. Zou, Hydrothermal synthesis of BiVO4/TiO2 composites and their application for degradation of gaseous benzene under visible light irradiation, Appl. Surf. Sci. 436 (2018) 319–326, https://doi.org/10.1016/J.APSUSC.2017.12.054.
[223] B.X. Lei, L.L. Zeng, P. Zhang, Z.F. Sun, W. Sun, X.X. Zhang, Hydrothermal synthesis and photocatalytic properties of visible-light induced BiVO4 with different morphologies, Adv. Powder Technol. 25 (2014) 946–951, https://doi.org/10.1016/J.APT.2014.01.014.
[224] T. Anukunprasert, C. Saiwan, E. Traversa, Microstructure effect of nanocrystalline titanium dioxide prepared by microemulsion technique on photocatalytic decomposition of phenol, J. Mater. Res 21 (2006) 3001–3008, https://doi.org/10.1557/jmr.2006.0373.
[225] N.I. Politova-Brinkova, S.R. Tsibranska-Gyoreva, S.S. Tcholakova, N.D. Denkov, T. Danner, Preparation of tio2 nanoparticle aggregates and capsules by the 'two-emulsion method', Colloids Interfaces 4 (4) (2020) 57, https://doi.org/10.3390/colloids4040057.
[226] A. Vahl, S. Veziroglu, B. Henkel, T. Strunskus, O. Polonskyi, O.C. Aktas, F. Faupel, Pathways to tailor photocatalytic performance of TiO2 thin films deposited by reactive magnetron sputtering, Materials 12 (17) (2019) 2840, https://doi.org/10.3390/ma12172840.
[227] B.K. Ozcelik, C. Ergun, Synthesis of ZnO nanoparticles by an aerosol process, Ceram. Int 40 (2014) 7107–7116, https://doi.org/10.1016/J.CERAMINT.2013.12.044.
[228] N. Sedefoglu, Green synthesis of ZnO nanoparticles by Myrtus communis plant extract with investigation of effect of precursor, calcination temperature and study of photocatalytic performance, Ceram. Int 50 (2024) 9884–9895, https://doi.org/10.1016/J.CERAMINT.2024.01.387.
[229] V. Gadore, S.R. Mishra, K.K. Yadav, M. Ahmaruzzaman, Green synthesis of novel Z-scheme SnS2/HAp nanocomposite using Ocimum tenuiflorum leaf extract and investigation of its photocatalytic activity, Sci. Rep. 14 (2024) 23493, https://doi.org/10.1038/s41598-024-74819-1.
[230] D. Ayu Larasati, D. Lismawenning Puspitarum, N. Imani Istiqomah, J. Partini, E. Suharyadi, D. Lismawenning Puspitarum, H. Ali, D. Ali, Novel green synthesis approach of eco-friendly magnetic/semiconductor nanocomposites as magnetically separable and reusable photocatalyst for organic dye degradation, Results Chem. 10 (2024) 101693, https://doi.org/10.1016/J.RECHEM.2024.101693.
[231] T.H. Kim, G.M. Go, H.B. Cho, Y. Song, C.G. Lee, Y.H. Choa, A novel synthetic method for N Doped TiO2 nanoparticles through plasma-assisted electrolysis and photocatalytic activity in the visible region, Front Chem. 6 (2018) 458, https://doi.org/10.3389/fchem.2018.00458.
[232] N. Deng, Y. Wang, G. Luo, A novel method for fast and continuous preparation of superfine titanium dioxide nanoparticles in microfluidic system, Particuology 60 (2022) 61–67, https://doi.org/10.1016/J.PARTIC.2021.04.015.
[233] M. Kumar, X. Xiong, Z. Wan, Y. Sun, D.C.W. Tsang, J. Gupta, B. Gao, X. Cao, J. Tang, Y.S. Ok, Ball milling as a mechanochemical technology for fabrication of novel biochar nanomaterials, Bioresour. Technol. 312 (2020) 123613, https://doi.org/10.1016/J.BIORTECH.2020.123613.
[234] F. Yang, C. Wang, L. Li, H. Diao, Y. Wang, X. Zheng, C. Li, Nickel-Doped TiO2 Nanoplate Synthesized via Mechanical Ball Milling-Assisted Sol–Gel Method for Photocatalytic Degradation of MB and NO, Processes 13 (2025) 1192, https://doi.org/10.3390/pr13041192.
[235] Q. Hu, J. Xu, D. Zhang, S. Sun, G. Zhang, Atomic layer deposition in the design of functional materials for sensing/removing toxic gases, Curr. Opin. Environ. Sci. Health 36 (2023) 100517, https://doi.org/10.1016/J.COESH.2023.100517.
[236] N.K.R. Eswar, S.A. Singh, J. Heo, Atomic layer deposited photocatalysts: Comprehensive review on viable fabrication routes and reactor design approaches for photo-mediated redox reactions, J. Mater. Chem. A Mater. 7 (2019) 17703–17734, https://doi.org/10.1039/c9ta04780h.
[237] C.Y. Su, L.C. Wang, W.S. Liu, C.C. Wang, T.P. Perng, Photocatalysis and hydrogen evolution of Al- and Zn-Doped TiO2 nanotubes fabricated by atomic layer deposition, ACS Appl. Mater. Interfaces 10 (2018) 33287–33295, https://doi.org/10.1021/acsami.8b12299.
[238] M. Liu, X. Bao, F. Ma, M. Wang, L. Zheng, Z. Wang, P. Wang, Y. Liu, H. Cheng, Y. Dai, Y. Fan, Z. Zheng, B. Huang, Enhanced stability and activity towards photocatalytic CO2 reduction via supercycle ALD of Cu and TiO2, Chem. Eng. J. 429 (2022) 132022, https://doi.org/10.1016/J.CEJ.2021.132022.

[239] W. Liu, Z. Zhang, D. Liu, Comparison of SiO2/TiO2 photocatalysts with different thicknesses synthesized by fluidized bed atomic layer deposition, Powder Technol. 438 (2024) 119613, https://doi.org/10.1016/J.POWTEC.2024.119613.
[240] S. Parsa Amouzesh, M. Zandjou, A. Ali Khodadadi, Y. Mortazavi, F. Hooriabad Saboor, S. Saris, A. Javanmard, S. Alirezayi, M. Asgari, Innovative photocatalyst design: advancing ZnO/MIL-100(Fe) through atomic layer deposition in hydrogen evolution, ChemCatChem 11 (2024) e202401016, https://doi.org/10.1002/cctc.202401016.
[241] S. Saedy, N. Hiemstra, D. Benz, H. Van Bui, M. Nolan, J.R. van Ommen, Dual promotional effect of CuxO clusters grown with atomic layer deposition on TiO2 for photocatalytic hydrogen production, Catal. Sci. Technol. 12 (2022) 4511–4523, https://doi.org/10.1039/d2cy00400c.
[242] N. Li, K. Tong, L. Yang, X. Du, Review of 3D printing in photocatalytic substrates and catalysts, Mater. Today Energy 29 (2022) 101100, https://doi.org/10.1016/J.MTENER.2022.101100.
[243] J.M. Aguirre-Cortés, A.I. Moral-Rodríguez, E. Bailón-García, A. Davó-Quiñonero, A.F. Pérez-Cadenas, F. Carrasco-Marín, 3D printing in photocatalysis: methods and capabilities for the improved performance, Appl. Mater. Today 32 (2023) 101831, https://doi.org/10.1016/J.APMT.2023.101831.
[244] X. Liu, S. Ma, P. He, M. Wang, X. Duan, D. Jia, P. Colombo, Y. Zhou, 3D printing of green and environment-friendly rGO@ZnO/GP for removal of methylene blue from wastewater, J. Phys. Chem. Solids 174 (2023) 111158, https://doi.org/10.1016/J.JPCS.2022.111158.
[245] A. Iborra-Torres, M. Huš, K. Nguyen, A. Vamvakeros, M.T. Sajjad, S. Dunn, M. Mertens, S. Jacques, A.M. Beale, B. Likozar, G. Hyett, S. Kellici, V. Middelkoop, 3D printed SrNbO2N photocatalyst for degradation of organic pollutants in water, Mater. Adv. 4 (2023) 3461–3472, https://doi.org/10.1039/d2ma01076c.
[246] J. Liu, L. Liang, B. Su, D. Wu, Y. Zhang, J. Wu, C. Fu, Transformative strategies in photocatalyst design: merging computational methods and deep learning, J. Mater. Inform. 4 (2024) 33, https://doi.org/10.20517/jmi.2024.48.
[247] D. Ješić, B. Pomeroy, K.M. Kamal, Ž. Kovačič, M. Huš, B. Likozar, Photo- and photoelectrocatalysis in nitrogen reduction reactions to ammonia: interfaces, mechanisms, and modeling simulations, Adv. Energy Sustain. Res. 5 (2024) 2400083, https://doi.org/10.1002/aesr.202400083.
[248] C. Zhao, W. Dong, K. Wang, Z. Tao, W. Li, Investigation on effects of LiCl, KCl and polyethylene oxide on electrochemical properties of cement-based capacitors, Constr. Build. Mater. 481 (2025) 141612.
[249] Y. Song, L. Huang, Y. Wang, Y. Du, Z. Song, Q. Dong, X. Zhao, J. Qi, G. Zhang, W. Li, L. Shi, Energy performance and fire risk of solar PV panels under partial shading: An experimental study, Renew. Energy 246 (2025) 22910.
[250] C. Zhao, W. Dong, J. Liu, S. Peng, W. Li, Toward intelligent buildings and civil infrastructure: A review on multifunctional concrete through nanotechnology, Cem. Concr. Compos. 163 (2025) 106165.
[251] D. Luo, K. Wang, D. Wang, A. Sharma, W. Li, I.H. Choi, Artificial intelligence in the design, optimization, and performance prediction of concrete materials: a comprehensive review, npj Mater, Sustain 3 (2025) 14.